Amirhossein Nikoofard

Control and Adaptive Observer Designs for Managed Pressure and Under Balanced Drilling

Amirhossein Nikoofard

Doctoral Thesis

NTNU
Norwegian University of
Science and Technology
Faculty of Information Technology,
Mathematics and Electrical Engineering
Department of Engineering Cybernetics

◉ NTNU
Norwegian University of
Science and Technology

◉ NTNU
Norwegian University of
Science and Technology

◉ NTNU

Amirhossein Nikoofard

Control and Adaptive Observer Designs for Managed Pressure and Under Balanced Drilling

Thesis for the degree of Philosophiae Doctor

Trondheim, February 2016

Norwegian University of Science and Technology
Faculty of Information Technology,
Mathematics and Electrical Engineering
Department of Engineering Cybernetics

◉ NTNU
Norwegian University of
Science and Technology

Dedicated to my parents,
and my sisters,
Without whom none of my success would be possible

Summary

Due to increasing the number of depleted formations, reservoirs with low pressure margins and high cost of field exploration and development, there has been increasing interest in under-balanced drilling (UBD) and managed pressure drilling (MPD). These types of drillings concepts have contributed to improved oil recovery and reduced drilling problems.

UBD and MPD have several advantages compared to conventional drilling such as increasing the ultimate recovery from the reservoir, reducing the non-productive time (NPT), increasing the rate of penetration (ROP), and extending control over bottom-hole pressure (BHP) for operational scenarios such as connections and trips and when the rig pumps are off, improvement in safety and well control resulting from more detailed design and planning required for accomplishment, decreasing invasive formation damage, and reducing drilling problems.

Since the pressure of the well is kept intentionally lower than the pressure of the reservoir in UBD operations, the UBD operations potentially have some risks and perils. Therefore, it is important to study the control system and monitoring methodology of UBD operations to improve the safety and efficiency of this method. Underbalanced drilling is not possible for some cases due to existence of high (H_2S) in the well or instability in wellbore.

MPD is an alternative overbalanced drilling method which can work on a narrow pressure window and reduce drilling problems. Offshore MPD operation in hostile environment, such as the North Sea, is a challenging problem in drilling, due to heave motion of floating platforms and ships. Without proper control, it leads to potential loss of mud, rig blowout and formation kicks. Therefore, it is vital to study the control of offshore MPD operations with heave motion.

Reservoir properties (i.e. production index, reservoir pore pressure) specify influx of formation fluids during UBD operations. Therefore, reservoir characterization has a significant effect in the success of UBD. In this work, we develop and compare methods that rely on distributed and low order lumped models to estimate the states and geological properties of the reservoir during UBD operation. In this study we also design a controller to attenuate heave disturbance in offshore MPD system.

A nonlinear moving horizon estimation (MHE) based on a nonlinear two-

phase fluid flow model is designed to estimate the total mass of gas and liquid in the annulus, and geological properties of the reservoir during UBD operation. This observer is evaluated and compared with an Unscented Kalman filter for the case of a pipe connection scenario where the main pump is shut off and the rotation of the drill string and the circulation of fluids are stopped. These adaptive observers are compared to each other in terms of speed of convergence, sensitivity of noise measurement and accuracy. The results show that both algorithms are capable of identifying the production constants of gas and liquid from the reservoir into the well, while the nonlinear MHE achieves better performance than the Unscented Kalman filter.

In addition, a nonlinear Lyapunov-based adaptive observer and an Unscented Kalman filter based on a low order lumped (LOL) model and an Unscented Kalman filter based on the distributed drift-flux model are designed to estimate the states and the production constants of gas and liquid from the reservoir into the well by using real-time measurements of the choke and the bottom-hole pressures during UBD operation. These adaptive observers are tested by two scenarios which are simulated with the OLGA simulator: a pipe connection scenario and a scenario with a changing production index. The OLGA dynamic multiphase flow simulator is a high fidelity simulation tool. The performance of the adaptive observers to detect and track the changes in production parameters is studied. Robustness of the adaptive observers is investigated despite uncertainties in the reservoir and well parameters of the models. The results show that all adaptive observers are capable of identifying the production constants of gas and liquid from the reservoir into the well, with some differences in performance. It is also found that the LOL model is sufficient for the purpose of reservoir characterization during UBD operations.

To estimate unmeasured states, production parameters and slip parameters using real time measurements of the bottom-hole pressure and liquid and gas rate at the outlet an Unscented Kalman filter based on simplified drift-flux model is designed. The drift-flux model uses a specific slip law which allows for transition between single and two phase flows. The performance is tested against the Extended Kalman Filter by using OLGA simulations for two drilling scenarios: a pipe connection scenario and a scenario with a changing production index. The number of cells in the discretization of the drift-flux model was found to not have a significant effect on accuracy of estimation. Robustness of the Unscented and Extended Kalman Filters for pipe connection scenario is studied in case of uncertainties and errors in the reservoir and well parameters of the model. The results show that these methods are very sensitive to errors in the reservoir pore pressure value.

However, there are robust in case of error in the liquid density value of the model.

Finally, a constrained model predictive control (MPC) scheme is applied to MPD operations for controlling of the annular pressure in a well when drilling from a floating offshore vessel. This controller is evaluated and compared with a standard proportional-integral-derivative (PID) control scheme to deal with heave disturbances. The heave disturbances are simulated by a stochastic model describing sea waves in the North Sea. The robustness of the controller to compensate for heave disturbances despite significant uncertainties in the friction factor and bulk modulus is investigated by Monte Carlo simulations. The results show that the constrained MPC has a good performance to regulate the set point and attenuate the effect of the heave disturbance. Heave motion can be predicted for short time based on forward-looking sensors such as ocean wave radar. It is found that the performance of MPC can be further improved by prediction of the heave motion about $10s$ ahead.

Preface

This thesis is submitted in partial fulfillment of the requirements for the degree of Doctor of Philosophy (PhD) at the Norwegian University of Science and Technology (NTNU). The research has been conducted at the Department of Engineering Cybernetics (ITK) from July 2012 to September 2015. The work has been funded by the Norwegian Research Council and Statoil ASA (NFR project 210432/E30 Intelligent Drilling), for which I am very grateful.

I wish to express my sincere gratitude to my supervisor professor Tor Arne Johansen for the continuous support of my PhD study and related research, for his patience, motivation, trust and guidance. His guidance helped me in all the time of research and writing of this thesis. I would also like to thank my co-supervisor adjunct associate professor Glenn-Ole Kaasa (also managing director at Kelda Drilling) for his valuable comments and suggestion for this work.

I would like to thank my project group and coauthors of the papers for comprehensive discussions and feedbacks, including Ulf Jakob Aarsnes, Anders Willersrud, Hessam Mahdianfar, Torbjørn Pedersen, Dr. Agus Hasan, Dr. Florent Di Meglio, Dr. Alexey Pavlov, Dr. Jan Einar Gravdal, professor Ole Morten Aamo, professor Lars Imsland, and adjunct professor Gerhard Nygaard.

I would also like to thank my colleagues in Department of Engineering Cybernetics, Kawthar Student Organization, and Iranian community of Trondheim. I express my special thanks to Hossein Mirzaei and Amirhossein Bakhtiari for their kind support and friendship during my short visit in USA and Canada. Many thanks to the department secretaries, Tove, Unni, Jan, Eva, Janne, and Bente for their appreciable help on all the bureaucracy. I would like to express my special thanks to Dr. Sara Nikoofard for constructive discussions and assistance during my PhD work.

Finally and foremost, I wish to express my thanks to my parents and my sisters for unconditional love and support in my whole life. I can say without shadow of doubt that without their support this work would not be happened.

Amirhossein Nikoofard

Trondheim, November 2015

Contents

List of figures

List of tables

Nomenclatures

UBD	Under-Balanced Drilling
UKF	Unscented Kalman Filter
LOL	Low-Order Lumped Model
LWD	Logging While Drilling
EKF	Extended Kalman Filter
ECD	Equivalent Circulating Density
MPD	Managed Pressure Drilling
MPC	Model Predictive Control
MHE	Moving Horizon Estimation
MWD	Measurement While Drilling
DFM	Drift-Flux Model
PI	Production Index
PID	Proportional-Integral-Derivative
PDE	Partial Differential Equation
WHP	Wellhead Pressure
ROP	Rate of Penetration
RCD	Rotating Control Devices
NPT	Non-Productive Time
NRV	Non-Return Valve
BOP	Blowout Preventer
BHA	Bottom-hole Assembly
WOB	Weight On Bit
LF	Low-Frequency
WF	Wave-Frequency
BHCP	Bottom-hole circulating pressure

CHAPTER 1

Introduction

The total consumption of oil and natural gas in the world has been increased rapidly over the last two decades. For instance, the average world oil demand raised from 70 million barrels per day (B/D) in 1995 to 92.5 million (B/D) in 2015[1] . Also, the world natural gas demand increased from 2.15 trillion cubic meters (tcm) in 1995 to almost 3.35 tcm in 2013[2]. The growing demand for oil and natural gas in China, India and other developing countries is the most significant factor for the rapid increase in oil and gas consumption in the world in the last two decades. Fast population growth, rapid economic development, further urbanization and industrialization in these countries are the main factors in rising fossil fuel demands. In the next decade, an increase in oil and natural gas demand is expected in the world[3].

Many giant oil fields in Saudi Arabia, Indonesia, the United States, Norway, Venezuela, and Russia are showing indubitable signs of aging by reducing quality and quantity of oil production. For instance, the oil production in Norway decreased form 3.22 million (B/D) in 2001 to 1.46 million (B/D) in 2013[3]. In the last forty years, supergiant oil fields have rarely been discovered. In addition, new oil discoveries in the world have been less than oil consumption during the year for more than 20 years [70]. Despite of recent developments in unconventional oil such as shale oil, tight oil or oil sands, conventional oil is still an important source of oil demand. Therefore, it is considered important to invest on developing advanced technology which can help to overcome the challenges in oil filed such as high pressure, high temperature reservoirs, deep water reservoirs, depleted reservoirs and reservoir with narrow pressure windows. Under balanced drilling (UBD), dual gradient drilling and managed pressure drilling (MPD) are some advanced

---

[1]http://www.IEA.org
[2]http://www.BP.com
[3]http://www.opec.org/

drilling technology for dealing with challenging reservoir and challenging drilling problems such as differential sticking, lost circulation and etc.

1.1   Drilling Technology

The first modern oil well was drilled under the supervision of Russian engineer V.N. Semyonov on north-east of Baku in 1840's. More than a decade later, the first oil well in the United States was drilled by Colonel Edwin Drake. This well was only $21m$ deep. The oil and gas drilling technology has been has been improved so much since then which enabled us to dig wells as deep as $12km$[4].

Advanced drilling technologies that are used nowadays utilizes a drilling fluid (mud) which is pumped down through the drill string and flows through the drill bit at the bottom of the well (Figure 1.1).

The mud flows up the well annulus carrying cuttings out of the well. The mud is separated at the surface from the return well flow, conditioned, and stored in storage tanks (pits) before it is pumped down into the well for further drilling. To avoid fracturing, collapse of the well, or influx of formation fluids surrounding the well, it is crucial to control the pressure in the open part of the annulus within a certain operating window.

There are three different drilling methods that are commonly used in the industry namely, conventional drilling (also known as over-balanced drilling), managed pressure drilling (MPD) and under-balanced drilling (UBD). Each method control the pressure in the open part of the annulus differently. In conventional drilling, this is done by using a mud of appropriate density and adjusting mud pump flow rates. In MPD and UBD, the annulus is sealed, and the mud exits through a controlled choke, allowing for faster and more precise control of the annular pressure. In conventional drilling and MPD, the pressure in the well is kept greater than the pressure of the reservoir to prevent influx from entering the well, while in UBD operations the pressure of the well is kept below the pressure of the reservoir, allowing formation fluid flow into the well during the drilling operation.

1.2   Under-balanced Drilling

The first well in Norway drilled with under-balanced techniques was a well at the Gullfaks field in 2008. The International Association of Drilling Contractors (IADC) has defined under-balanced drilling as " A drilling activity employing appropriate equipment and controls where the pressure exerted in the wellbore is intentionally less than the pore pressure in any part of

---

[4]http://news.exxonmobil.com/
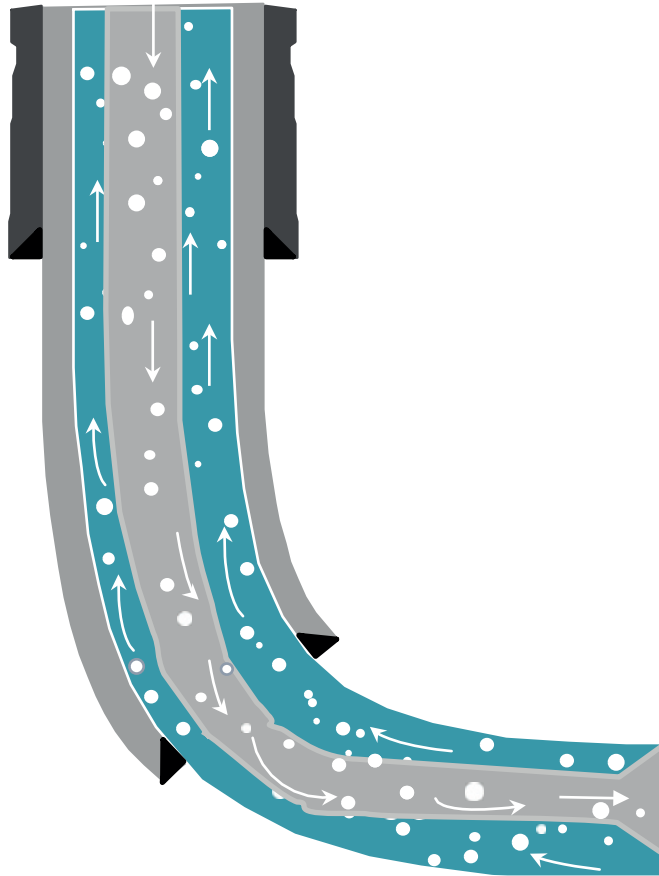
Figure 1.1: Schematic of a drilling system

the exposed formations with the intention of bringing formation fluids to the surface" [102]. So, the hydrostatic pressure of the well (p_{well}) must be kept greater than pressure of collapse (p_{coll}) and less than both pressure of formation reservoir (p_{res}) and formation fracture pressure (p_{frac})

$$p_{coll}(t,x) < p_{well}(t,x) < p_{res}(t,x) < p_{frac}(t,x) \qquad (1.1)$$

at all times t and positions x. UBD can be classified based on drilling fluid as follows:

- ■ Gas and air drilling
- ■ Drilling mud (flow drilling)
- ■ Mist drilling
- ■ Foam drilling

■ Gasified liquid drilling (Gaseated mud)

1.2.1   Gas and air drilling

The gas and air drilling technology is usually used for drilling operations in low pressure reservoirs and performance drilling operations in competent rock formations [59]. Compressed air, membrane generated Nitrogen, cryogenic Nitrogen, natural gas (hydrocarbon gas), and exhaust gas from combustion engines or turbines may be used in gas and air drilling technology. Compressed air is the cheapest and also widely used in mine-shafts drilling and water well drilling. But, air could be flammable, explosive and corrosive. Therefore, air could not be used in hydrocarbon bearing formation. Nitrogen is usually used in UBD operation, notably in offshore drilling. The characteristics of gas and air drilling can be summarized as follows:

- High penetration rate
- Low cost
- Good cement job
- Requiring minimal water influx
- Small surface facility

Currently, air and gas drilling technology is utilized by nearly 30% of land-based oil and natural gas recovery drilling and completion operations[59].

1.2.2   Drilling mud (flow drilling)

Flow drillings are usually suitable for the formation with high hydrostatic pressure. Density of the liquid mud is low enough to satisfy the desired under-balanced conditions. The liquid mud can be used both for water based or oil based type, and is very similar to the mud used in conventional drilling. The liquid mud must be an incompressible and homogenous liquid with constant density. In addition, it does not have any lost circulation materials (LCM) or bridging materials.

1.2.3   Mist drilling

In the mist drilling, the small quantities of liquid is injected into the gas stream. This method is very similar to the air drilling but the liquid mist assists in cleaning small cuttings around the drill bit. Typical mist mud comprises less than 2.5% liquid content. The characteristics of mist drilling can be summarized as follows [59]:

- High penetration rate
- Slugging can occur if the ratio of gas and liquid is incorrect

- Reduce formation of mud rings
- The mist provides some lubrication to the drill bit
- Since the gas in the mist attenuates the mud pulses of Measurement While Drilling (MWD) system, conventional MWD could not be used, instead an electro-magnetic MWD systems are often used.

1.2.4   Foam drilling

Stable foam has been used by the oil drilling industry since the early 1950s [32, 100]. Stable foam is usually generated by mixing liquid, gas, and surfactant foaming agent at surface. Stable foam usually comprises about 55 to 97 % gas at surface condition. In a standard deep drilling operation, the mixture is injected into the drill string. The surface mixture flows as an aerated fluid down the drill string to the bottom hole. The foam is formed at the jet nozzles of the drill bit and then flows up the annulus to the surface. The foam must be broken into its liquid and gas components at separator. Foam drilling is a cost effective method for large holes [59]. The characteristics of stable foam drilling can be summarized as follows:

- High carrying capacity
- Low density
- The stable foam can resist during pipe connection or limited circulation stoppages without affecting the removal of cuttings due to the bubble structures and high fluid yield point
- Reduced pump rates due to improved cuttings transport
- Large surface facility needed
- Since the gas in the stable foam debilitate the mud pulses of MWD system, conventional MWD could not be used, instead an electro-magnetic MWD systems are often used.
- Foam has ability to clean under the bit and the annulus.

1.2.5   Gasified liquid drilling (Gaseated mud)

In this technique, the gas is injected into the incompressible liquid mud to reduce the density. Therefore, gasified liquid drillings are usually suitable for the formation with low hydrostatic pressure. The mixing can be done either on the surface at the base of stand pipe or at the bottom of the well. The gas and liquid mud do not dissolve each other. The liquid mud can use both water based or oil based type. The multiphase flow of gasified liquid drilling complicates the hydraulics program. The characteristics of gasified liquid drilling can be summarized as follows:

- Lower bottom hole pressures can be achieved

- Less gas volumetric flow rate is required

- Increased amount of surface equipments due to the need to store and cleaning of the base fluid

- Conventional MWD cannot be used when the gas is injected at the top of the drill string

- Slugging can occur if the ratio of gas and liquid is incorrect

1.3   UBD advantages and drawbacks

The automatic UBD has several advantages compared to conventional drilling such as increasing the rate of penetration (ROP), increasing the ultimate recovery from the reservoir, reducing the non-productive time (NPT), reducing the risk of differential sticking, reducing the risk of lost circulation, improving the safety and control of the well by using a detailed design for implementation, increasing the bit life due to requiring less weight on the bit, decreasing/eliminating invasive formation damage, increasing economic benefits due to flush production during drilling, not exposing shales to mud filtrate, drilling faster compared to other methods, extending control over Bottom-Hole Pressure (BHP) to operational scenarios such as connections and trips and when the rig pumps are off, no need to clean up the well after drilling, reducing cutting size and plugging of the rocks in the reservoir, being able to find the most productive zones of the reservoir while drilling, reducing equivalent circulating density (ECD) in extended reach wells, limiting or avoiding near well-bore reservoir damage, and reducing drilling-fluid costs through the use of cheaper, lighter fluid systems [5, 9, 10, 91, 97].

While there are several advantages for UBD systems, there are a few drawbacks compared to conventional drilling including: well-bore instability during UBD, increasing string weight due to reduced buoyancy, discontinuous UBD conditions, compatibility with conventional MWD systems, possible abundant borehole erosion, possible increased torque and drag, increasing equipment requirement, gravity drainage in horizontal wells, and the increase cost of personnel due to acquaint with new professions, skills, and procedures [5, 9, 10, 91, 97].

1.4   UBD Equipments and Technology Components

The main surface equipments typically involved in normal UBD operations are as follows [20, 102]

- Nitrogen unit

- Rotating control devices (RCD)
- Chemical injection equipment
- Surface separation equipment
- Choke and manifold system
- Geologic sampler
- Emergency shut-down system
- Non-return valve (NRV)

These components are briefly introduced in the following sections.

1.4.1 Nitrogen unit

The nitrogen unit provides a supply of high-pressure and high-purity nitrogen gas for using in typical UBD operations. A nitrogen converter and a nitrogen generator are two common types of nitrogen unit. A nitrogen generator is a device that compresses and cools the air and then filters nitrogen out of the air for use in oil or gas wells, and a nitrogen converter is a device that converts high pressure liquid nitrogen to high-pressure gas at ambient temperature. For example,Figure 1.2 shows a high pressure compressor of nitrogen generation unit.
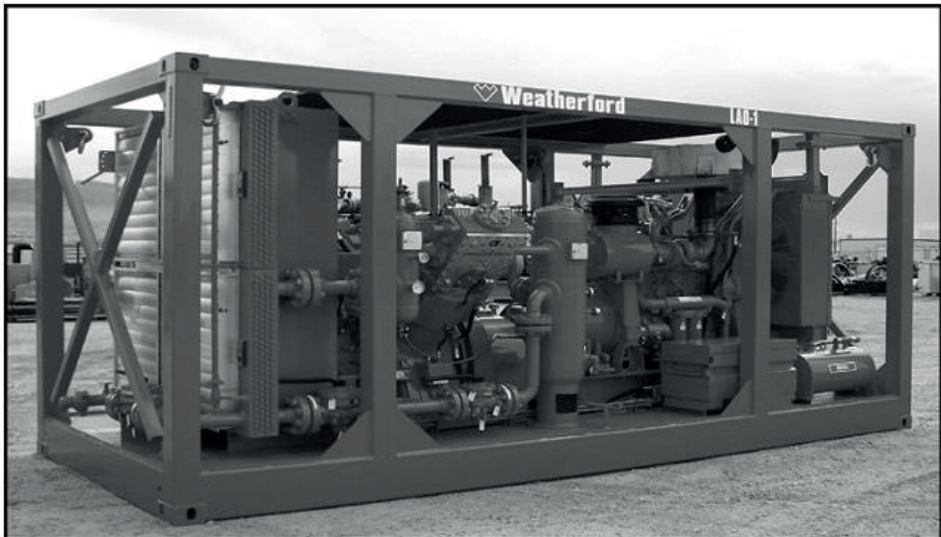
Figure 1.2: High pressure compressor unit of nitrogen generator (courtesy of Weatherford International [59])

1.4.2 Surface separation system

The well fluids contains oil, gas, heavy liquid such as water and drilling mud, and the formation rock cuttings. Therefore, it must be separated by pressurized four (or three) phase separators. The four-phase separator is a pressure vessel that separates the well fluids into different phases based on density. The heaviest phase is the formation rock cuttings (solids) that falls down to the bottom of the separator. The lightest phase is gas that exits from the top of the separator and the oil is stored and evacuated below the gas. The heavy liquid is stored and evacuated above the formation rock cuttings. Figure 1.3 shows structure of a four-phase separation system.
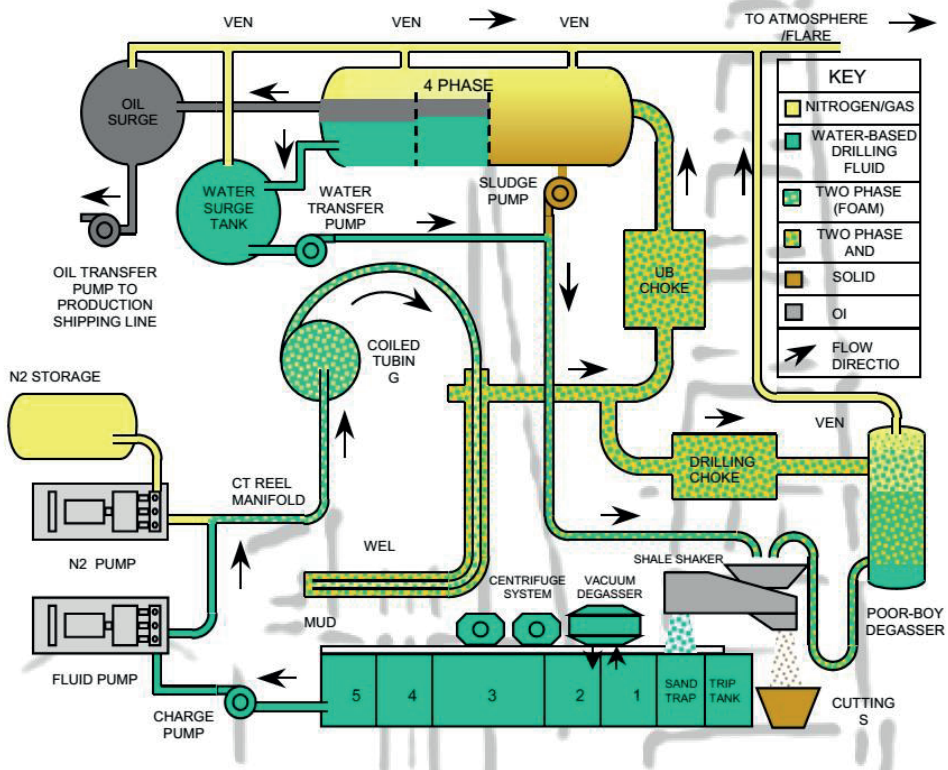
Figure 1.3: Structure of a four- phase separator [4]

1.4.3 Rotating control devices (RCD)

Rotating control devices (RCD) are used to seal around the drill string while allowing rotation of the drill string during UBD operations. It is installed

on top of the well. There are two types of RCD [101].

- **Passive system:** It uses the sealing rubber element and energy from the well pressure. It is usually called a Rotating control head.

- **Active system:** It uses external hydraulic pressure to energize the sealing rubber element. It is usually called a Rotating Annular Preventers.

1.4.4 Choke and manifold system

A choke valve is a component that restricts or blocks flow line or orifice. The main function of a choke valve is to adjust the rate of flow and to control the pressure in the well during UBD operations. It is normally used to control the bottom hole pressure in UBD. The choke manifold consists two chokes that can be installed in parallel on a pipe assembly for increasing the reliability of UBD operation. Figure 1.4 shows the structure of a choke valve.
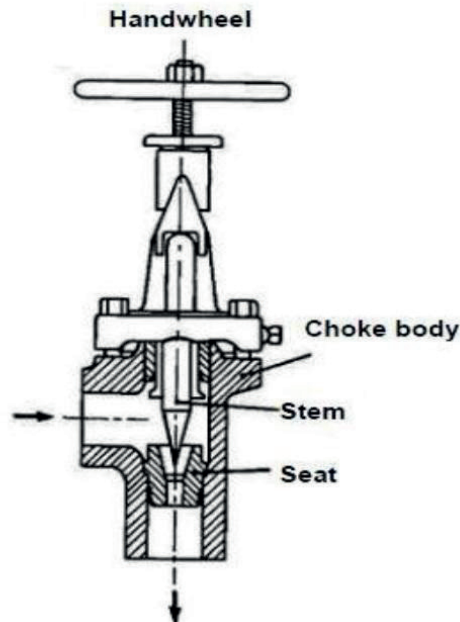
Figure 1.4: Structure of a choke valve [17]

1.4.5 Non-return valve (NRV)

The drill pipe Non-Return Valve (NRV) is used to avoid back-flow of drilling fluids from the annulus to the drill pipe. There are two types of NRVs based on their functions [17].

- **Bit floats:** It is placed at the bottom of the drill pipe above the bit. The functions of the bit floats are safety barrier and shielding the motor, the bit, and MWD against the back flow and plugging by cuttings [17]. There are different types of bit floats (NRV) such as Basic Piston-Type Float, Hydrostatic Control Valve, Inside BOP (Pump-Down Check Valve), and Retrievable NRV or Check Valve [101].

- **String floats:** It is placed in the drill string and normally 300 meters away from the surface. It is used to avoid blowing back gas in the drill string to the drill floor during pipe connection [17].

1.5 Managed Pressure Drilling

The IADC has defined Managed Pressure Drilling as "An adaptive drilling process used to precisely control the annular pressure profile throughout the wellbore. The objectives are to ascertain the downhole pressure environment limits and to manage the annular hydraulic pressure profile accordingly. MPD is intended to avoid continuous influx of formation fluids to the surface"[101]. In MPD operation, the dynamic pressure of the well must be kept higher than the reservoir pore pressure to prevent gas or formation fluids from entering the well and less than a formation fracture pressure at all times t and positions x.

$$p_{res}(x) < p_{well}(x,t) < p_{frac}(x) \qquad (1.2)$$

The automatic MPD system has several advantages compared to conventional drilling as follows [91]:

- Reducing the drilling costs as a result of reducing the nonproductive time.
- Increasing the rate of penetration.
- Improving well-bore stability.
- Minimizing the risk of lost circulation.
- Extending control over bottom-hole pressure (BHP) to operational scenarios such as connections and trips and when the rig pumps are off.
- Improvement in safety and well control resulting from more detailed design and planning required for accomplishment.

1.6   Background study on UBD operations

There are two primary safety barriers in conventional drilling: the mud column (the positive difference between the hydrostatic pressure of the well and the reservoir pressure) and the Blow-Out Preventer (BOP), whereas the primary safety barrier in UBD operations is the BOP. Since there is no mud column barrier in UBD, it is crucial to pay more attention to control and monitoring of UBD operations.

Since the hydrostatic pressure of the well in UBD operation is intentionally lower than the reservoir formation pressure, influx fluids (oil, free gas and water) from the reservoir are mixed with rock cuttings and mud fluid in the annulus. Therefore, modeling of the UBD operation should be considered as multiphase flow which can be modeled by a distributed model or a low-order lumped model. Due to the complexity of the multi-phase flow, dynamics of a UBD well coupled with a reservoir, the modeling, estimation and model based control of UBD operations is still considered as an emerging and challenging topic within drilling automation. This section introduces background on estimation and control of UBD operations.

1.6.1   Estimation in UBD system

The measurement while drilling (MWD) system in the bottom-hole assembly (BHA) is used to measure and transmit to the surface important information of the well such as

- Bottom-hole pressure

- Hole inclination and azimuth

- Load on the bit

These measurements are normally available in real-time. Logging while drilling (LWD) is used to measure and store information about properties of formation such as conductivity, porosity, bed thickness, gamma ray, acoustic velocity, etc. [88] Since this data is collected when the tool is pulled out from the well, these measurements usually have some delay. Real time knowledge of geological properties of the reservoir is very useful in many active controllers, fault detection systems and safety applications in the well during petroleum exploration and production drilling. Therefore, these parameters and states must be estimated online using proper measurements with MWD. Since the selection of a proper model plays the most important role in the success of model based estimators, estimation of states and parameters on UBD operation can be categorized based on the model as follows:

- Estimation based on distributed models

- Estimation based on low-order models

Estimation based on distributed models

Lorentzen et al.[55, 56] designed an ensemble Kalman filter to tune the nine uncertain parameters of a two-phase flow model based on drift flux model of the UBD operation. This method was applied to synthetic cases and full-scale experimental data. The robustness of the ensemble Kalman filter was investigated by using simulator data with different sets of model parameters. A least squares method was used to tune the uncertain parameters of the two-phase flow model instead of the ensemble Kalman filter in [54]. However, it was shown that the least squares approach is not suitable to online tuning due to more complexity in computation [56].

Vefring et al. [110, 111] compared and evaluated the performance of the ensemble Kalman filter and an off-line nonlinear least squares technique utilizing the Levenberg-Marquardt optimization algorithm to estimate reservoir pore pressure and reservoir permeability during UBD while performing an excitation of the bottom-hole pressure. The results show that excitation of the bottom-hole pressure might improve the estimation of the reservoir pore pressure and reservoir permeability.

Aarsnes et al. [2] introduced a simplified drift-flux model and estimation of the distributed multiphase dynamics during UBD operation. This model used a specific empirical slip law without flow-regime predictions . The estimation algorithm separates varying parameters slowly and potentially changing parameters more quickly such as the PI (this sentence is very hard to read think more about it). In this model, fast changing parameters were estimated online simultaneously with the states of the model, while other parameters were calibrated infrequently and offline.

Di Meglio et al. designed an adaptive observer based on a back stepping approach for a linear first-order hyperbolic system of Partial Differential Equations (PDEs) by using only boundary measurements with application to UBD [15]. It was shown that this method has exponential convergence for the distributed state and the parameter estimation. This adaptive observer was used to estimate distributed states and unknown boundary parameters of the well during UBD operations.

Gao Li et al. presented an algorithm for characterizing reservoir pore pressure and reservoir permeability during UBD of horizontal wells [51, 52]. Since the total flow rate from the reservoir has a negative linear correlation with the bottom hole pressure, reservoir pore pressure was identified by the crossing of the horizontal axis and the best-fit regression line between the total flow rate from the reservoir and the bottom hole pressure while performing an excitation of the bottom-hole pressure by changing the choke

valve opening or pump rates. The results show a reasonable performance for this method for reservoir characterization in horizontal well.

Estimation based on low-order models

Nygaard et al. compared and evaluated the performance of the extended Kalman filter, the ensemble Kalman filter and the unscented Kalman filter based on a low order model to estimate the states and the production index (PI) in UBD operation [82]. The results show that the unscented Kalman filter has a better performance than other methods.

Nazari et al. [69] designed and compared the performance of the ensemble Kalman filter and the unscented Kalman filter based on a low order model developed in [80] to estimate the states. For extracting more reliable information from several pressure sensors at each moment, two centralized and distributed estimation fusion schemes based on the unscented Kalman filter for estimating and monitoring mixture velocity of drill-string and annulus was developed. The result of central estimation fusion method was more accurate than the distributed estimation fusion method. But, the distributed fusion presented more robust results.

Reservoir characterization in Under-Balanced Drilling

As mentioned above, reservoir characterization can be estimated by using both low-order models and distributed models. Real-time updates of reservoir properties which are part of these models are able to improve efficiency of the overall well construction by calculating reservoir characterization accurately while drilling, ultimately enabling increased oil recovery by better well completion.

Reservoir characterization during UBD has been investigated by several researchers[39, 41, 52, 110, 111], focusing mainly on the estimation of the reservoir pore pressure and reservoir permeability by using the assumption that the total flow rate from the reservoir is known [110]. Since the total flow rate from the reservoir is usually unknown or unmeasurable online, this thesis has designed novel methods to estimate reservoir properties with only pressure measurements.This can highly improve safety and efficiency of UBD operations.

1.6.2 Control in UBD system

In oil and gas drilling operations, the main goal of automatic or manual controller is to control the annulus pressure in the well under both static and dynamic conditions. In addition, an other objective of well control in UBD operations is to control influx of formation fluids. The most important manipulated variables for control in UBD operations are the choke valve opening, drilling fluid density and the drilling fluid injection flow rates. These variables have different time-scales and effects on UBD operations. The choke valve opening is generally used to control the rapid pressure fluctuations during the UBD operations. The other manipulated variables can be used to adjust pressure and friction in the well for long time scale.

Perez Tellez et al. [94, 95]proposed UBD flow control procedure based on a mechanistic model for control of the bottom-hole pressure and influx of formation fluids during routine operation and pipe connections procedures. The mechanistic model was validated with both field measurements from a Mexican well and full-scale experimental data. Manipulated variables in this controller were the choke valve opening and the drilling fluid injection flow rates. In this study, the choke valve is adjusted manually based on the calculated set-point. This method can cause some errors if the planned pipe connection is not performed properly

Nygaard et al.[81] designed a nonlinear model predictive control(NMPC) based on a detailed model for regulating bottom-hole pressure during the drilling operations and pipe connections procedures. This controller was compared by two other control algorithms, a PI controller with feed-forward control of the pump rates and a manual controller. The PI scheme parameters were tuned by Ziegler-Nichols closed loop algorithm based on a low-order model. The performance of all algorithms was tested on the detailed model. The results showed that the nonlinear model predictive control has a better performance than the PI and the manual controller.

Nygaard et al. [84, 87] used a nonlinear model predictive control algorithm based on detailed model to obtain optimal choke pressure and pump rate for controlling the bottom-hole pressure during pipe connection in a gas dominant well. They used the unscented Kalman filter for nonlinear model to estimate the states, and the permeability of the reservoir. The reservoir was divided into three zones, and the permeability of the reservoir for each zone was estimated. The results show that this control algorithm can reduce fluctuations in the bottom hole pressure during UBD operations.

In Nygaard et al. [85], a finite horizon nonlinear model predictive control in combination with an unscented Kalman filter was designed for controlling the bottom-hole pressure based on a low order model developed in [81]. In this study the unscented Kalman filter (UKF) was used to estimate the

states, and the friction and choke coefficients.

1.7 Background on control of heave disturbance in offshore MPD

There is a specific disturbance occurring during drilling from floaters that significantly affects MPD operations. In this case, the rig moves vertically with the waves, referred to as heave motion. As drilling proceeds, the drill string needs to be extended with new sections. Thus, every couple of hours or so, drilling is stopped to add a new segment of about 27 m to the drill string. During drilling, a heave compensation mechanism is active to isolate the drill string from the heave motion of the rig. However, during connections, the pump is stopped, and the string is disconnected from the heave compensation mechanism and rigidly connected to the rig. The drill string then moves vertically with the heave motion of the floating rig and acts like a piston on the mud in the well. The heave motion may be more than 3 m in amplitude and typically has a period of 10–20 s, which causes severe pressure fluctuations at the bottom of the well. Pressure fluctuations have been observed to be an order of magnitude higher than the standard limits for pressure regulation accuracy in MPD (about ± 2.5 *bar*) [24]. Downward movement of the drill string into the well increases pressure (surging), and upward movement decreases pressure (swabbing). Excessive surge and swab pressures can lead to mud loss resulting from high-pressure fracturing of the formation or a kick-sequence (uncontrolled influx from the reservoir) that can potentially grow into a blowout as a consequence of low pressure.

Rasmussen et al.[99] compared and evaluated different MPD methods for the compensation of surge and swab pressure. In Nygaard et al. [86], it is shown that surge and swab pressure fluctuation in the BHP during pipe connection can be suppressed by controlling the choke and main pump. Nygaard et al. [87] used a nonlinear model predictive control (MPC) algorithm to obtain optimal choke pressure for controlling the BHP during pipe connection in a gas-dominant well. Pavlov et al. [93] presented two nonlinear control algorithms for handling heave disturbances in MPD operations. Mahdianfar et al. [61, 62] designed an infinite-dimensional observer that estimates the heave disturbance. This estimation is used in a controller to reject the effect of the disturbance on the downhole pressure. In all the above mentioned papers, the controllers are designed for the nominal case disregarding the uncertainty in the parameters, although several parameters in the well could be uncertain during drilling operations. In addition, the heave disturbance, which is inherently stochastic and contains many different spectral harmonics, is approximated by one or a couple of sinusoidal waves with known fixed

frequencies throughout controller design and simulations [50]. In this thesis, a stochastic model for the heave motion in the North Sea is given and used in simulations. This thesis develops a model predictive controller for the first time to control the annular pressure in a well to deal with heave disturbances during offshore MPD operations. This can improve safety and performance of MPD operations.

1.8   Research Objective

Based on background studies, the main research objective of this thesis is to develop methods using both distributed and low order model to estimate the states and geological properties of the reservoir during UBD operations. Since reservoir properties determine anticipated influx of formation fluids during UBD operations, reservoir characterization has important role in the safety and efficiency of UBD technology. Real-time updates of reservoir properties may improve efficiency of the overall well construction by accurate estimation of reservoir characterization while drilling. And consequently, enabling increased oil recovery by better well completion.

Since heave motion in offshore drilling induces severe pressure fluctuations at the bottom of the well, improper control leads to loss of mud, rig blowout and formation kicks. Therefore, in this work it has been developed algorithms to control the annular pressure in a well to deal with heave disturbances during offshore MPD operations. In some cases, short-term heave motion can be predicted based on forward-looking sensors such as ocean wave radar and used directly in MPC controller. Short-term heave motion prediction can also improve performance of MPC to deal with heave disturbance.

1.9   Summaries and Outline of the Thesis

Advancement of automation on drilling technologies solved quite a few challenges in this sector in the past few decades. However, still there are many more challenges that has to be addressed. This work addresses two of the important challenges that drilling technology faces nowadays :

1. Accurate reservoir characterization in UBD

2. Control of heave disturbance in offshore MPD operations

To solve these challenges, this thesis includes novel solutions. The summary of contributions of each chapter is as follows. Each of the following chapters is based on a number of papers that are published independently, or sub-

mitted for publication:

Chapter 2. Nonlinear Moving Horizon Observer for estimation of states and parameters in Under-Balanced drilling operations: This chapter describes a nonlinear Moving Horizon Observer to estimate the annular mass of gas and liquid, and production constants of gas and liquid from the reservoir into the well during UBD operations with measuring the choke pressure and the bottom-hole pressure. This observer algorithm which is based on a low-order lumped model is evaluated against Joint Unscented Kalman filter for two different simulations with low and high measurement noise covariance. The results show that both algorithms are capable of identifying the production constants of gas and liquid from the reservoir into the well, while the nonlinear Moving Horizon Observer achieves better performance than the Unscented Kalman filter. A version of the contents of this chapter was presented in [74].

Chapter 3. Reservoir characterization in Under-balanced Drilling using Low-Order Lumped Model: Estimation of the production index of oil and gas from the reservoir into the well during UBD operations is studied. This chapter compares a Lyapunov-based adaptive observer and a joint unscented Kalman filter (UKF) based on a low order lumped (LOL) model and the joint UKF based on the distributed drift-flux model by using real-time measurements of the choke and the bottom-hole pressures. Using the OLGA simulator, it is found that all adaptive observers are capable of identifying the production constants of gas and liquid from the reservoir into the well, with some differences in performance. The results show that the LOL model is sufficient for the purpose of reservoir characterization during UBD operations. Robustness of the adaptive observers is investigated in case of uncertainties and errors in the reservoir and well parameters of the models. A version of the contents of this chapter has been submitted in [79], based on preliminary results in [73] and [78].

Chapter 4. State and parameter estimation of a Drift-Flux Model for Under-Balanced Drilling operations: This chapter presents a drift-flux model describing multiphase (gas-liquid) flow during drilling. The drift-flux model uses a specific slip law which allows for transition between single and two phase flows. With this model, we design Unscented and Extended Kalman Filters (UKF and EKF) for estimation of unmeasured state, production and slip parameters using real time measurements of the bottom-hole pressure, outlet pressure and outlet flow-rate. The OLGA high-fidelity simulator is used to create two scenarios from UBD operations on which

the estimators are tested: A pipe connection scenario and a scenario with a changing production index. A performance comparison reveal that both UKF and EKF are capable of identifying the production constants of gas from the reservoir into the well with sufficient accuracy, while the UKF is more accurate than the EKF. Robustness of the UKF and EKF for the pipe connection scenario is studied in case of uncertainties and errors in the reservoir and well parameters of the model. It is found that these methods are very sensitive to errors in the reservoir pore pressure value. However, there are robust in case of error in the liquid density value of the model. A version of the contents of this chapter has been submitted in [77], based on preliminary results in [76].

Chapter 5. Design constrained MPC for heave disturbance attenuation in offshore Managed Pressure drilling systems: This chapter presents a constrained finite horizon model predictive control (MPC) scheme for regulation of the annular pressure in a well during managed pressure drilling from a floating vessel subject to heave motion. In addition to the robustness of a controller, the methodology to deal with heave disturbances despite uncertainties in the friction factor and bulk modulus is investigated. The stochastic model describing sea waves in the North Sea is used to simulate the heave disturbances. The results show that the closed-loop simulation without disturbance has a fast regulation response, without any overshoot, and is better than a proportional-integral-derivative controller. The constrained MPC for managed pressure drilling shows further improved disturbance rejection capabilities with measured or predicted heave disturbance. Monte Carlo simulations show that the constrained MPC has a good performance to regulate set point and attenuate the effect of heave disturbance in case of significant uncertainties in the well parameter values. A version of the contents of this chapter was presented in [75], based on preliminary results in [72].

Chapter 6. Conclusions. This chapter presents main conclusions of this thesis and possible future research directions.

1.10 Main Contributions

The main contributions of this work can be summarized as follows:

- Nonlinear Moving Horizon Observer using a Low-Order Lumped model for estimation of states and parameters in UBD operations, chapter 2.

■ The proof of stability of Lyapunov-based adaptive observer based on a Low-Order Lumped model for estimation of Production Index in UBD operations, chapter 3.

■ Comparasion of the joint unscented Kalman filter and a Lyapunov-based adaptive observer for estimating the states and production constant of gas and liquid from the reservoir into the well based on a Low-Order Lumped model for UBD operation, chapter 3.

■ Applying the unscented Kalman Filter for estimation of states and parameters of a Drift-Flux Model, chapters 3 & 4.

■ Constrained model predictive control (MPC) scheme for regulation of the annular pressure in a well and heave disturbance attenuation in offshore MPD systems, chapter 5.

1.11   Publications

The main contribution of this thesis presented in several conferences and journal papers which are listed below:

- **Nikoofard, A.**, Johansen, T. A., Mahdianfar, H., and Pavlov, A. (2013, June). Constrained MPC design for heave disturbance attenuation in offshore drilling systems. In OCEANS-Bergen, 2013 MTS/IEEE (pp. 1-7). IEEE.

- **Nikoofard, A.**, Johansen, T. A., Mahdianfar, H., and Pavlov, A. (2014). Design and comparison of constrained MPC with pid controller for heave disturbance attenuation in offshore managed pressure drilling systems. Marine Technology Society Journal, 48(2), 90-103.

- **Nikoofard, A.**, Johansen, T. A., and Kaasa, G. O. (2014, June). Design and comparison of adaptive estimators for Under-Balanced Drilling. In American Control Conference (ACC), 2014 (pp. 5681-5687). IEEE.

- **Nikoofard, A.**, Johansen, T. A., and Kaasa, G. O. (2014, October). Nonlinear Moving Horizon Observer for Estimation of States and Parameters in Under-Balanced Drilling Operations. In ASME 2014 Dynamic Systems and Control Conference (pp. V003T37A002-V003T37A002). American Society of Mechanical Engineers.

- **Nikoofard, A.**, Aarsnes, U. J. F., Johansen, T. A., and Kaasa, G. O. (2015, May). Estimation of States and Parameters of a Drift-Flux Model with Unscented Kalman Filter. In Proceedings of the 2015 IFAC Workshop on Automatic Control in Offshore Oil and Gas Production (Vol. 2, pp. 171-176).

- **Nikoofard, A.**, Johansen, T. A., and Kaasa, G. O. (2015, June). Evaluation of Lyapunov-based Adaptive Observer using Low-Order Lumped Model for Estimation of Production Index in Under-balanced Drilling. In Proceedings of 9th IFAC international symposium on advanced control of chemical processes (pp. 69-75)

- **Nikoofard, A.**, Johansen, T. A., and Kaasa, G. O. Reservoir characterization in Under-balanced Drilling using Low-Order Lumped Model. Journal of Process Control (submitted)

- **Nikoofard, A.**, Aarsnes, U. J. F., Johansen, T. A., and Kaasa, G. O. State and Parameter Estimation of a Drift-Flux Model for Under-Balanced Drilling Operations. IEEE Transactions Control Systems Technology (submitted)

Nonlinear Moving Horizon Observer for estimation of states and parameters in Under-Balanced drilling operations

2.1 Introduction

In recent years there has been increasing interest in Under-Balanced Drilling (UBD). UBD has the potential to both decrease drilling problems and improve hydrocarbon recovery. In conventional (over-balanced) drilling, or Managed Pressure Drilling (MPD), the pressure of the well must be kept greater than pressure of reservoir to prevent influx from entering the well. But in an UBD operation, the hydrostatic pressure in the circulating downhole fluid system must be kept greater than pressure of collapse and less than pressure of reservoir

$$p_{coll}(t,x) < p_{well}(t,x) < p_{res}(t,x) \qquad (2.1)$$

at all times t and positions x. Since hydrostatic pressure in the circulating downhole fluid system is intentionally lower than the reservoir formation pressure, influx fluids (oil, free gas, water) from the reservoir are mixed with rock cuttings and drilling fluid ("mud") in the annulus. Therefore, modeling of the UBD operation should be considered as multiphase flow. Different aspects of modeling relevant for UBD have been studied in the literature [19, 47, 81, 106].

Estimation and control design in MPD has been investigated by several researchers [38, 63, 72, 75, 92, 105, 113, 114]. However, due to the complexity of multi-phase flow dynamics in UBD operations, there are few studies on estimation and control of UBD operations [56, 73, 81, 82, 85]. Nygaard et al. [82] compared and evaluated the performance of the extended Kalman filter, the ensemble Kalman filter and the unscented Kalman filter to esti-

mate the states and production index in UBD operation. Lorentzen et al.[56] designed an ensemble Kalman filter to tune the uncertain parameters of a two-phase flow model in the UBD operation. In Nygaard et al [85], a finite horizon nonlinear model predictive control in combination with an unscented Kalman filter was designed for controlling the bottom-hole pressure based on a low order model developed in [81], and the unscented Kalman filter was used to estimate the states, and the friction and choke coefficients. Gao Li et al. presented an algorithm for characterizing reservoir pore pressure and reservoir permeability during UBD of horizontal wells [51, 52]. Since the total flow rate from the reservoir has a negative linear correlation with the bottom hole pressure, reservoir pore pressure can be identified by the crossing of the horizontal axis and the best-fit regression line between the total flow rate from the reservoir and the bottom hole pressure while performing an excitation of the bottom-hole pressure by changing the choke valve opening or pump rates. Nikoofard et al.[73] designed Lyapunov-based adaptive observer, recursive least squares and joint unscented Kalman filter based on a low-order lumped model to estimate states and parameters during UBD operations by using the total mass of gas and liquid as measurements calculated from pressure measurements using a model. The performance of adaptive estimators are compared and evaluated for two cases.The results show that all estimators were capable of identifying the production constants of gas and liquid from the reservoir into the well, while the Lyapunov based adaptive observer had the best performance comparing with other methods when there was a significant amount of noise. This chapter estimates states and parameters only by using real-time measurements of the choke and the bottom-hole pressures.

Due to mathematical complexity presented by nonlinearity, state and parameter estimation of nonlinear dynamical systems is one of the challenging topics in the control theory and has been the subject of many studies since its advent. The adaptive observer was proposed by Carrol et al. in 1973 [14]. The Lyapunov based adaptive observer is generally used to design a Luenberger type observer for the state while appropriate adaptive law to estimate the unknown parameters [33, 43, 68, 71]. If the observability and persistency excitation condition is satisfied, then both the state and the parameter estimation will converge to their true values. Nonlinear Moving Horizon Estimation is one of the powerful method which estimates states and parameters simultaneously [34, 65, 98]. At each sampling time, a Moving Horizon Estimation estimate the state and parameter by minimizing a cost function over the previous finite horizon, subject to the nonlinear model equations. Robustness to lack of persistent excitation and measurement noise is due to the use of an apriori prediction model as well as some modifications

to the basic MHE algorithm [35, 107]. The original Kalman filter based on linear model was developed to estimate both state and parameter of the system usually known as an augmented Kalman filter. Several Kalman filter techniques have been developed to work with non-linear system. The unscented Kalman filter has been shown to have a better performance than other Kalman filter techniques for nonlinear system in same cases [104, 112].

Total mass of gas and liquid in the well could not be measured directly, as well as some geological properties of the reservoir such as production constants of gas and liquid from the reservoir might vary and could be uncertain during drilling operations. Therefore, they must be estimated by adaptive estimators during UBD operations. It is assumed that the bottom-hole pressure (BHP) readings are transmitted continuously to the surface through a wired pipe telemetry with a pressure sensor at the measurement while drilling (MWD) tool [31]. This chapter presents the design of a non-linear Moving Horizon Estimation based on a nonlinear two-phase fluid flow model to estimate the total mass of gas and liquid in the annulus and geological properties of the reservoir during UBD operation. The performance of this methods is evaluated against Joint Unscented Kalman Filter for the case of pipe connection operations where the main pump is shut off and the rotation of the drill string and the circulation of fluids are stopped. The estimators are compared to each other in terms of speed of convergence, sensitivity of noise measurement, and accuracy.

This chapter consists of the following sections: The modeling section presents a low-order lumped model based on mass and momentum balances for UBD operation. The adaptive observer section explains nonlinear Moving Horizon Estimation for simultaneously estimating the states and model parameters of a nonlinear system from noisy measurements. In the Simulations section, the simulation results are provided for state and parameter estimation. At the end, the conclusion that has been made through this chapter are presented.

2.2   Modeling

Modeling of Under-balanced Drilling (UBD) in an oil well is a challenging mathematical and industrial research area. Due to existence of multiphase flow (i.e. oil, gas, drilling mud and cuttings) in the system, the modeling of the system is very complex. Multiphase flow can be modeled as a distributed (infinite dimension) model or a lumped (finite dimension) model. A distributed model is capable of describing the gas-liquid behavior along the annulus in the well. In this chapter, a low-order lumped (LOL) model is used. The lumped model considers only the gas-liquid behavior at the

drill bit and the choke system. This modeling method is very similar to the two-phase flow model found in [1, 81]. The simplifying assumptions of the LOL model are listed as below:

- Ideal gas behavior
- Simplified choke model for gas, mud and liquid leaving the annulus
- No mass transfer between gas and liquid
- Isothermal condition and constant system temperature
- Constant mixture density with respect to pressure and temperature.
- Liquid phase considers the total mass of mud, oil, water, and rock cuttings.

The simplified LOL model equations for mass of gas and liquid in an annulus are derived from mass and momentum balances as follows

$$\dot{m}_g = \quad w_{g,d} + w_{g,res}(m_g, m_l) - \frac{m_g}{m_g + m_l} w_{out}(m_g, m_l) \qquad (2.2)$$

$$\dot{m}_l = \quad w_{l,d} + w_{l,res}(m_g, m_l) - \frac{m_l}{m_g + m_l} w_{out}(m_g, m_l) \qquad (2.3)$$

where m_g and m_l are the total mass of gas and liquid, respectively. The liquid phase is considered incompressible, and ρ_l is the liquid mass density. The gas phase is compressible and occupies the space left free by the liquid phase. $w_{g,d}$ and $w_{l,d}$ are the mass flow rate of gas and liquid from the drill string, $w_{g,res}$ and $w_{l,res}$ are the mass flow rates of gas and liquid from the reservoir. The total mass outflow rate is denoted by w_{out}.

The total mass outlet flow rate is calculated by the valve equation

$$w_{out} = K_c Z \sqrt{\frac{m_g + m_l}{V_a}} \sqrt{p_c - p_{c0}} \qquad (2.4)$$

where K_c is the choke constant. Z is the control signal to the choke opening, taking its values on the interval $(0, 1]$. The total volume of the annulus is denoted by V_a. p_{c0} is the constant downstream choke pressure (atmospheric). The choke pressure is denoted by p_c, and derived from ideal gas equation

$$p_c = \frac{RT}{M_{gas}} \frac{m_g}{V_a - \frac{m_l}{\rho_l}} \qquad (2.5)$$

where R is the gas constant, T is the average temperature of the gas, and M_{gas} is the molecular weight of the gas. The flow from the reservoir into the well for each phase is commonly modeled by the linear relation with the

pressure difference between the reservoir and the well. The mass flow rates of gas and liquid from the reservoir into the well are given by

$$
w_{g,res} = \begin{cases} K_g(p_{res} - p_{bh}), & \text{if } p_{res} > p_{bh} \\ 0, & \text{otherwise.} \end{cases} \tag{2.6}
$$

$$
w_{l,res} = \begin{cases} K_l(p_{res} - p_{bh}), & \text{if } p_{res} > p_{bh} \\ 0, & \text{otherwise.} \end{cases} \tag{2.7}
$$

where p_{res} is the known pore pressure in the reservoir, and K_g and K_l are the production constants of gas and liquid from the reservoir into the well, respectively. Finally, the bottom-hole pressure is given by the following equation

$$
p_{bh} = p_c + \frac{(m_g + m_l)g\cos(\Delta\theta)}{A} + \Delta p_f \tag{2.8}
$$

where g is the gravitational constant, A is the cross sectional area of the annulus, $\Delta\theta$ is the average angle between gravity and the positive flow direction of the well, Δp_f is the friction pressure loss in the well

$$
\Delta p_f = K_f(w_{g,d} + w_{l,d})^2 \tag{2.9}
$$

and K_f is the friction factor.

Reservoir parameters could be evaluated by seismic data and other geological data from core sample analysis. But, local variations of reservoir parameters such as the production constants of gas and liquid may be revealed only during drilling. So, it is valuable to estimate the partial variations of some of the reservoir parameters while drilling is performed [82].

2.3 Adaptive Observer

In this section, first the Nonlinear Moving Horizon Estimation (MHE) to estimate states and parameters in UBD operation is explained. Then, the joint unscented Kalman filter is presented for same problem.The choke and the bottom-hole pressures are outputs and measurements of the system. The measurements and inputs of the observer are summarized in Table 2.1. The production constant of gas (K_g) and liquid (K_l) from the reservoir into the well are unknown and must be estimated. Below K_g and K_l are denoted by θ_1 and θ_2, respectively.

Table 2.1: Measurements and Inputs

Variables	Type
Choke pressure (p_c)	Measurement
Bottom-hole pressure (p_{bh})	Measurement
Drill string mass flow rate of gas ($w_{g,d}$)	Input
Drill string mass flow rate of liquid ($w_{l,d}$)	Input
Choke opening (Z)	Input

2.3.1 Nonlinear Moving Horizon Estimation

The LOL model based on equations (2.2)-(2.3) can be represented by a discrete explicit scheme given by

$$x_k = f(x_{k-1}, u_{k-1}) + q_k \qquad (2.10)$$

$$y_k = h(x_k) + r_k \qquad (2.11)$$

$$h(x_k) = [p_c, p_{bh}]^T \qquad (2.12)$$

where q_k and r_k are the process noise and the measurement noise, and u_k is the input. At time t, the information vector of the $N+1$ last measurements and the N last inputs is defined as

$$I_t = col(y_{t-N}, ..., y_t, u_{t-N}, ..., u_{t-1}) \qquad (2.13)$$

$N+1$ is the finite horizon or window length . This information can be summarized in a single vector for measurement and input as follow

$$Y_t = \begin{bmatrix} y_{t-N} \\ y_{t-N+1} \\ \vdots \\ y_t \end{bmatrix} \qquad U_t = \begin{bmatrix} u_{t-N} \\ u_{t-N+1} \\ \vdots \\ u_{t-1} \end{bmatrix} \qquad (2.14)$$

Nonlinear MHE cost function can be considered as follows

$$J(\hat{x}_{t-N,t}, \bar{x}_{t-N,t}, I_t) = \|W(Y_t - H_t(\hat{x}_{t-N,t}))\|^2 + \|V(\hat{x}_{t-N,t} - \bar{x}_{t-N,t})\|^2 \qquad (2.15)$$

where V, W are the positive definite weight matrices. Choosing the tuning matrices V, W in the MHE specify trade-offs in the MHE design. Choosing small tuning matrices V, W lead to faster track of data and convergence but more uncertainty in the estimation. Choosing larger tuning matrices W and V lead to slower track of data and convergence but less uncertainty in the estimation. The cost function (2.15) consists of two standard terms: one

is a term that penalizes the deviation between the measured and predicted outputs, the other term weights the difference between the estimated state at the start of the horizon from its prediction. The Nonlinear MHE minimizes the cost function (2.15) over the window of the current measurement and the historical measurement, subject to the nonlinear model equations. $x^o_{t-N,t}$ is the optimal solution of this problem. The sequence of the state estimates $\hat{x}_{i,t}$ $(i = t - N, \ldots, t)$ can be yielded from the noise free nonlinear model dynamics. So, a sequence of denoted as estimated output vectors $\hat{Y}_t$ can be formulated as follows

$$\hat{Y}_t = H(\hat{x}_{t-N,t}, U_t) = H_t(\hat{x}_{t-N,t}) = \begin{bmatrix} h(\hat{x}_{t-N,t}) \\ h(f^{u_{t-N}}(\hat{x}_{t-N,t})) \\ \vdots \\ h(f^{u_{t-1}}(\ldots(f^{u_{t-N}}(\hat{x}_{t-N,t})))) \end{bmatrix} \quad (2.16)$$

A one-step prediction $\bar{x}_{t-N,t}$ is determined from $x^o_{t-N-1,t-1}$ as follow

$$\bar{x}_{t-N,t} = f(x^o_{t-N-1,t-1}, u_{t-N-1}) \quad t = N+1, N+2, \ldots \quad (2.17)$$

For parameter estimation, x is augmented with the unknown parameter vector θ with the dynamic model $\theta_{t+1} = \theta_t$.

2.3.2 Joint Unscented Kalman Filter

The Unscented Kalman Filter (UKF) was introduced in [36, 37, 109]. The main idea behind the method is that approximation of a Gaussian distribution is easier than approximation on of an arbitrary nonlinear function. The UKF estimates the mean and covariance matrix of estimation error with a minimal set of sample points (called sigma points) around the mean by using a deterministic sampling approach known as the unscented transform. The nonlinear model is applied to sigma points instead of a linearization of the model. So, this method does not need to calculate explicit Jacobian or Hessian. More details can be found in [36, 104, 109, 112].

Two common approaches for estimation of parameters and state variables simultaneously are dual and joint UKF techniques. The dual UKF method uses another UKF for parameter estimation so that two filters run sequentially in every time step. At each time step, the state estimator updates with new measurements, and then the current estimate of the state is used in the parameter estimator. The joint UKF augments the original state variables with parameters and a single UKF is used to estimate augmented state vector. The joint UKF is easier to implement [109, 112].

Using the joint UKF, the augmented state vector is defined by $x^a = [X, \theta]$. The state-space equations for the the augmented state vector at time

instant k is written as:

$$
\begin{bmatrix} x_{1,k} \\ x_{2,k} \\ \theta_{1,k} \\ \theta_{2,k} \end{bmatrix} = \begin{bmatrix} f_1(X_{k-1}, \theta_{1,k-1}) \\ f_2(X_{k-1}, \theta_{2,k-1}) \\ \theta_{1,k-1} \\ \theta_{2,k-1} \end{bmatrix} = f^a(X_{k-1}, \theta_{k-1}, u_{k-1}) + q_k \qquad (2.18)
$$

m_g and m_l are denoted by x_1 and x_2, respectively. The discrete measurements of the system can be modeled as follows:

$$
y_k = h(X_k) + r_k \qquad (2.19)
$$

$$
h(X_k) = [p_c, p_{bh}]^T \qquad (2.20)
$$

where $r_k \sim N(0, R_k)$ is the zero mean Gaussian measurement noise.

2.4 Simulation Results

The parameter values for the simulated well, LOL model and reservoir are summarized in Table 2.2. These parameters are used from the offshore test of WeMod simulator[89]. WeMod is a high fidelity drilling simulator developed by the International Research Institute of Stavanger (IRIS). In WEMOD, the drift-flux model was used for modeling one-dimensional two-phase flow in well. To derive thermodynamic relations, it is generally assumed a system in thermodynamic equilibrium (PVT-models), ideal gas law, and a more detailed model for mud PVT properties[89]. The process noise covariance matrix used in this plant model (LOL model) is

$$
Q = diag[10^{-1}, 10^{-1}, 10^{-4}, 10^{-4}]
$$

UKF parameters are determined empirically and used in the series of equations presented in the Appendix.A. The parameter values for nonlinear MHE and joint UKF are summarized in Table 2.3.

The time-step used for discretizing the dynamic model and adaptive estimator was 1 seconds. The initial values for the estimated and real states and parameters are as follows

$$
x_1 = 5446.6, \quad x_2 = 54466.5, \quad \theta_1 = 5 \quad , \quad \theta_2 = 5
$$

$$
\hat{x}_1 = 4629.6, \quad \hat{x}_2 = 46296.2, \quad \hat{\theta}_1 = 4.25, \quad \hat{\theta}_2 = 4.25
$$

The scenario in this simulation is as follows, first the drilling in a steady-state condition is initiated, then at t = 10 min the main pump is shut off to perform a connection procedure. The rotation of the drill string and the circulation of fluids are stopped for 10 mins. Next after making the first pipe

Table 2.2: Parameter Values for Well and Reservoir

Name	LOL	Unit
Reservoir pressure (p_{res})	270	bar
Collapse pressure (p_{coll})	255	bar
Friction pressure loss (Δp_f)	10	bar
Well total length (L_{tot})	2300	m
Well vertical depth (L)	1720	m
Drill string outer diameter (D_d)	0.1397	m
Annulus volume (V_a)	252.833	m^3
Annulus inner diameter (D_a)	0.2445	m
Liquid flow rate ($w_{l,d}$)	44	Kg/s
Gas flow rate ($w_{g,d}$)	5	Kg/s
Liquid density (ρ_l)	1475	Kg/m^3
Production constant of gas (K_g)	5×10^{-6}	Kg/Pa
Production constant of liquid (K_l)	5×10^{-5}	Kg/Pa
Gas average temperature (T)	25	°C
Average angle ($\Delta\theta$)	0.726	rad
Choke constant (K_c)	0.013	m^2

Table 2.3: Parameter Values for Estimators

Parameter	Value	Parameter	Value
W	100	V	diag (0.1,0.1, 0.03, 0.05)
$N+1$	15	κ	0
β	2	α	0.5

connection at t = 20 min the main pump and rotation of the drill string are restarted. Then at t=52 min the second pipe connection procedure is started, and is completed after 12 mins. Two different simulations with low and high measurement noise covariances are performed. In the first simulation, the choke and the bottom-hole pressures measurements are corrupted by zero mean additive white noise with the following covariance matrix

$$R = diag[0.5^2, 0.5^2]$$

Figures 2.1 and 2.2 show the measured and estimated total mass of gas and liquid, respectively. The nonlinear MHE is more accurate than UKF to estimate the total mass of gas and liquid. The estimation of the production constants of gas and liquid from the reservoir into the well are shown in Figures 2.3 and 2.4, respectively. In estimation of the production constants of gas and liquid from the reservoir into the well, nonlinear MHE has a very fast convergence rate, about 30 seconds or less. UKF take much longer and

it is in the order of minutes. After convergence to the value, the correct nonlinear MHE has more small fluctuations than UKF for estimation of the production constants of gas and liquid.
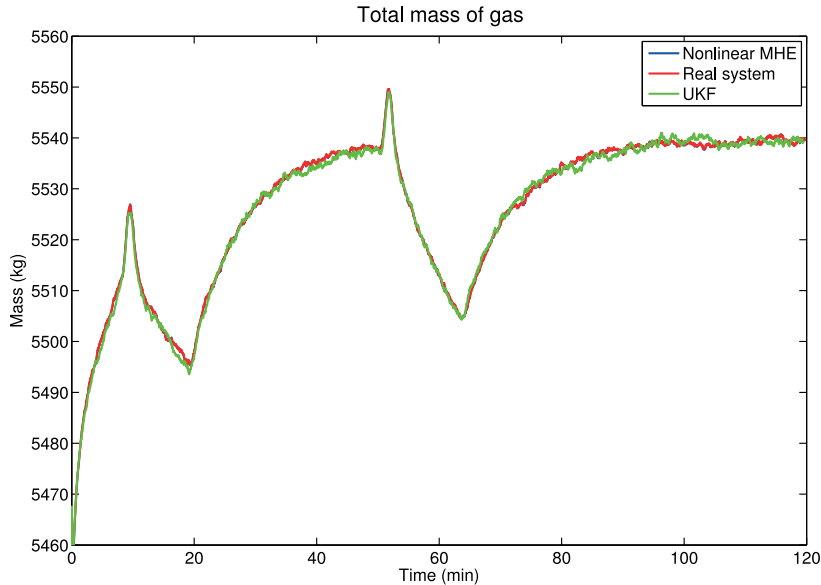
Figure 2.1: Total mass of gas with the low measurement noise covariance

In second simulation, the choke and the bottom-hole pressures are corrupted by zero mean additive white noise with the following covariance matrix

$$R = diag[50^2, 50^2]$$

Figures 2.5 and 2.6 show the measured and estimated total mass of gas and liquid, respectively. It is found that the nonlinear MHE is more accurate than UKF to estimate the total mass of gas and liquid. The estimation of the production constants of gas and liquid from reservoir into the well are illustrated in Figures 2.7 and 2.8, respectively. In estimation of the production constants of gas and liquid from the reservoir into the well, the nonlinear MHE has a very fast convergence rate, about 30 seconds or less, while the UKF takes almost 7 minutes.

In this section, performance of these adaptive estimators is evaluated through the root mean square error (RMSE) metric. The RMSE metric for nonlinear MHE and UKF in two cases are summarized in Table 2.4.
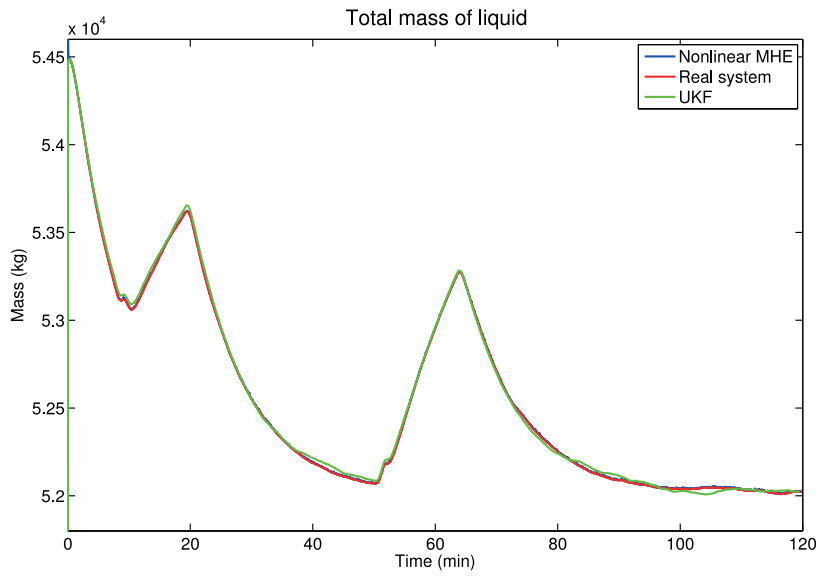
Figure 2.2: Total mass of liquid with the low measurement noise covariance
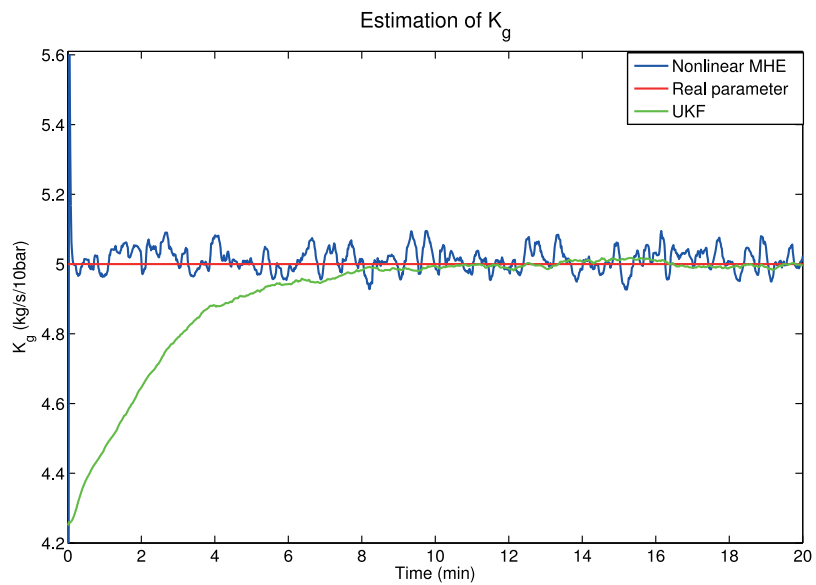
Figure 2.3: Production constant of gas with the low measurement noise covariance
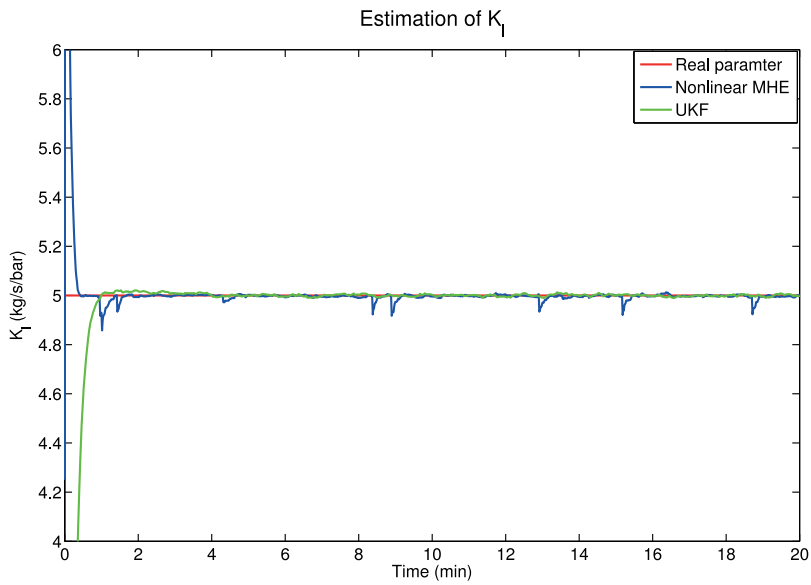
Figure 2.4: Production constant of liquid with the low measurement noise covariance
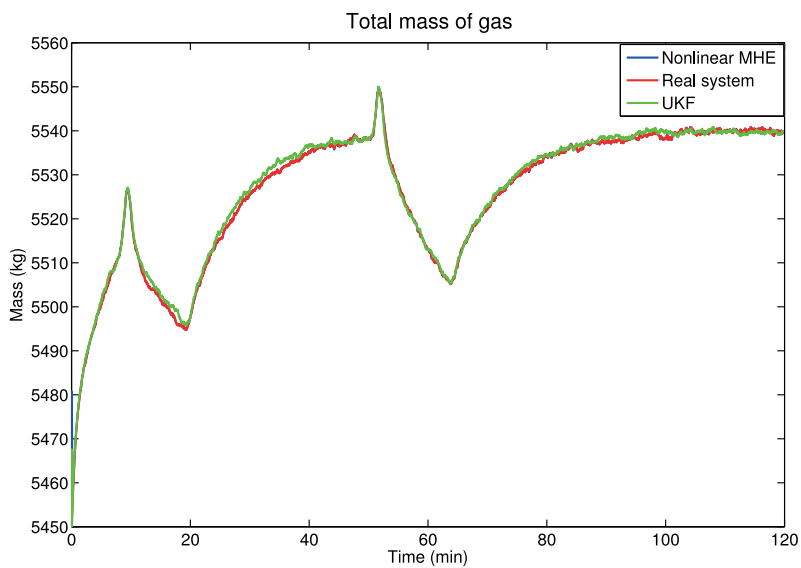
Figure 2.5: Total mass of gas with the high measurement noise covariance
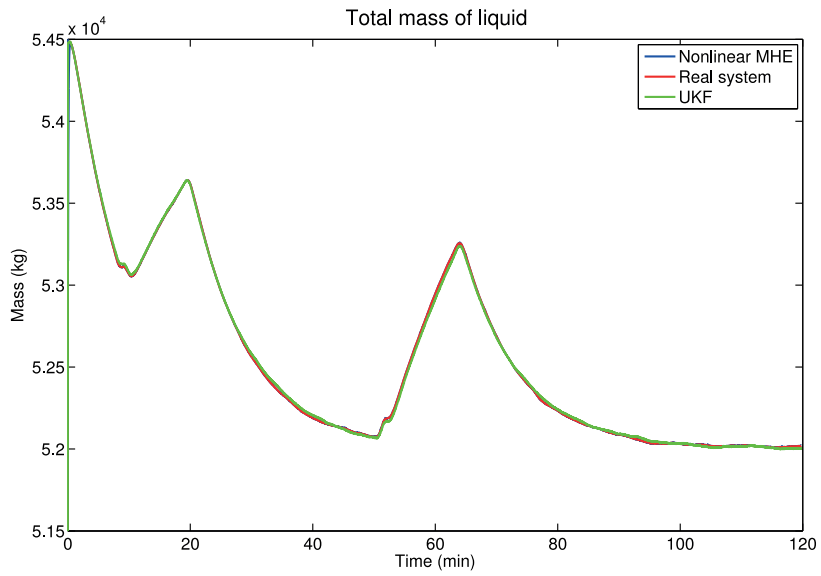
Figure 2.6: Total mass of liquid with the high measurement noise covariance
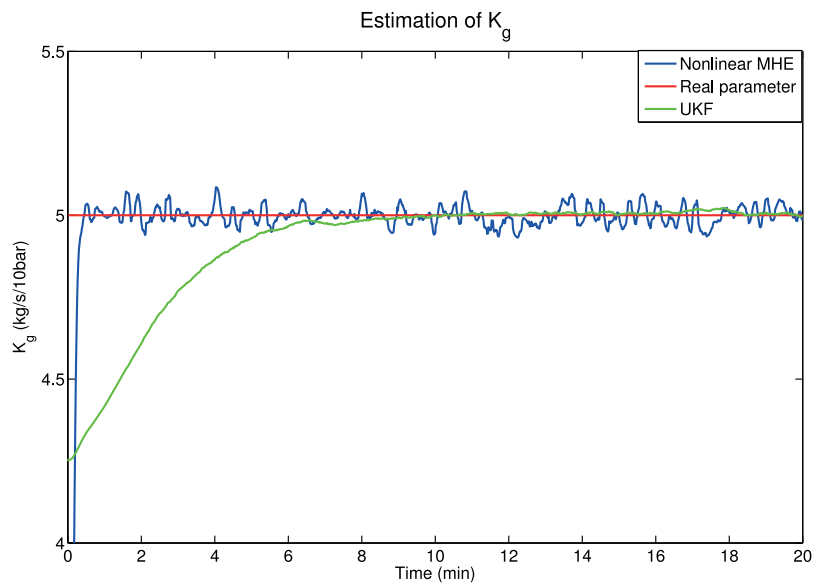
Figure 2.7: Production constant of gas with the high measurement noise covariance
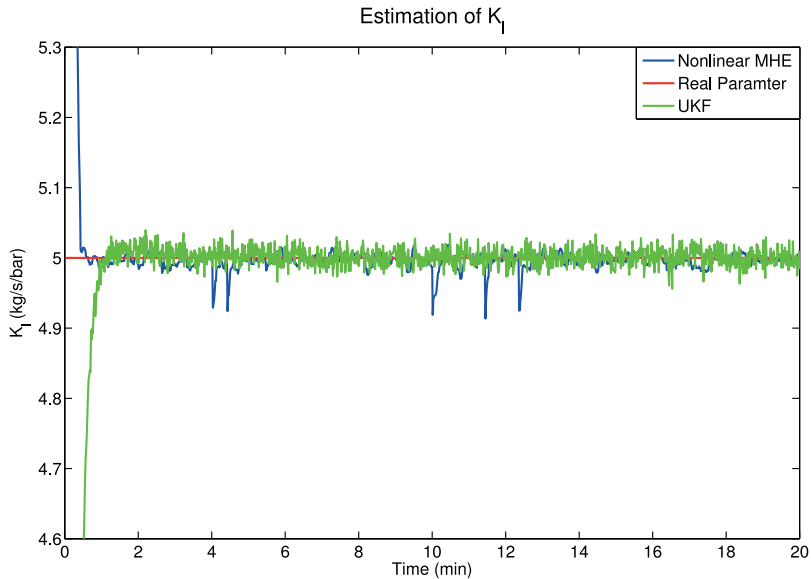
Figure 2.8: Production constant of liquid with the high measurement noise covariance

Table 2.4: RMSE metric

Method	R	x_1	x_2	θ_1	θ_2
MHE	Low	0.315	10.3	0.04	0.100
UKF	Low	0.328	36.4	0.078	0.152
MHE	High	0.978	34.9	0.115	0.667
UKF	High	1.631	96.3	0.084	0.177

According to the RMSE metric table, nonlinear Moving Horizon Observe has the better performance than joint UKF for state and parameter estimation while it has low and high measurement noise covariances.

2.5   Conclusions

This chapter describes nonlinear MHE to estimate states and parameters during pipe connection procedure in UBD operations. The low-order lumped model presented here only captures the major phenomena of the UBD operation. Simulation results demonstrate satisfactory performance of nonlinear MHE and joint UKF for state and parameter estimation during pipe connection procedure with low and high measurement noise covariances. It is

found that the nonlinear MHE shows better convergence and performance than joint UKF with low and high measurement noise covariances. According to the RMSE metric, nonlinear MHE can perform better in terms of accuracy and robustness to measurement noise.

Reservoir characterization in Under-balanced Drilling using Low-Order Lumped Model

3.1   Introduction

Since the number of depleted formations and cost of field exploration and development has increased, there has been increasing interest in new technology and automation of drilling process which can improve drilling efficiency and increase oil recovery for the past two decades. UBD is a technology that enables drilling with the downhole pressure lower than the pore pressure of the formation. The UBD has several advantages compared to conventional drilling in increasing the ultimate recovery from the reservoir, reducing the non-productive time (NPT), minimizing the risk of lost circulation, increasing the rate of penetration (ROP), reducing drilling-fluid costs through the use of cheaper, lighter fluid systems, and reducing drilling problems such as hole cleaning and differential sticking [9, 97].

Real-time updates of reservoir properties may improve efficiency of the overall well construction by more accurate reservoir characterization while drilling, ultimately enabling increased oil recovery by better well completion. Reservoir characterization during UBD has been investigated by several researchers[39, 41, 52, 110, 111], focusing mainly on the estimation of the reservoir pore pressure and reservoir permeability by using the assumption that the total flow rate from the reservoir is known [110]. Kneissl proposed an algorithm to estimate both reservoir pore pressure and reservoir permeability during UBD while performing an excitation of the bottom-hole pressure [41]. However, the variations of fluid flow behavior in the downhole and the annuls section might introduce significant uncertainties to estimation of the reservoir pore pressure. Vefring et al. [110, 111] compared and evaluated

the performance of the ensemble Kalman filter and an off-line nonlinear least squares technique utilizing the Levenberg-Marquardt optimization algorithm to estimate reservoir pore pressure and reservoir permeability during UBD while performing an excitation of the bottom-hole pressure. The result shows that excitation of the bottom-hole pressure might improve the estimation of the reservoir pore pressure and reservoir permeability [110, 111]. Gao Li et al. presented an algorithm for characterizing reservoir pore pressure and reservoir permeability during UBD of horizontal wells [51, 52]. The total flow rate from the reservoir has a negative linear correlation with the bottom hole pressure. Therefore, reservoir pore pressure can be found at the intersection of the horizontal axis and the best-fit regression line between the total flow rate from the reservoir and the bottom hole pressure. It must be performing an excitation of the bottom-hole pressure by changing the choke valve opening or pump rates for estimation of reservoir pore pressure (see example in section 3.5).

In this chapter, it is assumed that reservoir pore pressure is known by identifying from Li's method [52] or other algorithms. The main focus is to estimate both production constants of gas and liquid during UBD operations, simultaneously. Due to the complexity of the multi-phase flow dynamics of a UBD well coupled with a reservoir, the modeling, estimation and control of UBD operations is still considered an emerging and challenging topic in drilling automation. Nygaard et al. compared and evaluated the performance of the extended Kalman filter, the ensemble Kalman filter and the unscented Kalman filter based on a low order model to estimate the states and the production index (PI) in UBD operation [82]. Lorentzen et al. designed an ensemble Kalman filter based on a drift-flux model to tune the uncertain parameters of a two-phase flow model in the UBD operation [56]. In Nygaard et al. [85], a finite horizon nonlinear model predictive control in combination with an unscented Kalman filter was designed for controlling the bottom-hole pressure based on a low order model developed in [81], and the unscented Kalman filter (UKF) was used to estimate the states, and the friction and choke coefficients. A Nonlinear Moving Horizon Observer based on a low-order lumped model (LOL) was designed for estimating the total mass of gas and liquid in the annulus and geological properties of the reservoir during UBD operation for pipe connection procedure in [74]. Aarsnes et al. introduced a simplified drift-flux model and estimation of the distributed multiphase dynamics during UBD operation. This model used a specific empirical slip law without flow-regime predictions [2]. The estimation algorithm separates slowly varying parameters and potentially more quickly changing parameters such as the PI. Fast changing parameters are estimated online simultaneously with the states of the model, but other pa-

rameters are calibrated infrequently and offline. Nikoofard et al. designed an UKF for estimation of unmeasured states, production and slip parameters of simplified drift-flux model using real time measurements of the bottom-hole pressure and liquid and gas rate at the outlet [76]. Di Meglio et al. designed an adaptive observer based on a backstepping approach for a linear first-order hyperbolic system of Partial Differential Equations (PDEs) by using only boundary measurements with application to UBD [15]. It is shown that this method has exponential convergence for the distributed state and the parameter estimation. This adaptive observer is applied to estimate distributed states and unknown boundary parameters of the well during UBD operations. Nikoofard et al. designed Lyapunov-based adaptive observer, a recursive least squares estimator and a UKF based on a LOL model to estimate states and parameters during UBD operations by using the total mass of gas and liquid as measurements calculated from pressure measurements using a model [73]. The performance of the adaptive estimators were compared and evaluated for pipe connection procedure using a simple simulation model. This model was the extended version of adaptive observer used in [73] for directly using real-time measurements of the choke and the bottom-hole pressures to estimate states and parameters [78]. The performance of the adaptive observers was compared and evaluated for typical drilling case to estimate only production constant of gas using a simulated scenario with drift-flux model . In this chapter, the performance of the adaptive observers from [78] is compared and evaluated for an UBD case study to estimate both production constants of gas and liquid using some simulated scenarios with the OLGA simulator. The OLGA dynamic multiphase flow simulator is a high fidelity simulation tool which has become the de facto industry standard in oil and gas production, see [8]. These adaptive observers were tested by two challenging scenarios:

1. Changing for production constant of gas.

2. Pipe connection.

The performance of the estimation algorithms to detect and track the change in production parameters is investigated. It shows that how the estimators performs in a more realistic setting.

Lyapunov based adaptive observers and the Kalman filter are widely used for the estimation of state and parameters. A Lyapunov based adaptive observer is generally designed as Luenberger type observer for the state combined with an appropriate adaptive law to estimate the unknown parameters [33]. The unscented Kalman filter (UKF) has been shown to typically have a better performance than other Kalman filter techniques for nonlinear system [104, 112].

The purpose of the chapter is to evaluate the LOL model for reservoir characterization in UBD employing an adaptive observer that uses the bottom hole and choke pressure measurements from a simulated scenario with the OLGA simulator. This chapter presents the design of a Lyapunov-based adaptive observer and an UKF based on LOL model, and an UKF based on a simplified drift-flux model to estimate the states and geological properties of the reservoir (production parameters) during UBD operation. The performance of the adaptive observers based on LOL model is evaluated against UKF based on a simplified drift-flux model by using measurements from the OLGA simulator. The adaptive observers are compared with each other in terms of rate of convergence and accuracy. Robustness of the adaptive observers is investigated in case of errors in the reservoir and well parameters of the models.

This chapter consists of the following sections: Section 3.2 describes the basic concept of the UBD process. The modeling section presents a LOL and simplified drift-flux model based on mass and momentum balances for UBD operation and the reservoir model. Section 3.4 explains the Lyapunov-based adaptive observer for and joint UKF methods for simultaneously estimating the states and model parameters from real-time measurements. At the end the conclusion of the chapter is presented.

3.2   Under balanced drilling

In drilling operations, the drilling fluid is pumped down through the drill string and the drill bit (see Figure 3.1). The annulus is sealed with a rotating control device (RCD), and the drilling fluid exits through a controlled choke valve, allowing for faster and more precise control of the annular pressure. The drilling fluid carries cuttings from the drill bit to the surface.

In conventional (over-balanced) drilling, or managed pressure drilling (MPD), the pressure in the well is kept greater than pressure of reservoir to prevent influx from entering the well [29]. In UBD operations, on the other hand the pressure of the well is kept below the pressure of the reservoir, allowing formation fluid flow into the well during the drilling operation.

Nitrogen unit, Rotating control devices (RCD), Chemical injection equipment, Surface separation equipment, choke and manifold system, geologic sampler, emergency shut-down system and Non-return valve (NRV) are the main surface equipments involved in normal UBD operations [102]. The pump flow rate, choke valve and density of the drilling fluid (mud) are the various inputs used to adjust the pressure in the well-bore. The choke valve is the most common input used to regulate the pressure in the annulus during MPD and UBD operations. Furthermore, real time knowledge of states
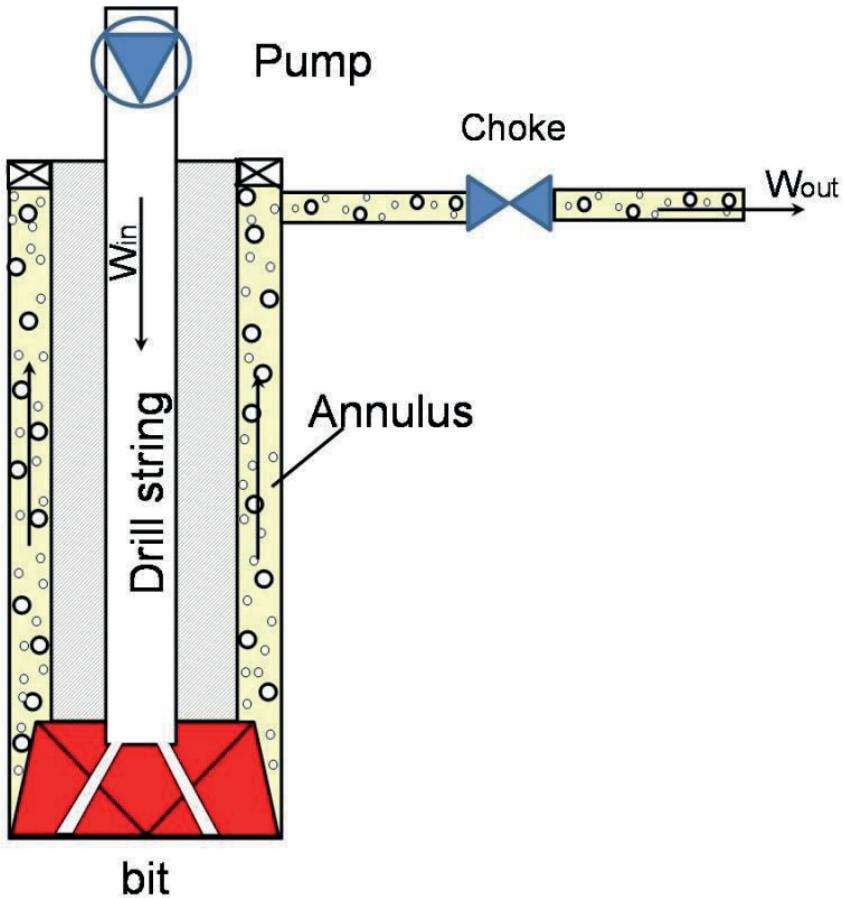
Figure 3.1: Schematic of an UBD system

and parameters of a dynamic model for the multi phase flow in the well is very useful in controllers, fault detection systems and safety applications in the well during petroleum exploration and production drilling. Some states for a dynamic model of multi phase flow in the well can not be measured directly or have a delay or low measurement frequency, and some parameters may be varied only during drilling. So, states and parameters for the dynamic model of multi phase flow in the well must be estimated.

3.3   Modeling

Due to the existence of multiphase flow (i.e. oil, gas, water, drilling mud and cuttings) in the system, the modeling of the system is challenging. Multiphase flow can be modeled by a distributed model or a simplified LOL

model. A distributed model is capable of describing the gas-liquid behavior along the annulus in the well. The simplified LOL model is based on some simplifying assumptions, and considers only the gas-liquid behavior at the drill bit and the choke system. The LOL model used in this chapter is very similar to the two-phase flow model found in [1, 81]. In the simplified drift-flux model and the LOL model, the drilling fluid, oil, water, and rock cuttings are lumped into the liquid phase. All models neglect the effects of cutting transport as one of their assumption.

3.3.1 Simplified drift-flux model

There are two common methods for modeling distributed multiphase flow in UBD operations. The most general and detailed method is called a two-fluid model. This method uses four partial differential equations (PDE's) for conservation of mass and momentum in each phase. The two-fluid model is difficult to solve both analytically or numerically, because the source terms reflecting interphase drag are stiff and this can lead to significant problems in the numerical computation [19]. Due to the complexity of the two-fluid model, the drift-flux model is derived by merging the momentum equations of both phases (gas/liquid) into one equation. Therefore, difficult phase interaction terms cancel out, and the missing information in the mixture momentum equation must be replaced by a slip equation which gives a relation between the flow velocities of the phases. The mechanistic models use different relations between the phase slip velocities and pressure loss terms for different flow patterns [46, 56]. These models need to predict flow patterns at each time step. In this chapter, a simplified drift-flux model (DFM) is used. The simple DFM uses a specific empirical slip law, without flow-regime predictions, but which allows for transition between single and two phase flows. The isothermal simple DFM formulation of the conservation of mass and momentum balance are given by [3]

$$\frac{\partial m}{\partial t} + \frac{\partial mv_l}{\partial x} = 0, \tag{3.1}$$

$$\frac{\partial n}{\partial t} + \frac{\partial nv_g}{\partial x} = 0, \tag{3.2}$$

$$\frac{\partial(mv_l + nv_g)}{\partial t} + \frac{\partial(P + mv_l^2 + nv_g^2)}{\partial x} = -(m+n)g\cos\Delta\theta - \frac{2f(m+n)v_m|v_m|}{D}. \tag{3.3}$$

where the mass variables are defined as follows

$$m = \alpha_l \rho_l, \qquad\qquad n = \alpha_g \rho_g$$

where $k = l, g$ denoting iquid and gas, respectively, ρ_k is the phase density, and α_k is the volume fraction satisfying

$$\alpha_l + \alpha_g = 1. \tag{3.4}$$

Further v_k denotes the velocities, and P the pressure. All of these variables are functions of time and space. We denote $t \geq 0$ the time variable, and $x \in [0, L]$ the space variable, corresponding to a curvilinear abscissa with $x = 0$ corresponding to the bottom hole and $x = L$ to the outlet choke position. In the momentum equation (3.3), the term $(m + n)g \cos \Delta\theta$ represents the gravitational source term, g is the gravitational constant and $\Delta\theta$ is the mean angle between gravity and the positive flow direction of the well, while $-\frac{2f(m+n)v_m|v_m|}{D}$ accounts for frictional losses. The closure relations, boundary conditions and discretization schemes for this model can be found in [3].

3.3.2 LOL model

The so-called low-order lumped (LOL) model is perhaps the simplest method for modeling multiphase flow in UBD. A LOL model is suitable for conventional model-based control design methods and can be used for prediction and estimation in an observer and controller algorithms. The most important simplifying assumptions of the LOL model are listed as below:[81, 106]

- Ideal gas behavior
- Simplified choke model for gas, mud and liquid leaving the annulus
- No mass transfer between gas and liquid
- Isothermal condition and constant system temperature
- Constant liquid density with respect to pressure and temperature
- Uniform flow pattern along the whole drill string and annulus

The simplified LOL model equations for mass of gas and liquid in the annulus are derived from mass and momentum balances as follows [73]

$$\dot{m}_g = w_{g,d} + w_{g,res}(m_g, m_l) - \frac{m_g}{m_g + m_l} w_{out}(m_g, m_l) \tag{3.5}$$

$$\dot{m}_l = w_{l,d} + w_{l,res}(m_g, m_l) - \frac{m_l}{m_g + m_l} w_{out}(m_g, m_l) \tag{3.6}$$

where m_g and m_l are the total mass of gas and liquid, respectively. The liquid phase is assumed incompressible, and ρ_l is the liquid mass density. The gas phase is compressible and occupies the volume left free by the liquid phase. $w_{g,d}$ and $w_{l,d}$ are the mass flow rates of gas and liquid from the drill string,

and $w_{g,res}$ and $w_{l,res}$ are the mass flow rates of gas and liquid from the reservoir. The total mass outflow rate is

$$w_{out} = K_c Z \sqrt{\frac{m_g + m_l}{V_a}} \sqrt{p_c - p_{c0}} \qquad (3.7)$$

where K_c is the choke constant. Z is the control signal to the choke opening, taking its values on the interval $(0, 1]$. The total volume of the annulus is denoted by V_a, and p_{c0} is the constant downstream choke pressure (atmospheric). The choke pressure is denoted by p_c, and derived from ideal gas equation

$$p_c = \frac{RT}{M_{gas}} \frac{m_g}{V_a - \frac{m_l}{\rho_l}} \qquad (3.8)$$

where R is the gas constant, T is the average temperature of the gas, and M_{gas} is the molecular weight of the gas. The bottom-hole pressure is given by the following equation

$$p_{bh} = p_c + \frac{(m_g + m_l)g \cos(\Delta\theta)}{A} + \Delta p_f \qquad (3.9)$$

where A is the cross sectional area of the annulus, Δp_f is the friction pressure loss in the well

$$\Delta p_f = K_f (w_{g,d} + w_{l,d})^2 \qquad (3.10)$$

and K_f is the friction factor.

3.3.3   Reservoir flow

The mass flow from the reservoir into the well for each phase is modeled by a linear relation

$$w_{g,res} = \begin{cases} K_g(p_{res} - p_{bh}), & \text{if } p_{res} > p_{bh} \\ 0, & \text{otherwise.} \end{cases} \qquad (3.11)$$

$$w_{l,res} = \begin{cases} K_l(p_{res} - p_{bh}), & \text{if } p_{res} > p_{bh} \\ 0, & \text{otherwise.} \end{cases} \qquad (3.12)$$

where p_{res} is the known pore pressure in the reservoir, and K_g and K_l are the production constants of gas and liquid from the reservoir into the well, respectively. Reservoir parameters could be evaluated by seismic data and other geological data from core sample analysis. Still, local variations of reservoir parameters such as the production constants of gas and liquid may be revealed only during drilling. So, it is valuable to estimate the partial variations of some of the reservoir parameters while drilling is performed ([82]).

3.4 Estimation Algorithm

In this section, first a Lyapunov-based adaptive observer to estimate states and parameters in UBD operation for the LOL model is derived. Then, the joint unscented Kalman filter is presented for both the distributed and LOL models. The measurements and inputs of models are summarized in Table 3.1. We assume the pore pressure p_{res} is known, and the production constant of gas (K_g) and liquid (K_l) from the reservoir into the well are unknown and must be estimated. We will later mention why p_{res} can be assumed known by considering offline estimation and study the sensitivity to errors in p_{res}. K_g and K_l are named by θ_1 and θ_2, respectively, for notational purposes.

Table 3.1: Measurements and Inputs

Variables	Measurement/Input
Choke pressure (p_c)	Measurement
Bottom-hole pressure (p_{bh})	Measurement
Drill string mass flow rate of gas $(w_{g,d})$	Input
Drill string mass flow rate of liquid $(w_{l,d})$	Input
Choke opening (Z)	Input

The friction factor (k_f) and choke constant (k_c) of the model are known. These parameters could be estimated offline by using separation flow rates and topside data. Other parameters that are used in this chapter such as density, temperature and well volume come from well data.

3.4.1 Lyapunov-based adaptive observer

A full-order state observer for the system (2.2)-(2.3) is

$$\dot{\hat{m}}_g = w_{g,d} + \hat{w}_{g,res}(\hat{\theta}_1) - \frac{\hat{m}_g}{\hat{m}_g + \hat{m}_l}\hat{w}_{out}(\hat{m}_g, \hat{m}_l) + k_1(p_{bh} - \hat{p}_{bh}) \quad (3.13)$$

$$\dot{\hat{m}}_l = w_{l,d} + \hat{w}_{l,res}(\hat{\theta}_2) - \frac{\hat{m}_l}{\hat{m}_g + \hat{m}_l}\hat{w}_{out}(\hat{m}_g, \hat{m}_l) + k_1(p_{bh} - \hat{p}_{bh}) \quad (3.14)$$

where

$$\hat{w}_{g,res} = \hat{\theta}_1(p_{res} - p_{bh}) \quad (3.15)$$

$$\hat{w}_{l,res} = \hat{\theta}_2(p_{res} - p_{bh}) \quad (3.16)$$

$$\hat{w}_{out} = K_c Z \sqrt{\frac{\hat{m}_g + \hat{m}_l}{V_a}} \sqrt{p_c - p_{c0}} \qquad (3.17)$$

$$\hat{p}_{bh} = p_c + \frac{(\hat{m}_g + \hat{m}_l)g\cos(\Delta\theta)}{A} + \Delta p_f \qquad (3.18)$$

Note that the observer gains are chosen equal ($k_1 = k_2$) since it is based on Lyapunov theorem. However, in practice it might be possible to choose different gains based on tuning since Lyapunov theorem is conservative. $\frac{k_1}{A} = l_1$ has to be chosen sufficiently large positive. $\hat{m}_g$ and $\hat{m}_l$ are estimates of states m_g and m_l. Defining the state estimation errors $e_1 = m_g - \hat{m}_g$ and $e_2 = m_l - \hat{m}_l$, $\hat{\theta}_1$ and $\hat{\theta}_2$ are estimates of parameters $\theta_1 = K_g$ and $\theta_2 = K_l$.

$$\dot{\hat{\theta}}_1 = q_1(p_{res} - p_{bh})e_1 \qquad (3.19)$$

$$\dot{\hat{\theta}}_2 = q_2(p_{res} - p_{bh})e_2 \qquad (3.20)$$

where the gains q_1 and q_2 are positive tuning parameters that specify trade-offs in the observer design. Choosing larger gains results in faster convergence but large overshoot and undershoot in estimation, or sometimes instability. Choosing smaller gains results in slower convergence and small overshoot and undershoot, or sometimes without any overshoot in estimation. Since the total mass of gas and liquid in the well could not be measured directly, they are computed by solving a series of nonlinear algebraic equations (3.8)-(3.9) using measurements of the choke and the bottom-hole pressures.

$$m_l^c = \frac{1}{1 - \frac{p_c M_{gas}}{RT\rho_l}}\left(\frac{(p_{bh} - p_c - \Delta p_f)A}{g\cos(\Delta\theta)} - \frac{p_c M_{gas} V_a}{RT}\right) \qquad (3.21)$$

$$m_g^c = \frac{p_c M_{gas}(V_a - \frac{m_l^c}{\rho_l})}{RT} \qquad (3.22)$$

The adaptation laws (3.19)-(3.20) can be implemented by using $e_1 = m_g^c - \hat{m}_g$ and $e_2 = m_l^c - \hat{m}_l$. The error dynamics can be written as follows

$$\dot{e}_1 = (\theta_1 - \hat{\theta}_1)(p_{res} - p_{bh}) - \left(\frac{m_g}{m_g + m_l}w_{out} - \frac{\hat{m}_g}{\hat{m}_g + \hat{m}_l}\hat{w}_{out}\right)$$
$$- l_1 g\cos(\Delta\theta)(e_1 + e_2) \qquad (3.23)$$

$$\dot{e}_2 = (\theta_2 - \hat{\theta}_2)(p_{res} - p_{bh}) - \left(\frac{m_l}{m_g + m_l}w_{out} - \frac{\hat{m}_l}{\hat{m}_g + \hat{m}_l}\hat{w}_{out}\right)$$
$$- l_1 g\cos(\Delta\theta)(e_1 + e_2) \qquad (3.24)$$

Let $\tilde{\theta}_1 = \theta_1 - \hat{\theta}_1$, $\tilde{\theta}_2 = \theta_2 - \hat{\theta}_2$, and the Lyapunov function candidate for adaptive observer design be defined as

$$V(e, \tilde{\theta}) = \frac{1}{2}(e_1^2 + e_2^2 + q_1^{-1}\tilde{\theta}_1^2 + q_2^{-1}\tilde{\theta}_2^2) \qquad (3.25)$$

It is easy to check that $V(e, \tilde{\theta})$ is positive definite, and we continue to analyze if it can be made decrescent. From (3.23) and (3.24), the time derivative of $V(e, \tilde{\theta})$ along the trajectory of the error dynamics is

$$
\begin{aligned}
\dot{V}(e, \tilde{\theta}) = & -l_1 g \cos(\Delta\theta)(e_1 + e_2)^2 - \frac{e_1^2 w_{out}}{m_g + m_l} + \tilde{\theta}_1 \left[(p_{res} - p_{bh})e_1 + q_1^{-1}\dot{\tilde{\theta}}_1\right] \\
& + \tilde{\theta}_2 \left[(p_{res} - p_{bh})e_2 + q_2^{-1}\dot{\tilde{\theta}}_2\right] - \frac{\hat{m}_l e_2(w_{out} - \hat{w_{out}})}{\hat{m}_g + \hat{m}_l} - \frac{e_2^2 w_{out}}{m_g + m_l} \\
& + \frac{\hat{m}_l e_2(e_1 + e_2)w_{out}}{(m_g + m_l)(\hat{m}_g + \hat{m}_l)} + \frac{\hat{m}_g e_1(e_1 + e_2)w_{out}}{(m_g + m_l)(\hat{m}_g + \hat{m}_l)} \\
& - \frac{\hat{m}_g e_1(w_{out} - \hat{w_{out}})}{\hat{m}_g + \hat{m}_l}
\end{aligned}
\tag{3.26}
$$

The detail calculations of the derivative of the Lyapunov function is presented in Appendix B:

$$
\begin{aligned}
\implies \dot{V}(e, \tilde{\theta}) < & -l_1 g \cos(\Delta\theta)(e_1^2 + e_2^2) - \frac{w_{out}(\ e_1^2 + e_2^2)}{m_g + m_l + \sqrt{m_g + m_l}\sqrt{\hat{m}_g + \hat{m}_l}} \\
& - e_1 e_2 \Big(\ 2l_1 g \cos(\Delta\theta) - \frac{w_{out}(\frac{\sqrt{\hat{m}_g + \hat{m}_l}}{\sqrt{m_g + m_l}})}{m_g + m_l + \sqrt{m_g + m_l}\sqrt{\hat{m}_g + \hat{m}_l}}\Big)
\end{aligned}
\tag{3.27}
$$

By choosing l_1 sufficiently large, then

$$
0 \leq \left(\ 2l_1 g \cos(\Delta\theta) - \frac{w_{out}(\frac{\sqrt{\hat{m}_g + \hat{m}_l}}{\sqrt{m_g + m_l}})}{m_g + m_l + \sqrt{m_g + m_l}\sqrt{\hat{m}_g + \hat{m}_l}}\right) < 2l_1 g \cos(\Delta\theta)
\tag{3.28}
$$

The lower bound of l_1 is

$$
2l_1 g \cos(\Delta\theta) - (\frac{w_{out}}{m_g + m_l})\left(\frac{\sqrt{\hat{m}_g + \hat{m}_l}}{\sqrt{m_g + m_l} + \sqrt{\hat{m}_g + \hat{m}_l}}\right) \geq 0
$$

$$
\left(\frac{\sqrt{\hat{m}_g + \hat{m}_l}}{\sqrt{m_g + m_l} + \sqrt{\hat{m}_g + \hat{m}_l}}\right) < 1 \quad , (\frac{w_{out}}{m_g + m_l}) < \gamma
\tag{3.29}
$$

$$
\implies l_1 > \frac{\gamma}{2g \cos(\Delta\theta)}
\tag{3.30}
$$

In real drilling problem we usually have ($\gamma \ll 1$), therefore the lower bound of l_1 is small, and this gives

$$\dot{V}(e, \tilde{\theta}) < -l_1 g \cos(\Delta\theta)(e_1^2 + e_2^2) + 2l_1 g \cos(\Delta\theta)|e_1||e_2|$$
$$- \frac{w_{out}(e_1^2 + e_2^2)}{m_g + m_l + \sqrt{m_g + m_l}\sqrt{\hat{m}_g + \hat{m}_l}} \tag{3.31}$$

By using Young's inequality $2|e_1||e_2| \leq e_1^2 + e_2^2$,

$$\dot{V}(e, \tilde{\theta}) < -\frac{w_{out}(e_1^2 + e_2^2)}{m_g + m_l + \sqrt{m_g + m_l}\sqrt{\hat{m}_g + \hat{m}_l}} \leq 0 \tag{3.32}$$

which implies that all signals $e_1, e_2, \tilde{\theta}_1, \tilde{\theta}_2$ are bounded. From (3.23),(3.24) and $e_1, e_2, \tilde{\theta}_1, \tilde{\theta}_2 \in \mathcal{L}_\infty$, $\dot{e}_1, \dot{e}_2$ are bounded. It follows by using Barbalat's lemma that e_1, e_2 converge to zero. Based on equation (3.19)-(3.20), the adaptation laws can be written as follows:

$$\dot{\hat{\theta}} = \begin{bmatrix} \dot{\hat{\theta}}_1 \\ \dot{\hat{\theta}}_2 \end{bmatrix} = \begin{bmatrix} q_1 & 0 \\ 0 & q_2 \end{bmatrix} \begin{bmatrix} p_{res} - p_{bh} & 0 \\ 0 & p_{res} - p_{bh} \end{bmatrix} \begin{bmatrix} e_1 \\ e_2 \end{bmatrix}$$

$$\Gamma = \begin{bmatrix} q_1 & 0 \\ 0 & q_2 \end{bmatrix}, \quad \phi = (p_{res} - p_{bh})I, \quad \zeta = \begin{bmatrix} e_1 \\ e_2 \end{bmatrix} \implies \dot{\hat{\theta}} = \Gamma\phi\zeta \tag{3.33}$$

Based on the persistency excitation theorem,$\lim_{t\to\infty} \hat{\theta} = \theta^*$ if and only if there exists some $\alpha, T > 0$ such that, for any $t > 0$, the following inequality is satisfied ([33]):

$$\int_t^{t+T} \phi(\tau)\phi^T(\tau) \, d\tau \geq \alpha I > 0, \quad \forall t \geq t_0 \tag{3.34}$$

So,

$$\int_t^{t+T} \phi(\tau)\phi^T(\tau) \, d\tau = \int_t^{t+T} (p_{res}(\tau) - p_{bh}(\tau))^2 I \, d\tau \geq \alpha I > 0, \quad \forall t \geq t_0 \tag{3.35}$$

Thus according to theorem 4.9 in [40], the adaptive observer system is globally asymptotically stable if the persistency excitation condition is satisfied. There must be flow from the reservoir to satisfy persistence exciting condition.

3.4.2 Joint Unscented Kalman Filter

The Kalman filter using linearization to estimate both the state and parameter vectors of the system is usually known as an augmented Kalman filter.

The UKF technique has been developed to work with non-linear systems without using an explicit linearization of the model ([36, 37]). The UKF estimates the mean and covariance matrix of the estimation error with a minimal set of sample points (called sigma points) around the mean by using a deterministic sampling approach known as the unscented transform. The nonlinear model is applied to propagate uncertainty of sigma points instead of using a linearization of the model. So, this method does not need to calculate the explicit Jacobian or Hessian. More details can be found in ([36, 104]).

The augmented state vector is defined by $x^a = [X, \theta]$ where X is the state of the model. The discrete state-space equations for the the augmented state vector at time instant k is written as:

$$\begin{bmatrix} X_k \\ \theta_k \end{bmatrix} = \begin{bmatrix} f(X_{k-1}, \theta_{k-1}) \\ \theta_{k-1} \end{bmatrix} + q_k = f^a(X_{k-1}, \theta_{k-1}) + q_k \tag{3.36}$$

where $q_k \sim N(0, Q_k)$ is the zero mean Gaussian process noise (model error). Here, we apply the UKF to both the LOL and DFM. When using the DFM, the number of states that must be estimated by the joint UKF is equal to three times of the number of spatial discretization cells in the drift-flux model. The discrete measurements of the system can be modeled as follows:

$$y_k = h(X_k) + r_k \tag{3.37}$$

$$h(X_k) = [p_c, p_{bh}]^T \tag{3.38}$$

where $r_k \sim N(0, R_k)$ is the zero mean Gaussian measurement noise.

3.5 Simulation Results

The parameter values for the simulated well and reservoir are summarized in Table 3.2, and used in the OLGA simulator. The measurements have been synthetically generated by using the OLGA dynamic multiphase flow simulator. The OLGA simulator uses the same model for the mass flow from the reservoir into the well as in equations (3.11)-(3.12).

A discretization of the time and space variables is required for using numerical methods. The PDE of the drift-flux model are discretized by using a finite volumes method for the joint UKF based on DFM. where 6 cells were used for the spatial discretization. A measurement sampling period of 10 seconds were used and the model was run with time steps of 10 seconds. The parameter values for the nonlinear adaptive observer and UKF for both models are summarized in Table 3.3.

The initial values for the estimated and real parameters are as follows:

$$K_g = 0.05, \quad K_l = 0.1, \quad \hat{K}_g = 0.07, \quad \hat{K}_l = 0.13$$

Table 3.2: Parameter Values for Well and Reservoir

Name	DFM	Unit
Reservoir pressure (p_{res})	279	bar
Collapse pressure (p_{coll})	155	bar
Well total length (L_{tot})	2530	m
Drill string outer diameter (D_d)	0.1206	m
Annulus inner diameter (D_a)	0.1524	m
Liquid flow rate $(w_{l,d})$	13.33	kg/s
Gas flow rate $(w_{g,d})$	0	kg/s
Liquid density (ρ_L)	1000	kg/m^3
Production constant of liquid (K_L)	0.1	kg/s/bar
Gas average temperature (T)	285.15	K
Average angle $(\Delta\theta)$	0	rad
Choke constant (K_c)	0.0057	m^2

Table 3.3: Parameter Values for Model and Estimators

Parameter	Value	Parameter	Value
q_1	2.5×10^{-13}	k_1	4×10^{-9}
q_2	5×10^{-14}	L	4
κ_{LOL}	0	κ_{DFM}	0
α_{LOL}	0.00001	α_{DFM}	0.00001
β_{LOL}	2	β_{DFM}	2

The case study that is used in this chapter considers UBD operation of a vertical well drilled into an oil and gas reservoir. Two scenarios are simulated. In first scenario, first drilling in a steady-state condition is initiated with the choke opening of 12 %. After 1 hour, there is a linear decrease in the choke opening from 12 % to 8 % for 1 hour. After 4 hours, there is a linear increase in the choke opening from 8 % to 12 % for 1 hour. After 7 hours, there is a linear and sharp increase in the production constant of gas from 0.05 kg/s/bar to 0.07 kg/s/bar (change of reservoir height). Choke opening in this simulation is illustrated in Figure 3.2. The parameter covariance matrix of UKF used for both models and scenarios is

$$Q = diag[8 * 10^{-9}, 2 * 10^{-8}]$$

Choosing the process noise covariance matrix in the UKF (Q_k) specify trade-offs in the UKF design. Choosing larger process noise in the UKF (Q_k) leads to faster track of data and convergence but typically more uncertainty in the estimation. Choosing smaller process noise in the UKF (Q_k) leads to slower track of data and convergence but typically less uncertainty in
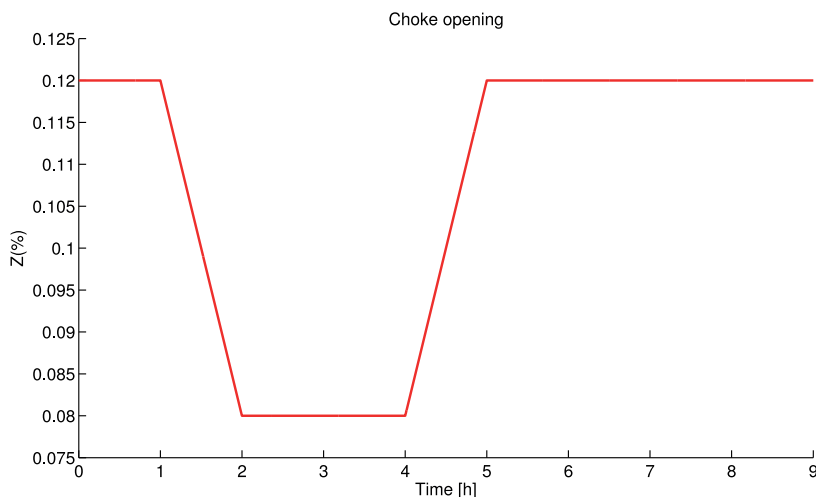
Figure 3.2: Choke opening

the estimation. The choke and the bottom-hole pressure measurements are corrupted by zero mean additive white noise with the following covariance matrix

$$R = \begin{bmatrix} 0.9 * 0.4^2 & 0 \\ 0 & 0.9 * 0.2^2 \end{bmatrix} (bar^2)$$

In order to estimation the reservoir pressure offline, consider Li's method. Figure 3.3 shows the best-fit regression line between the three points of estimation based on two characteristics of the well, total gas flow rate from the reservoir and the bottom hole pressure. The time of testing points are chosen 1.5, 3 and 6 hours. The offline estimation of reservoir pressure is 278.8, calculated by using Li's method. This estimation is very close to the actual value of 279 bar obtained from OLGA simulator. The total flow rate from the reservoir can be estimated by the Lyapunov-based adaptive observer in section 3.4 by changing adaptation laws for estimation of the total gas flow rate from the reservoir instead of the production constants.

The estimation of the production constants of gas and liquid from the reservoir into the well are shown in Figures 3.4 and 3.5, respectively. The estimates of all algorithms are converging to the true value quite fast, about 0.5 hour. UKF based on LOL model produces less accurate results than the other methods for estimation of the production constant of gas from the reservoir into the well during transient time. The results is shown that reasonable performance of the estimation algorithms to detect and track changing at production constant of gas. The Lyapunov-based adaptive ob-
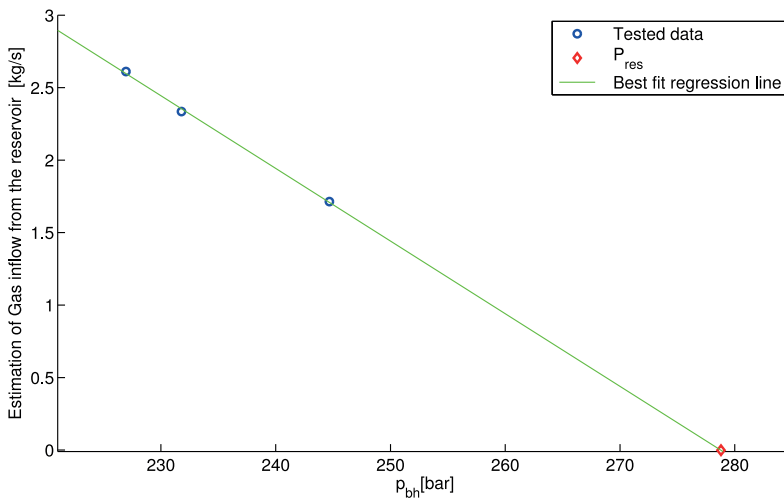
Figure 3.3: Estimation of total gas flow rate from the reservoir versus the bottom hole pressure and the best-fit regression line.

server has better performance than the other methods for estimation of the production constants of gas and liquid from the reservoir into the well when the production constant of gas is increased from 0.05 kg/s/bar to 0.07 kg/s/bar. In DFM, it is shown that estimation of the slip parameters can improve accuracy of the production parameters estimation [76]. Therefore, errors in slip parameters might cause small bias in the estimation of the production parameters with UKF based on DFM when the reservoir parameters change.

The measured and estimated bottom-hole pressure and choke pressure at the wellhead are illustrated in Figures 3.6 and 3.7, respectively. The only error measurement that was injected to the nonlinear Lyapunov-based adaptive observer is bottom hole pressure. Since the choke pressure in LOL model during transient time has an error, estimation of choke pressure with nonlinear Lyapunov-based adaptive observer has a small bias during transient time and estimation of bottom hole pressure with UKF has a small bias during transient time. Since the LOL model is a much simpler model than the distributed model, it has some mismatch with OLGA simulator. So, this mismatch influences the estimation of parameters and states. The measurement covariance of the UKF determines the priority of measurements for the UKF. The Lyapunov adaptive observer tries to reduce errors of states and parameters by injecting the error between estimation and measurement of bottom hole pressure (the last terms in Equations (3.13) and (3.14)). The
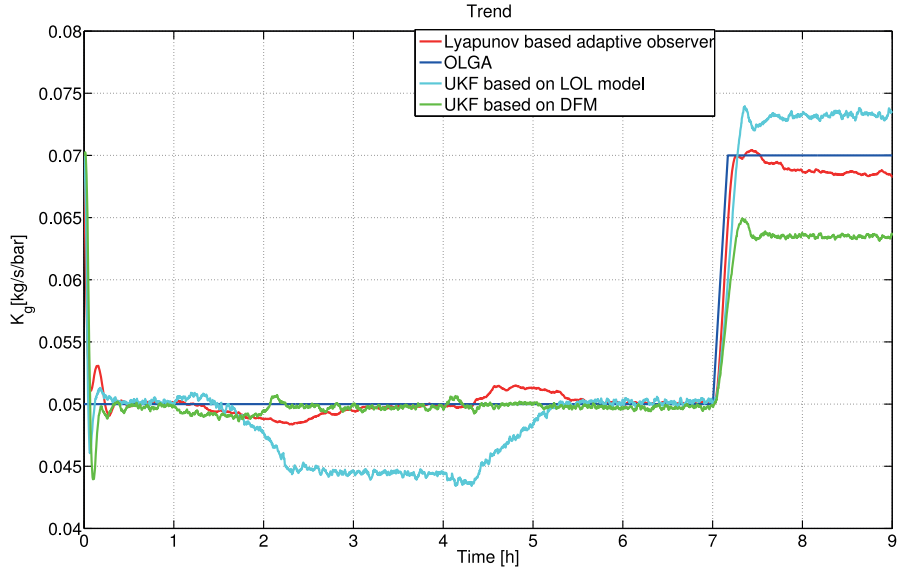
Figure 3.4: Actual value and estimated production constant of gas
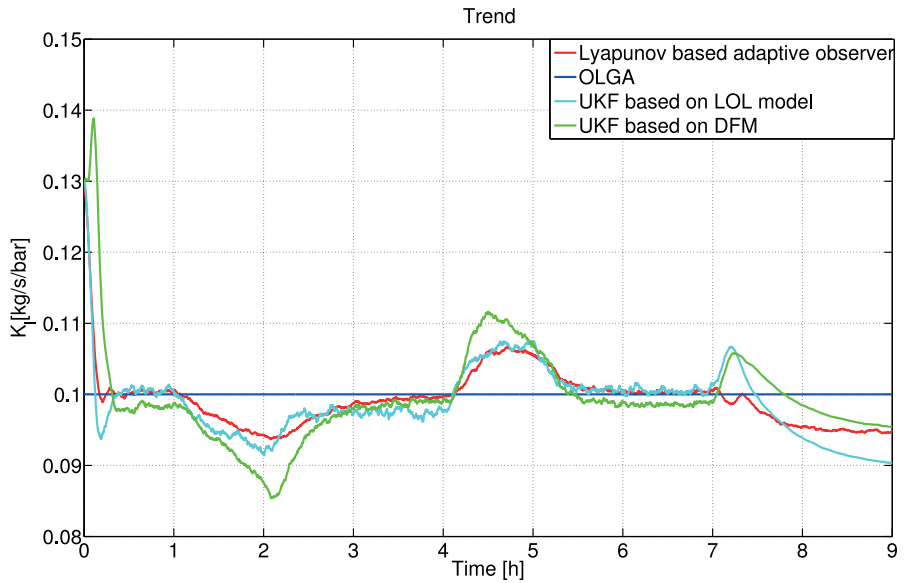
Figure 3.5: Actual value and estimated production constant of liquid

bottom hole pressure and the choke pressure are correlated with each other with the mass and momentum balances. So, the error between estimation and measurement of choke pressure is indirectly affected by the Lyapunov adaptive observer. But, the error between estimation and measurement of bottom hole pressure is affected directly by the Lyapunov adaptive observer. Simulation time of adaptive observers based on LOL model executes at least 100 times faster than joint UKF based on DFM.
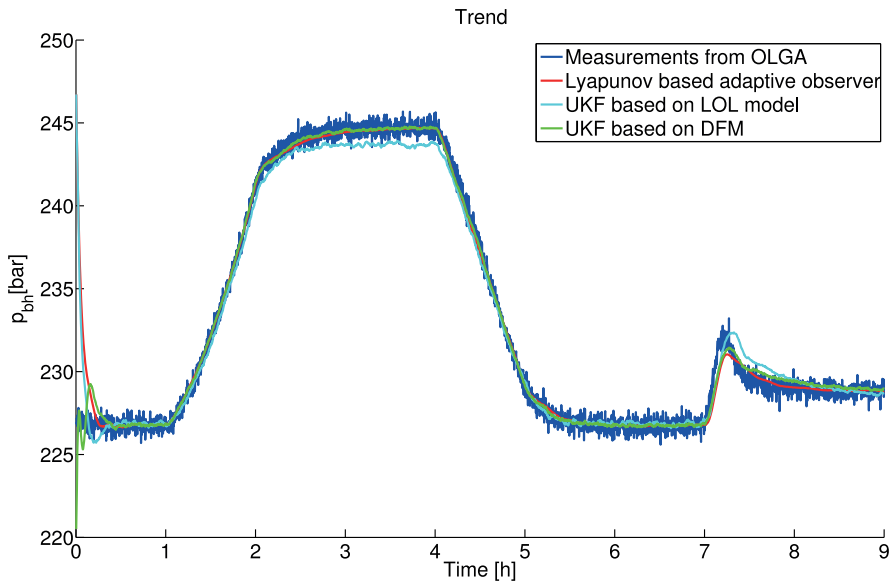
Figure 3.6: Measured and estimated bottom-hole pressure

In this chapter, performance of these adaptive observers is evaluated through the root mean square error (RMSE) metric for the parameters K_g and K_l. The RMSE metric for Lyapunov-based adaptive observer and UKF for both models during the whole estimation period and after initial transient ($t \geq 0.5 hour$) are summarized in Table 3.4.

According to the RMSE metric Table 3.4, the Lyapunov-based adaptive observer has better performance than the other methods for estimation of the production constants of gas and liquid from the reservoir into the well.

Robustness of the adaptive observers is tested in case of errors in the reservoir and well parameters of the models. This test is performed in case of errors in the reservoir pore pressure and liquid density. The RMSE metric for the adaptive observers in two case of 1% error on the reservoir pore pressure and 10% error on the liquid density are summarized in Table 3.5 and 3.6, respectively.
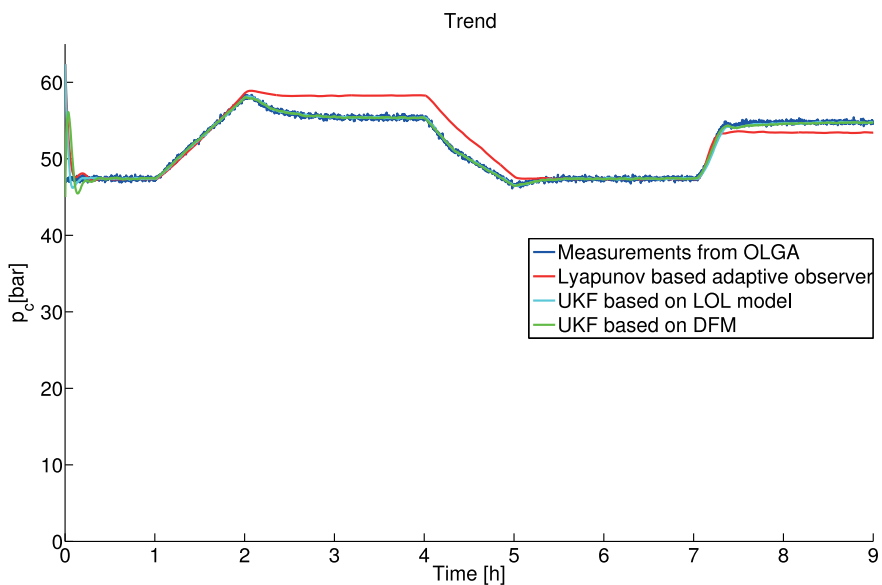
Figure 3.7: Measured and estimated choke pressure

Table 3.4: RMSE metric

Method	Whole estimation period		After initial transient	
	K_g	K_l	K_g	K_l
Lyapunov method	1.4×10^{-3}	4.0×10^{-3}	1.1×10^{-3}	3.3×10^{-3}
UKF based on LOL model	3.6×10^{-3}	5.0×10^{-3}	3.4×10^{-3}	4.5×10^{-3}
UKF based on DFM	3.5×10^{-3}	6.8×10^{-3}	3.3×10^{-3}	5.2×10^{-3}

Table 3.5: RMSE metric in case of error in the reservoir pressure value

Method	K_g	K_l	p_{res} true	p_{res} model
Lyapunov method	4×10^{-3}	8×10^{-3}	279	282
UKF based on LOL model	5.7×10^{-3}	9×10^{-3}	279	282
UKF based on DFM	5.9×10^{-3}	9.9×10^{-3}	279	282

Table 3.6: RMSE metric in case of error in the liquid density value

Method	K_g	K_l	ρ_L true	ρ_L model
Lyapunov method	2.6×10^{-3}	5.2×10^{-3}	1000	1100
UKF based on LOL model	3.4×10^{-3}	6.4×10^{-3}	1000	1100
UKF based on DFM	3.6×10^{-3}	6.9×10^{-3}	1000	1100

Since the reservoir pore pressure has a direct effect on the mass flow rates from the reservoir into the well, small inaccuracies in the reservoir pore pressure have a significant effect on the estimation of production constants. Therefor these methods are very sensitive to errors in the reservoir pore pressure value. Adaptive observers based on LOL model are more sensitive to errors in the liquid density value than UKF based on DFM.

The second scenario in this case study is as follows, first the drilling in a steady-state condition is initiated with the choke opening of 10 %, then at t = 1 hour and 35 min the main pump is shut off to perform a connection procedure, and the choke is closed to 6 %. The rotation of the drill string and the circulation of fluids are stopped for 15 mins. Next after making the first pipe connection at t = 1 hour and 50 min the main pump and rotation of the drill string are restarted. After 1 hour and 45 min (i.e. 3 hour and 35 min), the choke is closed to 5 %, and the second pipe connection procedure is started, and is completed after 15 mins. Then the choke is opened to 10 % at t= 3 hours and 50 min. The measured bottom-hole pressure (p_{bh}), choke pressure (p_c), choke opening (Z), and mass flow rate of liquid from the drill string ($w_{l,d}$) is illustrated in Figure 3.8.

Figure 3.8: Measured bottom-hole pressure, choke pressure, choke opening, and mass flow rate of liquid from the drill string for pipe connection scenario

The parameter values for the nonlinear adaptive observer and UKF for both models for pipe connection scenario are the same as previous scenario.

The initial values for the estimated and real parameters are as follows:

$$K_g = 0.07, \quad K_l = 0.1, \quad \hat{K}_g = 0.091, \quad \hat{K}_l = 0.13$$

The estimation of the production constants of gas and liquid from the reservoir into the well are shown in Figures 3.9 and 3.10, respectively. These parameters are identified correctly by all estimators. In estimation of production constant of liquid from the reservoir into the well, Lyapunov-based adaptive observer has better performance than the other methods. Since the model is significantly less accurate during the pipe connection, we need to prevent that the PI estimates drift away. Hence, the gains value (q_1 and q_2) for Lyapunov-based adaptive observer and the parameter covariance of UKF for both models are 1000 times smaller than the nominal value during the pipe connection. For the same reason, the measurement covariance of UKF for both models are 1000 times larger than the nominal value during the pipe connection.
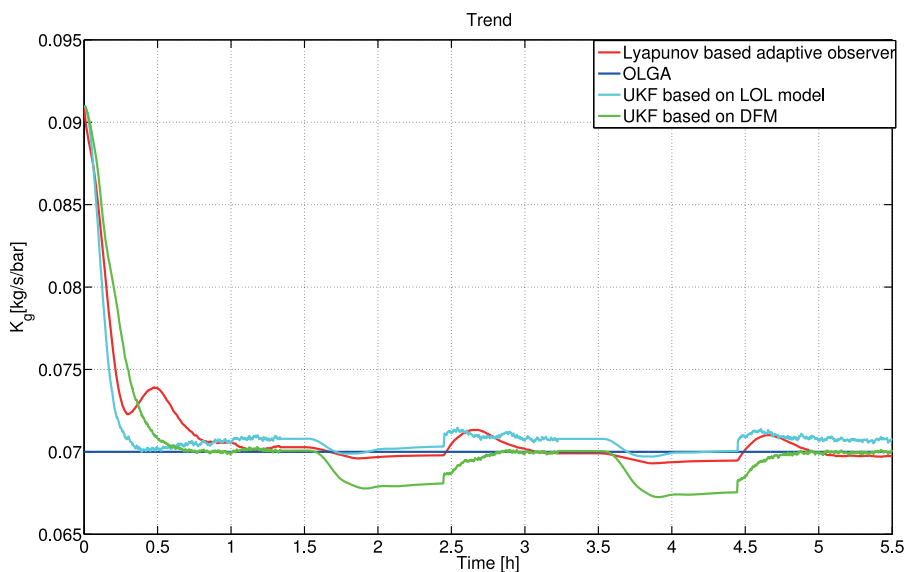
Figure 3.9: Actual value and estimated production constant of gas for pipe connection scenario

The measured and estimated bottom-hole pressure and choke pressure at the wellhead for pipe connection scenario are illustrated in Figures 3.11 and 3.12, respectively. This results show that adaptive observers have error in estimation of the bottom hole and choke pressure during pipe connection because the model is less accurate during pipe connection. Since the bottom
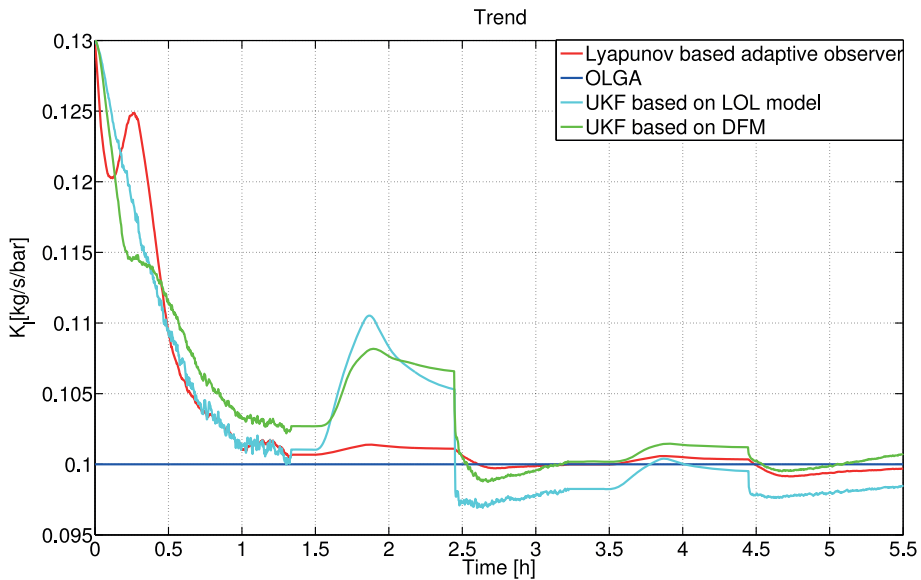
Figure 3.10: Actual value and estimated production constant of liquid for pipe connection scenario

hole and choke pressure are measured, errors of the bottom hole and choke pressure are not the main concern in this situation. Based on Nygaard et al. studied that some parameters of the model such as friction factor varies during pipe connection [85]. Since we assumed these parameters are constant, it introduces some errors to the model during pipe connection.

The RMSE metric of the parameters K_g and K_l for Lyapunov-based adaptive observer and UKF for both models after initial transient ($t \geq 0.5 hour$) are summarized in Table 3.7.

Table 3.7: RMSE metric for estimate of K_g and K_l for pipe connection scenario

Method	K_g(after $t \geq 0.5h$)	K_l(after $t \geq 0.5h$)
Lyapunov-based adaptive observer	0.7×10^{-3}	1.6×10^{-3}
UKF based on LOL model	0.7×10^{-3}	3.7×10^{-3}
UKF based on DFM	1.3×10^{-3}	3.7×10^{-3}

According to the RMSE metric Table 3.7, the Lyapunov-based adaptive observer has better performance than the other methods for estimation of the production constants of gas and liquid from the reservoir into the well in pipe connection scenario.
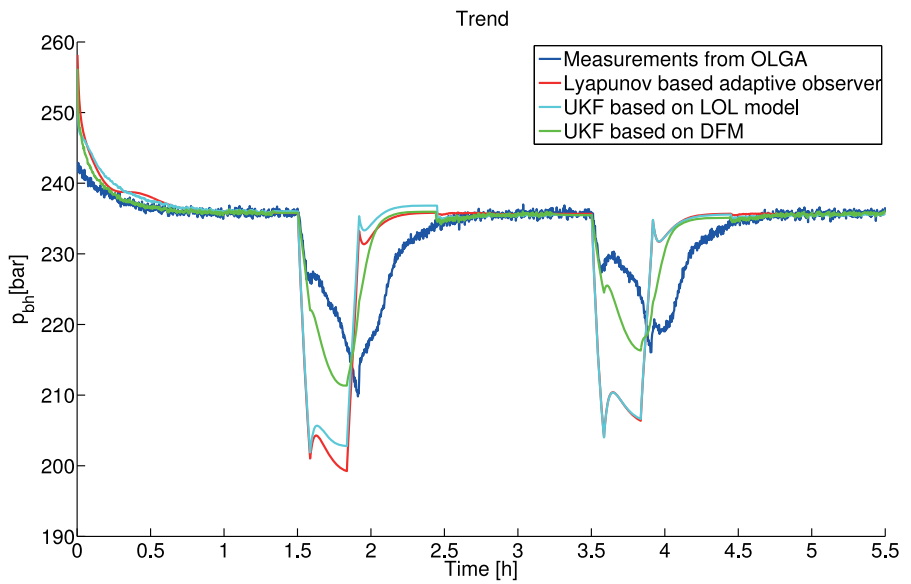
Figure 3.11: Measured and estimated bottom-hole pressure for pipe connection scenario
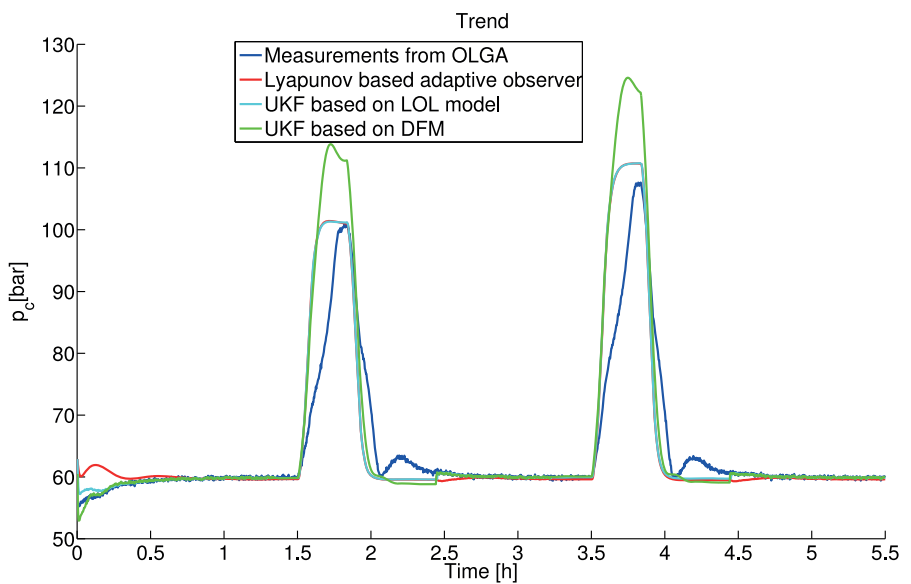
Figure 3.12: Measured and estimated choke pressure for pipe connection scenario

3.6 Conclusion

A simplified DFM and a LOL model describing a multiphase (gas-liquid) flow in the well during UBD has been used. This chapter presents Lyapunov-based adaptive observer and joint UKF based on LOL model for reservoir characterization during UBD operations. Furthermore, it describes a joint UKF to estimate parameters and states for the simplified DFM by using real-time measurements of the choke and the bottom-hole pressures from OLGA simulator. The results show that all estimators are capable of identifying the production constants of gas and liquid from the reservoir into the well. All adaptive observers have a quite fast convergence rate, about 0.5 hour. Simulation results demonstrated reasonable performance of the estimation algorithms to detect and track a changing gas production coefficient using a simulated scenario with OLGA. The nonlinear Lyapunov-based adaptive observer has better accuracy than the other methods for estimation of the production constants of gas and liquid from the reservoir into the well. Adaptive observers based on the LOL model are computationally simpler than joint UKF based on DFM. However, adaptive observers based on LOL model are more sensitive to errors in the reservoir and well parameters of the model than joint UKF based on DFM.

State and parameter estimation of a Drift-Flux Model for Under-Balanced Drilling operations

4.1 Introduction

There have been an increasing research focus on automation of drilling for exploration and production of hydrocarbons in the recent years. Modeling for estimation, and model-based control techniques have been studied in a wide range of drilling and production scenarios. In Managed Pressure Drilling (MPD), a back-pressure pump in conjunction with a back pressure choke is used to control the pressure in the well, posing new control and estimation challenges. In a typical scenario, the control goal is to keep the pressure of the well ($p_{\mathrm{well}}(t, x)$) greater than pressure of the reservoir ($p_{\mathrm{res}}(t, x)$) to prevent influx from entering the well, but lower than the fracture pressure ($p_{\mathrm{frac}}(t, x)$) to avoid the loss of drilling fluids to the reservoir [24]

$$p_{\mathrm{res}}(t, x) < p_{\mathrm{well}}(t, x) < p_{\mathrm{frac}}(t, x) \qquad (4.1)$$

at all times t and along the well profile $x \in [0, L]$.

In an alternative approach, known as Under-Balanced Drilling (UBD), the pressure in the well is kept greater than the collapse pressure of the well but lower than the pressure of the reservoir [9]

$$p_{\mathrm{coll}}(t, x) < p_{\mathrm{well}}(t, x) < p_{\mathrm{res}}(t, x) \qquad (4.2)$$

In this case, due to the pressure drawdown (meaning the positive difference of the reservoir pressure and well pressure) inflow fluid, in many cases gas, is produced continuously from the reservoir. The rate of reservoir inflow is typically approximated mathematically by a so-called Production Index (PI)

parameter

$$q_{influx} = \mathrm{PI} * \max(p_{\mathrm{res}} - p_{\mathrm{bh}}, 0). \qquad (4.3)$$

Especially for under-balanced wells producing gas, the magnitude of the PI has a significant impact on the dynamics of the UBD and thus also on the control problem. Hence, accurate estimates of the PI and reservoir pressure are important for an UBD operation.

Modeling of UBD operations and MPD scenarios handling influx requires a multiphase model. A popular model in the literature is the Drift-Flux Model (DFM) [19, 45, 56]. The drift flux model is a set of first order non-linear hyperbolic partial differential equations (PDE). In case of two-phase flow, it consists of three governing equations. The Low-Order Lumped (LOL) models are simpler methods that can be used. However, these models are only able to capture the major effects in the well and for the general purpose it produces less accurate results [73, 81, 106].

Due to the complexity of the multi-phase flow dynamics of a UBD well coupled with a reservoir, the modeling, estimation and model based control of UBD operations is still considered an emerging and challenging topic within drilling automation. Nygaard et al.[82] compared and evaluated the performance of the extended Kalman filter, the ensemble Kalman filter and the unscented Kalman filter based on a low order model to estimate the states and the PI in UBD operation. In Nygaard et al. [85], a finite horizon non-linear model predictive control in combination with an unscented Kalman filter was designed for controlling the bottom-hole pressure based on a low order model developed in [81] for a pipe connection scenario. The unscented Kalman filter was used to estimate the states, and the friction and choke coefficients. Nikoofard et al.[73] designed a Lyapunov-based adaptive observer, a recursive least squares estimation and a joint unscented Kalman filter based on a low-order lumped model to estimate states and parameters during UBD operations. This model was the extended version of an adaptive observer used in [73] for directly using real-time measurements of the choke and the bottom-hole pressures to estimate states and parameters [78]. The performance of the adaptive observers was compared and evaluated for a typical drilling case to estimate only production constant of gas using a simulated scenario with a drift-flux model. A Nonlinear Moving Horizon Observer based on a low-order lumped model was designed for estimating the total mass of gas and liquid in the annulus and geological properties of the reservoir during UBD operation in [74]. The problem of parameter estimation in multiphase flows is often referred to as 'soft-sensing' in the context of production, see[11, 28, 57, 58, 108].

Lorentzen et al. designed an ensemble Kalman filter based on the drift-

flux model to tune the uncertain parameters of a two-phase flow model in the UBD operation [56]. Vefring et al.[110, 111] compared and evaluated the performance of the ensemble Kalman filter and an off-line nonlinear least squares technique utilizing the Levenberg-Marquardt optimization algorithm to estimate reservoir pore pressure and reservoir permeability during UBD while performing an excitation of the bottom-hole pressure. The result shows that excitation of the bottom-hole pressure might improve the estimation of the reservoir pore pressure and reservoir permeability [110, 111]. Aarsnes et al.[2] used a drift-flux model and an Extended Kalman Filter to estimate the states and PI online, and suggested a scheme combining this with off-line calibration using the algorithm in [110]. The provided analysis also suggests how such a scheme fits into the UBD operating envelope as proposed by [26], and explored in [3]. Di Meglio et al. designed an adaptive observer based on a backstepping approach for a linear first-order hyperbolic system of Partial Differential Equations (PDEs) by using only boundary measurements with application to UBD [15]. It is shown that this method has exponential convergence for the distributed state and the parameter estimation. This adaptive observer is applied to estimate distributed states and unknown boundary parameters of the well during UBD operations. Gao Li et al. presented an algorithm for characterizing reservoir pore pressure and reservoir permeability during UBD of horizontal wells [52]. Since the total flow rate from the reservoir has a negative linear correlation with the bottom hole pressure, reservoir pore pressure can be identified by the crossing of the horizontal axis and the best-fit regression line between the total flow rate from the reservoir and the bottom hole pressure while performing an excitation of the bottom-hole pressure by changing the choke valve opening or pump rates. The unscented Kalman filter (UKF) has been shown to typically have a better performance than other Kalman filter techniques for nonlinear systems ([104, 112]). Nikoofard et al. used an UKF with the drift-flux model for the first time [76]. They designed an UKF for estimation of unmeasured states, production and slip parameters of simplified drift-flux model using real time measurements of the bottom-hole pressure and liquid and gas rate at the outlet [76]. This chapter is an extended version of work published in [76] which presents the design of a UKF based on a simplified drift-flux model to estimate the states, geological properties of the reservoir and slip parameters during UBD operation. In this work, both production constants of gas and liquid and unmeasured states are estimated by using only measurements of the choke and the bottom-hole pressures during UBD operation for a pipe connection procedure. The performance of UKF is evaluated against EKF by using measurements from the OLGA simulator and the consequences of not estimating slip parameters are discussed.These

adaptive observers were tested by two challenging scenarios:

1. Changing the production constant of gas.

2. Pipe connection.

The performance of the estimation algorithms to detect and track the change in production parameters is investigated. Robustness of the UKF and EKF for the pipe connection scenario is studied in case of uncertainties and errors in the reservoir and well parameters of the model. This chapter is organized as follows: Section 4.2 presents the simplified drift-flux model based on mass and momentum balances for UBD operation. Section 4.3 explain UKF and EKF for simultaneously estimating the states and parameters of a simplified drift-flux model from OLGA simulator measurements. In the section 4.4, the simulation results are provided for state and parameter estimation. The conclusions are presented at the end of the chapter.

4.2 The drift flux model

The model employed is the same as the one used in [3]. It expresses the mass conservation law for the gas and the liquid separately, and a combined momentum equation. The mud, oil and water are lumped into one single liquid phase. In developing the model, the following mass variables are used

$$m = \alpha_L \rho_L, \qquad\qquad n = \alpha_G \rho_G$$

where for $k = L, G$ denoting liquid or gas, ρ_k is the phase density, and α_k is the volume fraction satisfying

$$\alpha_L + \alpha_G = 1. \tag{4.4}$$

Further v_k denotes the velocities, and P the pressure. All of these variables are functions of time and space. We denote $t \geq 0$ the time variable, and $x \in [0, L]$ the space variable, corresponding to a curvilinear abscissa with x = 0 corresponding to the bottom hole and x = L to the outlet choke position (see Fig. 4.1). The isothermal equations are as follows,

$$\frac{\partial m}{\partial t} + \frac{\partial m v_L}{\partial x} = 0, \tag{4.5}$$

$$\frac{\partial n}{\partial t} + \frac{\partial n v_G}{\partial x} = 0, \tag{4.6}$$

$$\frac{\partial (m v_L + n v_G)}{\partial t} + \frac{\partial (P + m v_L^2 + n v_G^2)}{\partial x}$$
$$= -(m + n) g \cos \Delta \theta - \frac{2 f (m + n) v_m |v_m|}{D}. \tag{4.7}$$
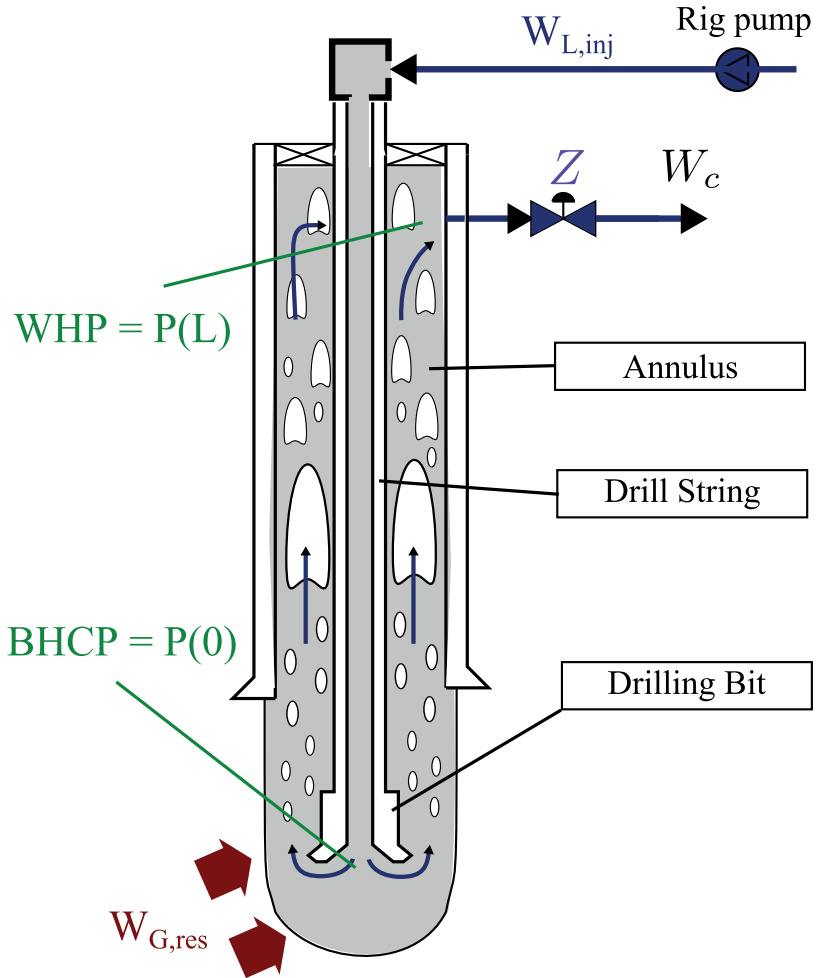
Figure 4.1: Drilling process schematic for UBD.

In the momentum equation (4.7), the term $(m+n)g\cos\Delta\theta$ represents the gravitational source term, g is the gravitational constant and $\Delta\theta$ is the mean angle between gravity and the positive flow direction of the well, while $-\frac{2f(m+n)v_m|v_m|}{D}$ accounts for frictional losses. The mixture velocity is given as

$$v_m = \alpha_G v_G + \alpha_L v_L. \tag{4.8}$$

Along with these distributed equations, algebraic relations are needed to describe the system.

4.2.1 Closure Relations

Both the liquid and gas phase are assumed compressible. This is required for the model to handle the transition from two-phase to single-phase flow. The densities are thus given as functions of the pressure as follows

$$\rho_G = \frac{P}{c_G^2}, \qquad\qquad \rho_L = \rho_{L,0} + \frac{P}{c_L^2}, \qquad (4.9)$$

where c_k is the velocity of sound and $\rho_{L,0}$ is the reference density of the liquid phase given at vacuum. Notice that the velocity of sound in the gas phase c_G depends on the temperature as suggested by the ideal gas law. The temperature profile is assumed to be known.

Combining (4.9) with (4.4) we obtain the following relations for finding volume fractions from the mass variables:

$$\alpha_G = \frac{1}{2} - \frac{\frac{c_G^2}{c_L^2}n + m + \sqrt{\Delta}}{2\rho_{L,0}}, \qquad (4.10)$$

$$\Delta = \left(\rho_{L,0} - \frac{c_G^2}{c_L^2}n - m\right)^2 + 4\frac{c_G^2}{c_L^2}n\rho_{L,0} \qquad (4.11)$$

Then the pressure can be found using a modified expression to ensure pressure is define when the gas vanishes

$$P = \begin{cases} \left(\frac{m}{1-\alpha_G} - \rho_{L,0}\right)c_L^2, & \text{if } \alpha_G \leq \alpha_G^* \\ \frac{n}{\alpha_G}c_G^2, & \text{otherwise.} \end{cases} \qquad (4.12)$$

α_G^* is typically chosen as 0.5. Because the momentum equation (4.7) was written for the gas-liquid mixture, a so-called *slip law* is needed to empirically relate the velocities of gas and liquid. To handle the transition between single and two-phase flow, a relation with state-dependent parameters is needed ([18, 103]).

$$v_G = (K - (K-1)\alpha_G)v_m + \alpha_L S \qquad (4.13)$$

where $K \geq 1$ and $S \geq 0$ are constant parameters.

4.2.2 Boundary Conditions

Boundary conditions are given by the mass-rates of gas and liquid injected from the drilling rig and flowing in from the reservoir. Denoting the cross sectional flow area by A, the boundary fluxes are given as:

$$mv_L|_{x=0} = \frac{1}{A}\Big(W_{L,res}(t) + W_{L,inj}(t)\Big), \qquad (4.14)$$

$$nv_G|_{x=0} = \frac{1}{A}\Big(W_{G,res}(t) + W_{G,inj}(t)\Big). \qquad (4.15)$$

The injection mass-rates of gas and liquid, $W_{G,inj}, W_{L,inj}$, are specified by the driller and can, within some constraints, be considered as manipulated variables. The inflow from the reservoir is dependent on the pressure on the left boundary, for which, within the operational range of a typical UBD operation, an affine approximation should suffice, i.e.

$$W_{L,res} = k_L \max(P_{res} - P(0), 0) \tag{4.16}$$

$$W_{G,res} = k_G \max(P_{res} - P(0), 0) \tag{4.17}$$

Here P_{res} is the reservoir pore pressure and k_G, k_L are the production index (PI) of the gas and liquid respectively.

The topside boundary condition is given by a choke equation relating topside pressure to mass flow rates

$$\frac{mv_L}{\sqrt{\rho_L}} + \frac{nv_G}{Y\sqrt{\rho_G}}\bigg|_{x=L} = \frac{C_v(Z)}{A}\sqrt{\max(P(L,t) - P_s, 0)}, \tag{4.18}$$

where C_v is the choke opening given by the manipulated variable Z. $Y \in [0, 1]$ is a gas expansion factor for the gas flow and P_s is the separator pressure, i.e. the pressure downstream the choke.

4.2.3 Numerical Implementation

The drift flux model described above was implemented using a fully implicit Backwards Time-Central Space (BTCS) finite differences numerical scheme with an explicitly derived Jacobian as described in [3].

The state vector consists of the conserved mass variables m and n and the combined momentum $I = mv_L + nv_L$, $\mathbf{u} = \begin{bmatrix} m & n & I \end{bmatrix}^T$. For each of the states we use the following definition for finite differences,

$$m_i^k = m(k\Delta t, i\Delta x), \quad \text{etc.}$$

where $i = 0, 1, \ldots, N$ and $k = 0, 1, \ldots$. We arrange the terms into a vector

$$\mathbf{u}_k = \left[m_1^k, m_2^k, \ldots, m_N^k, n_1^k, \ldots, n_N^k, I_1^k, \ldots, I_N^k \right].$$

Consequently, propagating the states in time from $\mathbf{u}_k$ to $\mathbf{u}_{k+1}$ equates to solving a set of nonlinear equations that are implicit in $\mathbf{u}_{k+1}$, which we denote as

$$F(\mathbf{u}_{k+1}, \mathbf{u}_k) = 0, \qquad F : \mathbb{R}^{3N} \times \mathbb{R}^{3N} \to \mathbb{R}^{3N}. \tag{4.19}$$

These are solved using Newton steps which require the inverse of the Jacobian of F w.r.t. X_{k+1} denoted $F_{X_{k+1}}$. We note that the existence of this inverse is guaranteed by the $1/\Delta t$ terms making up the diagonal of $F_{X_{k+1}}$.

4.3   Unscented and Extended Kalman Filter

4.3.1   UKF

The implemented drift-flux model based on equations (4.5)-(4.18), although solved implicitly, can conceptually be represented as

$$X_k = f(X_{k-1}, \theta) + q_k \tag{4.20}$$

$$y_k = h(X_k) + r_k \tag{4.21}$$

where $q_k \sim N(0, Q_{k-1})$ is the zero mean white Gaussian process noise and model error, and $r_k \sim N(0, R_k)$ is the zero mean white Gaussian measurement noise.

The Kalman filter based on a linearized model was developed to estimate both state and parameter of the system usually known as an augmented Kalman filter. The augmented state vector is defined by $x^a = [X, \theta]$. The state-space equations for the the augmented state vector at time instant k are written as:

$$\begin{bmatrix} X_k \\ \theta_k \end{bmatrix} = \begin{bmatrix} f(X_{k-1}, \theta_{k-1}) + q_k \\ \theta_{k-1} \end{bmatrix} = f^a(X_{k-1}, \theta_{k-1}) + q_k^a \tag{4.22}$$

The UKF technique has been developed to work with non-linear systems without using an explicit linearization of the model ([36, 37, 109]). The UKF estimates the mean and covariance matrix of the estimation error with a minimal set of sample points (called sigma points) around the mean by using a deterministic sampling approach known as the unscented transform. The nonlinear model is applied to sigma points to predict uncertainty instead of using a linearization of the model. More details can be found in ([36, 104, 109]).

Dual and joint UKF techniques are two common approaches for estimation of parameters and state variables simultaneously. The dual UKF method uses another UKF for parameter estimation so that two filters run sequentially in every time step; the state estimator updates with new measurements, and then the current estimate of the state is used in the parameter estimator. The joint UKF augments the original state variables with parameters and a single UKF is used to estimate augmented state vector. In this chapter, the joint UKF is used.

4.3.2   EKF

For the implementation of an Extended Kalman Filter,to be used for comparison we need the Jacobian of the explicit formulation of the system equation. A first order Taylor series expansion around the trajectory $\bar{\mathbf{u}}$, noting

that $F(\bar{\mathbf{u}}_{k+1}, \bar{\mathbf{u}}_k) = 0$, yields

$$F_{X_{k+1}}(\bar{\mathbf{u}}_{k+1}, \bar{\mathbf{u}}_k)\tilde{\mathbf{u}}_{k+1} + F_{X_k}(\bar{\mathbf{u}}_{k+1}, \bar{\mathbf{u}}_k)\tilde{\mathbf{u}}_k = 0. \qquad (4.23)$$

where $F_{X_k}(\bar{\mathbf{u}}_{k+1}, \bar{\mathbf{u}}_k)$ is F with respect to a X_k. Hence, for the system Jacobian, we get

$$J = -F_{X_{k+1}}^{-1}(\bar{\mathbf{u}}_{k+1}, \bar{\mathbf{u}}_k)F_{X_k}(\bar{\mathbf{u}}_{k+1}, \bar{\mathbf{u}}_k)$$

where the partial derivatives are evaluated at the trajectory. We recognize $F_{X_{k+1}}$ to be the Jacobian, previously discussed, the inverse of which is known to exist.

4.4   Simulation results

4.4.1   Simulation with perfect model data

First, the presented DFM, (4.5)-(4.15) was used to create the measurements and true states in this simulation study. In this case the estimated states and parameters, in several configurations of unknown parameters to be estimated, converged to the true states (results not shown). Convergence transients were typically 0.5 hours for the UKF and 1.5 hours for the EKF. Of significantly more interest, however, is how the estimators performs in a more realistic setting where we would have model errors to deal with. Such a scenario is considered next.

4.4.2   Simulation with OLGA data

The parameter values for the simulated well and reservoir are summarized in Table 4.1. These parameters are used from the OLGA simulator. The OLGA dynamic multiphase flow simulator is a high fidelity simulation tool which has become the de facto industry standard in oil and gas production, see [8]. The measurements have been synthetically generated by using OLGA. The OLGA simulator uses the same model for the mass flow from the reservoir into the well as in equations (4.16)-(4.17).
 In the following, a measurement sampling interval of 10 seconds was used, and the model was run with time steps of 10 seconds using different spatial discretization cells ($N = 6, 12, 20$).
    Two scenarios are simulated. The first scenario of this chapter is the same simulation scenario as [2], considering UBD operation of a vertical well drilled into a dry gas reservoir (i.e. $W_{L,res} = K_L = 0$). The scenario in this simulation is as follows. First drilling in a steady-state condition is initiated with the choke opening of 10 % , then the choke is closed to 8 % at 1 hour. After 2 hours, the choke is closed to 7 %. After 3.5 hours, there

Table 4.1: Parameter Values for Well and Reservoir

Name	DFM	Unit
Reservoir pressure (p_{res})	279	bar
Collapse pressure (p_{coll})	155	bar
Well total length (L_{tot})	2530	m
Drill string outer diameter (D_d)	0.1206	m
Annulus inner diameter (D_a)	0.1524	m
Liquid flow rate ($w_{l,d}$)	13.33	kg/s
Gas flow rate ($w_{g,d}$)	0	kg/s
Liquid density (ρ_L)	1000	kg/m^3
Gas average temperature (T)	285.15	K
Average angle ($\Delta\theta$)	0	rad
Choke constant (K_c)	0.0053	m^2

is a linear and sharp increase in the production constant of gas from 0.072 kg/s/bar to 0.12 kg/s/bar. Then the choke is closed to 6 % at 6 hours, and after 8 hours, the choke is closed to 5.5 %. The choke opening of this simulation scenario is summarized in Table 4.2.

In the first scenario, it is assumed that only bottom-hole pressure ($P(0)$)

Table 4.2: Choke opening used in this scenario

Time	Choke Opening
0-1 h	10 %
1-2 h	8 %
2-6 h	7 %
6-8 h	6 %
8-10 h	5.5 %

and liquid and gas rate at the outlet are measured. The joint UKF and EKF estimate the states, production constant of gas, and slip parameters (S, K) simultaneously. The initial values for the estimated production constant of gas is ($\hat{K}_G = 0.08$ kg/s/bar). UKF parameters are determined empirically ($\kappa = 0$, $\beta = 2$, $\alpha = 0.00001$). The measurement noise covariance matrix is $R = diag[0.01, 0.0004, 0.04]$. The covariance matrix used in this simulation for both EKF and UKF is

$$Q = diag[Q_s, Q_p]$$
$$Q_p = diag[10^{-3}, 2 * 10^{-6}, 2 * 10^{-5}] \ , \ p = [K_G, K, S]$$

where Q_s and Q_p are the state covariance matrix and parameter covariance matrices, respectively. We used the same the state covariance matrix for
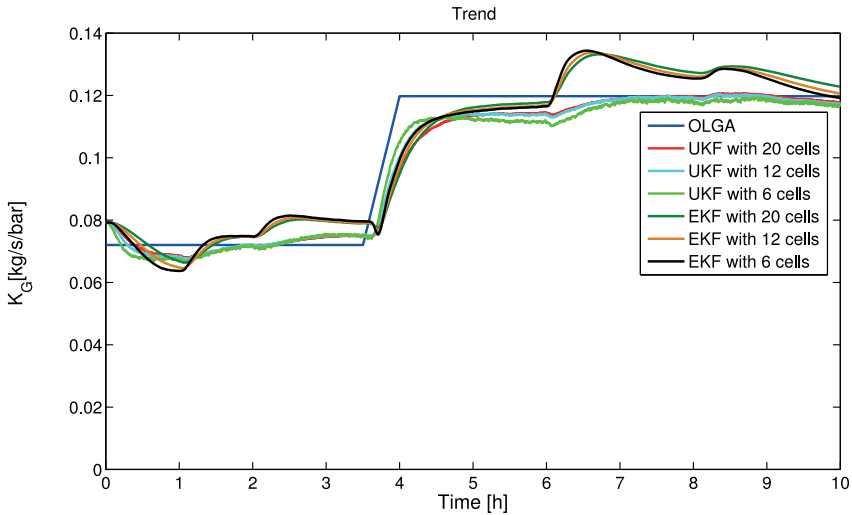
Figure 4.2: Estimating production constant of gas with different spatial discretizations

two scenarios. The estimations of the production constant of gas from the reservoir into the well for different spatial discretizations for both UKF and EKF are shown in Figure 4.2. The estimation algorithms are quite fast to detect and track changing at production constant of gas. However, there is a small deviation between the estimated and actual value of the production constant of gas. The number of steps in the spatial discretization does not have a significant effect on the accuracy of estimation, although the results show that decreasing number of steps can improve the convergence rate.

Figures 4.3 and 4.4 show the estimated slip parameters K and S for different spatial discretization cells for both UKF and EKF, respectively. The estimation of slip parameters does not always converges to constant values for steady state. However, estimation of production constant of gas has some errors during most of the scenario. On the other hand, estimation of production constant of gas in UKF has less error. In this case estimation of slip parameters varies during steady state. Since slip parameters are artificial parameters and has no reference value their convergence may not be important. As a production constant is a physical parameter, the convergence for estimation of production constant is vital for success of UBD operations.

Figure 4.5 shows the estimation of the production constant of gas with different fixed slip parameters by using UKF with 6 spatial discretization

71
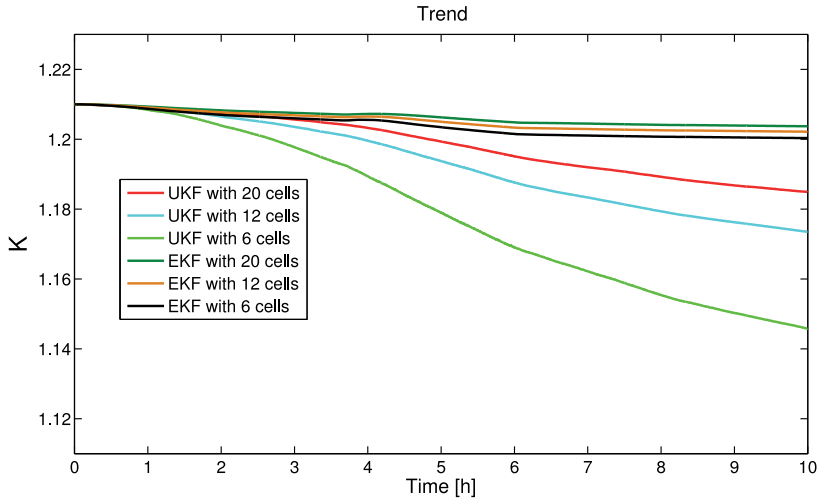
Figure 4.3: Estimating slip parameter (K) for different spatial discretization cells
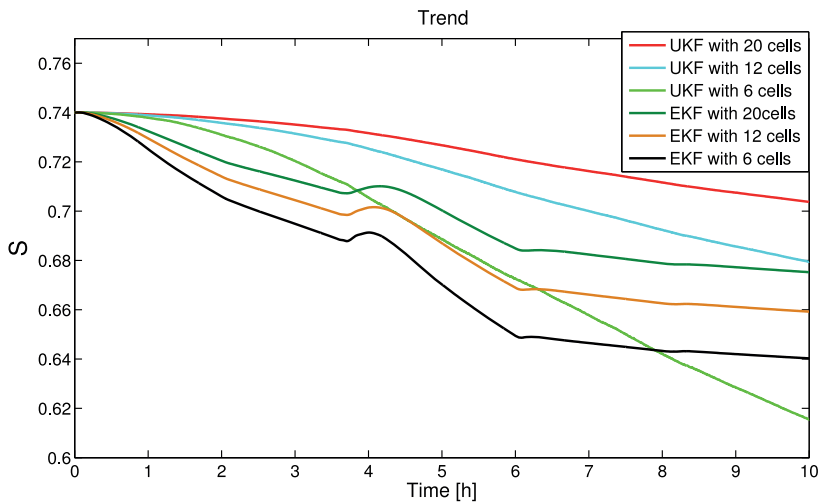
Figure 4.4: Estimating slip parameter (S) for different spatial discretization cells
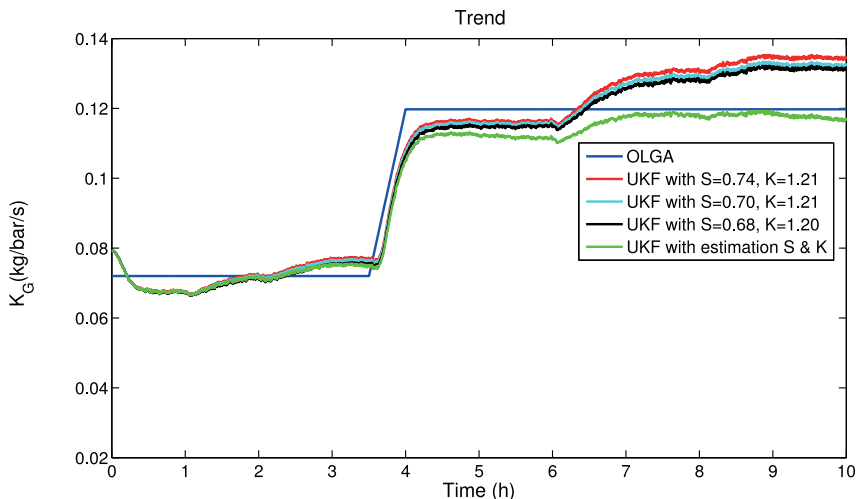
Figure 4.5: Estimating production constant of gas with fixed slip parameters

Table 4.3: Simulation runtime for different spatial discretization cells

Number of Cells	UKF (seconds)	EKF(seconds)
6	630.38	63.88
12	1110.82	67.27
20	2326.35	78.16

cells. The results show that estimation of the slip parameters can improve accuracy of the estimation of the production constant of gas. The measured bottom-hole pressure and choke pressure is illustrated in Figure 4.6.

The runtime of the simulations for different spatial discretization cells for both UKF and EKF are summarized in Table 4.3 by using 3.00 GHz Processor with 4 GB RAM running MATLAB, the runtime of the simulations for EKF are less than the runtime of the simulations for UKF, but we emphasize that the implementation is not optimized for computational efficiency.

Performance of these adaptive observers is evaluated through the root mean square error (RMSE) metric for the parameter K_G. The RMSE metric for UKF and EKF for different number of spatial discretization cells is summarized in Table 4.4.

According to the RMSE metric table, UKF with fewer cells in the spatial discretization has a slightly better performance than UKF with larger number of spatial discretization cells and EKF with different number of spatial
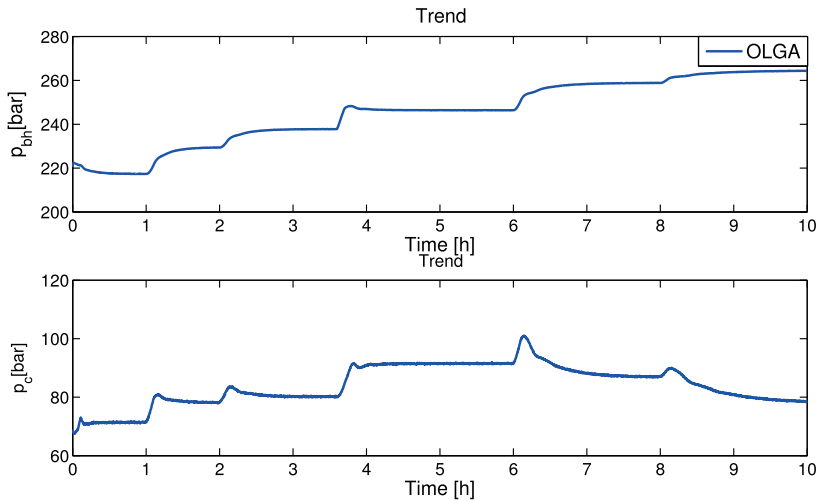
Figure 4.6: Bottom-hole pressure and choke pressure

Table 4.4: RMSE metric for estimate of K_G

Number of Cells	UKF	EKF
6	4.8×10^{-3}	8.2×10^{-3}
12	4.8×10^{-3}	8×10^{-3}
20	5.16×10^{-3}	8.3×10^{-3}

discretization cells for PI estimation, although the number of cells in the spatial discretization does not have a significant effect on the accuracy of estimation.

The second case study that is reported in this chapter considers UBD operation of a vertical well drilled into an oil and gas reservoir. First the drilling in a steady-state condition is initiated with the choke opening of 10 %, then at t = 1 hour and 35 min the main pump is shut off to perform a connection procedure, and the choke is closed to 6 %. The rotation of the drill string and the circulation of fluids are stopped for 15 mins. Next after making the first pipe connection at t = 1 hour and 50 min the main pump and rotation of the drill string are restarted. After 1 hour and 45 min (i.e. 3 hour and 35 min), the choke is closed to 5 %, and the second pipe connection procedure is started, and is completed after 15 mins. Then the choke is opened to 10 % at t= 3 hours and 50 min. The measured bottom-hole pressure (p_{bh}), choke pressure (p_c), choke opening (Z), and mass flow rate of liquid from the drill string ($w_{l,d}$) is illustrated in Figure 4.7.

Figure 4.7: Measured bottom-hole pressure, choke pressure, choke opening, and mass flow rate of liquid from the drill string for pipe connection scenario

Since these two scenarios model two drilling cases with different specifications, different measurements and different parameters for each scenario was used. Due to the fact that the liquid and gas flow rate at the outlet are sometimes measured by flow meter after separator, these measurements have usually some delay. Also, these measurements are sometimes not available. Therefore, the purpose of the second scenario is to show how the estimator works without these measurements. This way we can answer a wide range of problems in UBD operation with choosing different measurements by using these two scenarios.

In the second scenario, it is assumed that only bottom-hole pressure ($P(0)$) and choke pressure ($P(L)$) are measured. The UKF and EKF estimate the states and production constants of gas and liquid (K_G, K_L). Slip parameters in this simulation are fixed ($K = 1.15, S = 0.56$). The parameter values for the UKF for pipe connection scenario are the same as previous scenario. The initial values for the estimated and real parameters are as follows:

$$K_G = 0.07, \quad K_L = 0.1, \quad \hat{K}_G = 0.091, \quad \hat{K}_L = 0.13$$

The choke and the bottom-hole pressure measurements are corrupted by

zero mean additive white noise with the following covariance matrix

$$R = \begin{bmatrix} 0.9 * 0.4^2 & 0 \\ 0 & 0.9 * 0.2^2 \end{bmatrix} (bar^2)$$

The covariance matrix for parameter variations uses in this simulation for both EKF and UKF is

$$Q_p = diag[4 * 10^{-4}, 2 * 10^{-3}], \quad p = [K_G, K_L].$$

Figures 4.8 and 4.9 show the estimated production constants of gas and liquid from the reservoir into the well for different spatial discretization cells for both UKF and EKF, respectively.

The RMSE metric of the parameters K_G and K_L for UKF and EKF for different spatial discretization cells after initial transient $(t \geq 0.5 hour)$ are summarized in Table 4.5. The results show that UKF and EKF with fewer cells in the spatial discretization for the estimation of gas and liquid production constants have a better accuracy than UKF and EKF with larger spatial discretization cells with different spatial discretization cells for the estimation of gas and liquid production constants during the pipe connection. Since the model is significantly less accurate during the pipe connection, we need to prevent that the PI estimates drift away in order to compensate for other model errors. Hence, the Q_p of UKF and EKF is 1000 times smaller than the nominal value during the pipe connection. For the same reason, the measurement covariance of UKF and EKF is tuned 1000 times larger than the nominal value during the pipe connection.

Table 4.5: RMSE metric for estimate of K_G and K_L for pipe connection scenario

Number of Cells	K_G (after $t \geq 0.5h$)		K_L (after $t \geq 0.5h$)	
	UKF	EKF	UKF	EKF
6	1.4×10^{-3}	1.5×10^{-3}	3.6×10^{-3}	3.6×10^{-3}
12	1.8×10^{-3}	2.2×10^{-3}	3.8×10^{-3}	3.8×10^{-3}
20	2.4×10^{-3}	3.1×10^{-3}	4.8×10^{-3}	4.9×10^{-3}

Based on the RMSE metric in Table 4.5, UKF with fewer cells in the spatial discretization for the estimation of gas production constant (K_G) has a slightly better performance than UKF with larger spatial discretization cells and EKF with different spatial discretization cells for the estimation of K_G.
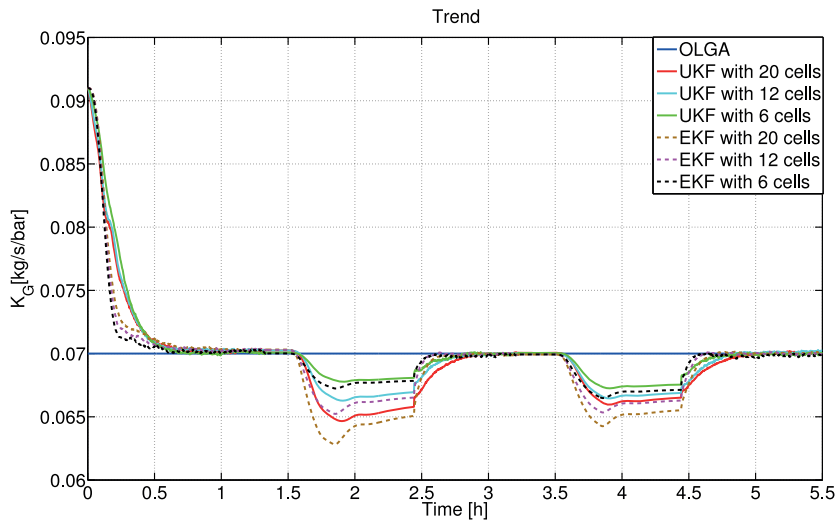
Figure 4.8: Estimating production constant of gas with different spatial discretization cells for pipe connection
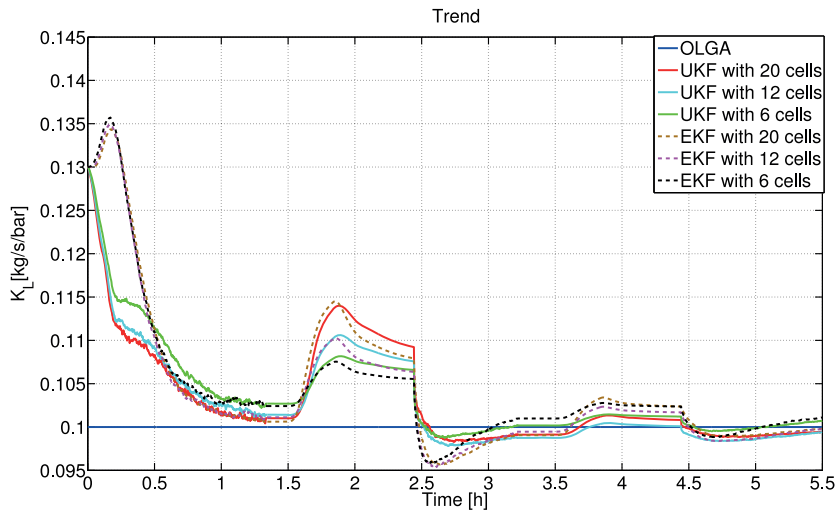

Figure 4.9: Estimating liquid production constant with different spatial discretization cells for pipe connection

4.4.3 Robustness analysis of UKF and EKF in case of uncertainties and errors in the reservoir and well parameters of the model

Robustness of the adaptive observers is investigated in case of errors in the reservoir and well parameters of the model. This test is performed in case of errors in the reservoir pore pressure and liquid density for pipe connection scenario. The RMSE metric for UKF and EKF in the two cases of 1% error on the reservoir pore pressure ($p_{res,model} = 282$ bar) and 10% error on the liquid density ($\rho_{L,model} = 1100$ kg/m^3)for different spatial discretization cells after initial transient ($t \geq 0.5hour$) are summarized in Table 4.6 and 4.7, respectively.

Table 4.6: RMSE metric in case of error in the reservoir pressure value for pipe connection scenario

Number of Cells	K_G (after $t \geq 0.5h$)		K_L (after $t \geq 0.5h$)	
	UKF	EKF	UKF	EKF
6	5.4×10^{-3}	5.6×10^{-3}	5.2×10^{-3}	5.3×10^{-3}
12	5.8×10^{-3}	6.0×10^{-3}	6.0×10^{-3}	6.0×10^{-3}
20	6.2×10^{-3}	6.7×10^{-3}	6.1×10^{-3}	6.3×10^{-3}

Table 4.7: RMSE metric in case of error in the liquid density value for pipe connection scenario

Number of Cells	K_G (after $t \geq 0.5h$)		K_L (after $t \geq 0.5h$)	
	UKF	EKF	UKF	EKF
6	1.4×10^{-3}	1.6×10^{-3}	3.7×10^{-3}	3.8×10^{-3}
12	1.9×10^{-3}	2.2×10^{-3}	3.9×10^{-3}	3.9×10^{-3}
20	2.4×10^{-3}	3.1×10^{-3}	4.8×10^{-3}	5.0×10^{-3}

Since the reservoir pore pressure has a direct effect on the mass flow rates from the reservoir into the well, small inaccuracies in the reservoir pore pressure have a significant effect on the estimation of production constants. Therefore these methods with different number of spatial discretization cells are very sensitive to errors in the reservoir pore pressure value. The results show that UKF and EKF with different number of spatial discretization cells are robust in case of error in the liquid density value of the model.

4.5 Conclusion

In this chapter, the joint UKF and EKF have been applied to the drift-flux model for different spatial discretization cells to estimate the distributed unmeasured states, geological properties of the reservoir (PI) and slip parameters (S, K) during UBD operations using measurement of the bottom-hole pressure and liquid and gas rate at the outlet. Furthermore, both production constants of gas and liquid and unmeasured states were estimated by using only measurements of the choke and the bottom-hole pressures for the pipe connection procedure. Simulation results demonstrated reasonable performance of the joint UKF and EKF to detect and track a changing gas production coefficient using the simulated scenario with OLGA. Even though the simulation scenario is somewhat idealized the results are encouraging. The number of spatial discretization cells was found to not have a significant effect on accuracy of estimation. The UKF was also found to estimate more accurately than the EKF. The results show that these methods are very sensitive to errors in the reservoir pore pressure value.

Design constrained MPC for heave disturbance attenuation in offshore Managed Pressure drilling systems

5.1 Introduction

In drilling operations, a drilling fluid (mud) is pumped down through the drill string and flows through the drill bit at the bottom of the well (Figure 5.1). The mud flows up the well annulus carrying cuttings out of the well. The mud is separated at the surface from the return well flow, conditioned, and stored in storage tanks (pits) before it is pumped down into the well for further drilling.To avoid fracturing, collapse of the well, or influx of formation fluids surrounding the well, it is crucial to control the pressure in the open part of the annulus within a certain operating window. In conventional drilling, this is done by using a mud of appropriate density and adjusting mud pump flow rates. In managed pressure drilling (MPD), the annulus is sealed, and the mud exits through a controlled choke, allowing for faster and more precise control of the annular pressure. In MPD operation, the dynamic pressure of the well must be kept higher than the reservoir pore pressure to prevent gas or formation fluids from entering the well and less than a formation fracture pressure at all times t and positions x.

$$p_{res}(x) < p_{well}(x,t) < p_{frac}(x) \tag{5.1}$$

where are reservoir pore pressure, well pressure, and formation fracture pressure, respectively. In automatic MPD systems, the choke is controlled to keep the annular mud pressure between specified upper and lower limits. There are several studies about different aspects of MPD modeling (e.g., see [38, 48, 50, 63, 96]). Estimation and control design in MPD have been investigated by several researchers (e.g., see [12, 25, 38, 83, 113, 114]). These

studies are mainly focused on pressure control during drilling from a fixed platform without any heave motion.

The automatic MPD system has several advantages compared to conventional drilling as follows:

- Reducing the drilling costs as a result of reducing the nonproductive time.

- Increasing the rate of penetration.

- Improving well-bore stability.

- Minimizing the risk of lost circulation.

- Extending control over bottom-hole pressure (BHP) to operational scenarios such as connections and trips and when the rig pumps are off.

- Improvement in safety and well control resulting from more detailed design and planning required for accomplishment.

When designing MPD control systems, one should take into account various operational procedures and disturbances that affect the pressure inside the well. There is a specific disturbance occurring during drilling from floaters that significantly affects MPD operations. In this case, the rig moves vertically with the waves, referred to as heave motion. As drilling proceeds, the drill string needs to be extended with new sections. Thus, every couple of hours or so, drilling is stopped to add a new segment of about 27 m to the drill string. During drilling, a heave compensation mechanism is active to isolate the drill string from the heave motion of the rig. However, during connections, the pump is stopped, and the string is disconnected from the heave compensation mechanism and rigidly connected to the rig. The drill string then moves vertically with the heave motion of the floating rig and acts like a piston on the mud in the well. The heave motion may be more than 3 m in amplitude and typically has a period of 10–20 s, which causes severe pressure fluctuations at the bottom of the well. Pressure fluctuations have been observed to be an order of magnitude higher than the standard limits for pressure regulation accuracy in MPD (about ± 2.5 *bar*) [24]. Downward movement of the drill string into the well increases pressure (surging), and upward movement decreases pressure (swabbing). Excessive surge and swab pressures can lead to mud loss resulting from high-pressure fracturing of the formation or a kick-sequence (uncontrolled influx from the reservoir) that can potentially grow into a blowout as a consequence of low pressure.

Hauge et al.[30] designed an adaptive observer to estimate the unknown states, the magnitude and location of the in /out flux and parameters of the hydraulic system during MPD. It is also used control law for choke to attenuate the in/out flux during drilling. This adaptive observer is verified with several experimental and simulation results. Carlsen et al.[13] designed
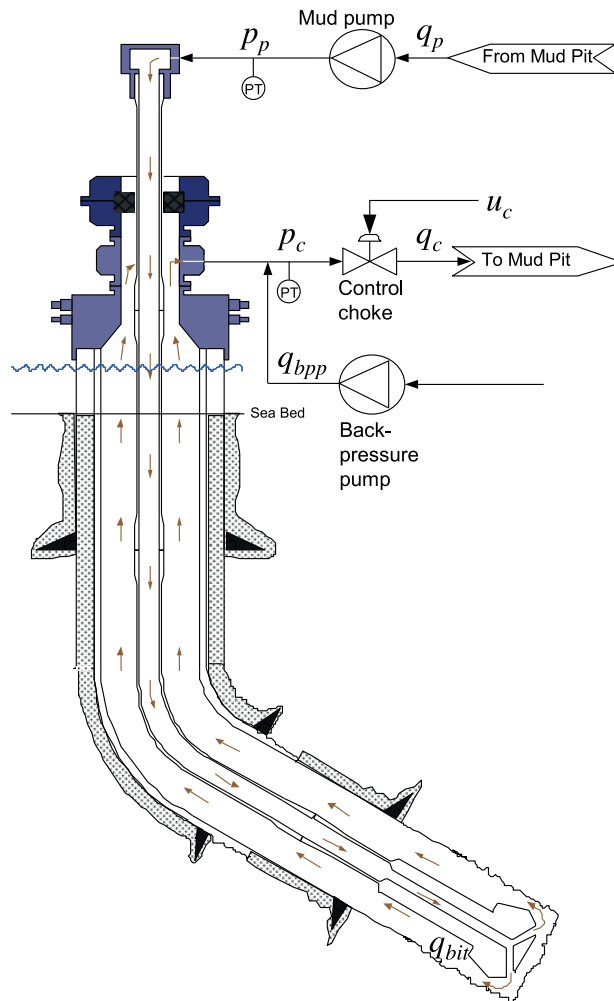
Figure 5.1: Schematic of an MPD system (courtesy of Dr. Glenn-Ole Kaasa, Statoil Research Centre).

linear MPC, PI and internal model controller based on simple first order model to stabilize the well pressure during MPD operations. The performance of these controllers was evaluated on three different drilling scenarios while the well kicked during these scenarios. Manipulated variables in the linear MPC and the internal model controller are choke valve and pump. while manipulated variable in the PI is only choke valve. The simulations show that the controllers have a good performance to stabilize the well pressure in case of change in drilling conditions and disturbances. Asgharzadeh et al.[7] designed nonlinear MPC (NMPC) with adaptive observer for kick detection and attenuation, regulation of the bottom hole pressure and rate of penetration (ROP) with direct pressure measurements from wired pipe telemetry technology during MPD. This Controller works for both normal drilling and kick event. Some parameters of the drilling model drilling could not be measured directly. Therefore, the annulus friction factor and density is estimated by a nonlinear moving horizon estimator. In this case the gas influx flow rate is estimated by an extended Kalman filter with measurement of choke valve, down-hole and pump pressures. Manipulated variables in the NMPC are mud pump flow rate, choke valve position, drill string rotation rate, and weight-on-bit (WOB). The objective function of the NMPC is using an $\ell_1$norm instead of conventional squared error norm for better noise and drift rejection. Asgharzadeh et al.[6] studied effect of temporarily communication loss in the NMPC during kick event. This paper shows that distributed pressure measurements with multiple sensor can improve kick attenuation of NMPC during kick event due to availability of a sensor closer to the influx location [6].

Rasmussen et al.[99] compared and evaluated different MPD methods for the compensation of surge and swab pressure. In Nygaard et al. [86], it is shown that surge and swab pressure fluctuation in the BHP during pipe connection can be suppressed by controlling the choke and main pump. Nygaard et al. [87] used a nonlinear model predictive control (MPC) algorithm to obtain optimal choke pressure for controlling the BHP during pipe connection in a gas-dominant well. Pavlov et al. [93] presented two nonlinear control algorithms for handling heave disturbances in MPD operations. Mahdianfar et al. [61, 62] designed an infinite-dimensional observer that estimates the heave disturbance. This estimation is used in a controller to reject the effect of the disturbance on the downhole pressure. In all the above mentioned papers, the controllers are designed for the nominal case disregarding the uncertainty in the parameters, although several parameters in the well could be uncertain during drilling operations. In addition, the heave disturbance, which is inherently stochastic and contains many different harmonics, is approximated by one or a couple of sinusoidal waves with

known fixed frequencies throughout controller design and simulations. In this chapter, a stochastic model for the heave motion in the North Sea is given and is used in simulations.

MPC is one of the most popular controller design methodologies for complex constrained multivariable control problems in the industry and has been the subject of many studies since the 1970s(e.g. see [23, 60, 64, 67]). At each sampling time, an MPC control action is acquired by the online solution of a finite horizon open-loop optimal control problem. Only the first part of the optimal control trajectory is applied to the system. At the next sampling time, the computation is repeated with new measurements obtained from the system. The purpose of this chapter is to study a constrained MPC scheme for controlling the pressure during MPD oil well drilling using measurements and optionally predictions of the heave disturbances. In some cases, short-term heave motion prediction based on forward-looking sensors such as ocean wave radar may be predictable [44], and we can use them directly in our MPC controller. One of the criteria for evaluating the controller performance is its ability to handle heave disturbances. This scheme is compared with a standard proportional-integral-derivative (PID) control scheme. Furthermore, the robustness of the controller to deal with heave disturbances despite significant uncertainties in the friction factor and bulk modulus is investigated by Monte Carlo simulations.

In the following sections, a model based on mass and momentum balances that provides the governing equations for pressure and flow in the annulus is given. A stochastic modeling of waves in the North Sea is used, and the heave disturbance induced by the elevation motion of the sea surface is modeled. The design of a constrained MPC scheme is presented and applied on MPD. In the cases with and without the predictive heave disturbance feed-forward and prediction, it is shown that this controller outperforms a PID controller. Finally robust performance of an MPC controller is evaluated through Monte-Carlo simulations.

5.2   Mathematical Modeling

In this section, the distribution of single-phase flows and pressures in the annulus and the drill string is modeled by two coupled partial differential equations (PDEs). Then, the PDE model is discretized by using the finite volume method. Finally, the model describing the vessel's heave motion in response to the stochastic sea waves in the North Sea is presented and used as the heave disturbance.

5.2.1 Annulus flow dynamics

The governing equations for flow in an annulus are derived from mass and momentum balances based on 1-D hydraulic transmission line [50].

$$\frac{\partial p}{\partial t} = -\frac{\beta}{A}\frac{\partial q}{\partial x} \tag{5.2}$$

$$\frac{\partial q}{\partial t} = -\frac{A}{\rho_0}\frac{\partial p}{\partial x} - \frac{F}{\rho_0} + Ag\cos(\alpha(x)) \tag{5.3}$$

where $p(x,t)$ and $q(x,t)$ are the pressure and volumetric flow rate at location x and time t, respectively. The bulk modulus of the mud is denoted by β. $A(x)$ is the cross section area, ρ is the (constant) mass density, F is the friction force per unit length, g is the gravitational constant and $\alpha(x)$ is the angle between gravity and the positive flow direction at location x in the well (Figure 5.2). To derive a set of ordinary differential equations describing the dynamics of the pressures and flows at different positions in the well, equations (5.2) and (5.3) are discretized by using a finite volumes method. To solve this problem, the annulus is divided into a number of control volumes, as shown in Figure 5.2, and integrating (5.2) and (5.3) over each control volume. This model will be used for the MPC design.

Landent et al. [50] found that five control volumes could capture the main dynamics of the system in the case of heave disturbance for a well from the Ullrigg test facility with a particular length of about 2,000 m and with water-based mud. Ullrigg is a full scale drilling test facility located at the International Research Institute of Stavanger (IRIS). The parameters corresponding to that well are used as a base case throughout this chapter. The set of nine ordinary differential equations describing five control volumes in the annulus are shown below ([48, 49])

$$\dot{p}_1 = \frac{\beta_1}{A_1 l_1}(-q_1 - v_d A_d) \tag{5.4}$$

$$\dot{p}_2 = \frac{\beta_2}{A_2 l_2}(q_1 - q_2) \tag{5.5}$$

$$\dot{p}_3 = \frac{\beta_3}{A_3 l_3}(q_2 - q_3) \tag{5.6}$$

$$\dot{p}_4 = \frac{\beta_4}{A_4 l_4}(q_3 - q_4) \tag{5.7}$$

$$\dot{p}_5 = \frac{\beta_5}{A_5 l_5}(q_4 - q_c + q_{bpp}) \tag{5.8}$$
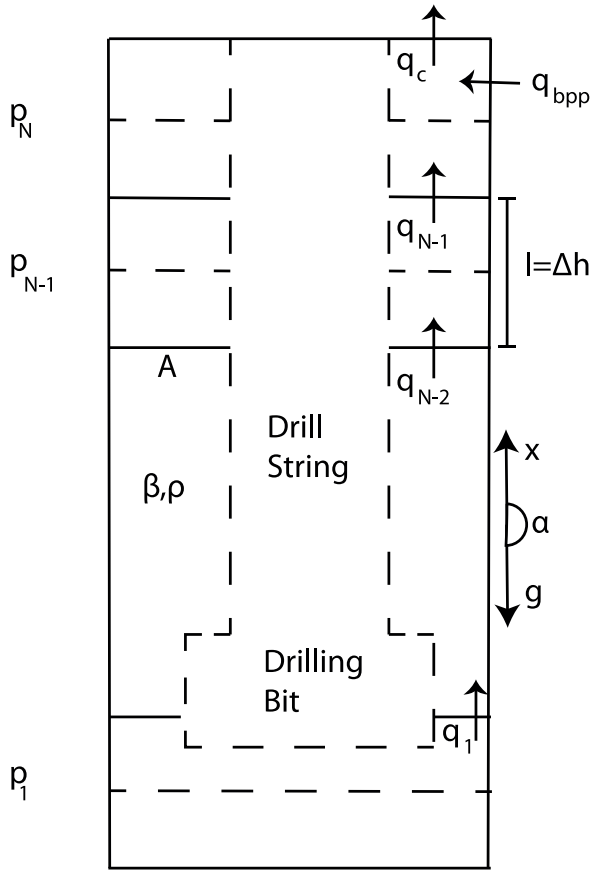
Figure 5.2: Control volumes of annulus hydraulic model [50]

$$\dot{q}_i = \frac{A_i}{l_i \rho_i}(p_i - p_{i+1}) - \frac{F_i(q_i)A_i}{l_i \rho_i} - A_i g \frac{\Delta h_i}{l_i} \tag{5.9}$$

$$q_c = K_c \sqrt{p_c - p_0} G(u) \tag{5.10}$$

where, $i = 1, ..., 4$, and the numbers $1, ..., 5$ refer to control volume number, with 1 being the lower most control volume representing the down hole pressure ($p_1 = p_{bit}$), and 5 being the upper most volume representing the choke pressure ($p_5 = p_c$). v_d is the heave vertical velocity due to ocean waves. The length of each control volume is denoted by l, and the height difference is Δh_i. Since the well may be non-vertical, l_i and Δh_i may in general differ from each other. The means for pressure control are the back pressure pump flow q_{bpp} and the choke flow q_c. The flow from the back pressure pump q_{bpp} is linearly related to the pump frequency and cannot be changed fast enough to compensate for the heave-induced pressure fluctuations. Therefore, it is the

choke flow that is used primarily for control, which is modeled by nonlinear orifice equation 5.10. K_c is the choke constant corresponding to the area of the choke and the density of the drilling fluid. p_0 is the (atmospheric) pressure downstream the choke and $G(u)$ is a strictly increasing and invertible function relating the control signal to the actual choke opening, taking its values on the interval $[0, 1]$.

Based on experimental results from full scale tests at Ullrigg, the friction force in the annulus is considered to be a linear function of the flow rate [50]. Friction force on the ith control volume is approximately modeled as

$$F_i(q_i) = \frac{k_{fric}q_i}{A_i} \tag{5.11}$$

where k_{fric} is the constant friction coefficient.

Some components of the transient hydraulic model, equations (5.2) - (5.3), have significant uncertainties, such as the following [63]:

- **Rheology and viscosity of drilling fluid**: Most drilling fluids are non-Newtonian, that is, with a nonlinear relation between shear stress and shear rate. Consequently, the viscosity will not be constant over a cross-sectional flow area. To measure the shear stress-shear rate relationship, the viscometer measurements must be correlated with the rheological model applied. However, information is limited and normally inadequate for a model of high accuracy, particularly for modern oil-based muds. Also, viscosity may depend on pressure and temperature. Manual rheology measurements are normally performed periodically on the rig at the atmospheric pressure and temperature of the mud in the pit. Thus, information on the influence of temperature and pressure variations is missing [21, 27, 53].

- **Frictional pressure loss models for drill pipe and annulus**: The frictional pressure loss depends on the mean cross-sectional velocity, drilling fluid viscosity, flow regime, hydraulic diameter, and pipe roughness. The accuracy of all these derived parameters is questionable. Moreover, the Fanning friction factor is a function of Reynolds number where the Reynolds number is a function of the fluid viscosity for a characteristic diameter [21, 38, 53].

- **Effective bulk modulus**: A bulk modulus is used because the degree of mechanical compliance of casing, pipe, hoses, and other components is uncertain and also because it is impossible to predict the amount of gas pockets, bubbles, or breathing of the well [38].

5.2.2 Waves Response Modeling

Environmental forces in the vertical direction due to waves are considered disturbances to the motion control system of floating vessels. These forces, which can be described in stochastic terms, are conceptually separated into low-frequency (LF) and wave-frequency (WF) components, [22]. The LF part is not considered any farther since it is very slow compared to the dynamics of the mud circulation system and dealt with by other controllers and operationally (e.g., pipe connection).

During normal drilling operations, the WF part of the drill-string motion is compensated by the heave control system ,[16, 42, 44]. However, during connections, the drill string is disconnected from the heave compensation mechanism and rigidly connected to the rig. Thus, it moves vertically with the heave motion of the floating rig and causes severe downhole pressure fluctuations.

Linear Approximation for WF Position

When simulating and testing feedback control systems, it is useful to have a simple and effective way of representing the wave forces. Here, the motion response amplitude operators(RAOs) are represented as a state-space model where the wave spectrum is approximated by a linear filter. In this setting, the RAO vessel model is represented in Figure 5.3, where $H_{rao}(s)$ is the wave amplitude-to-force transfer function and $H_v(s)$ is the force-to-motion transfer function. In addition to this, the response of the motion RAOs and the linear vessel dynamics in cascade is modeled as constant tunable gains, [22]. This means that the RAO vessel model is approximated as (Figure 5.3)

$$\boldsymbol{K} = \mathrm{diag}\{K^1, K^2, K^3, K^4, K^5, K^6\} \tag{5.12}$$

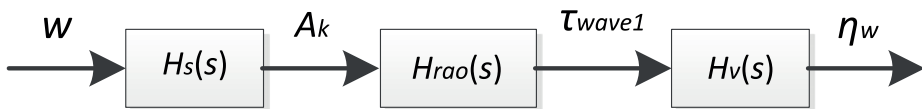$$H_{rao}(s)H_v(s) \approx K \tag{5.13}$$

Figure 5.3: Linear approximation for computation of wave-induced positions.

Since the vessel is typically designed to avoid resonances in the dominant WF, the fixed-gain approximation [equation 5.13] produces good results in a closed-loop system where the purpose is to test the robustness and performance of a feedback control system in the presence of waves.

Then, the generalized WF position vector η_w in Figure 5.3 becomes

$$\eta_w = K H_s(s) w(s) \tag{5.14}$$

where $H_s(s)$ is a diagonal matrix containing transfer function with the spectral factors of the wave spectrum $S(\omega)$. The WF position for the degree of freedom related to heave motion becomes

$$\eta_w^h = K^h \xi^h \tag{5.15}$$
$$\xi^h(s) = h^h(s) w^h(s) \tag{5.16}$$

where $h^h(s)$ is the spectral factor of the wave spectral density function $S(\omega)$ and $w^h(s)$ is a zero-mean Gaussian white noise process with unity power across the spectrum:

$$P_{ww}^h(\omega) = 1.0 \tag{5.17}$$

Hence, the power spectral density (PSD) function for $\xi^h(s)$ can be computed as

$$P_{\xi\xi}^h(\omega) = |h^h(j\omega)|^2 P_{ww}^h(\omega) = |h^h(j\omega)|^2 \tag{5.18}$$

Joint North SeaWave Project Spectrum

The Joint North Sea Wave Project (JONSWAP) formulation is based on an extensive wave measurement program known as the JONSWAP carried out in 1968 and 1969 in the North Sea, between the island Sylt in Germany and Iceland. The JONSWAP spectrum is representative of wind-generated waves under the assumption of finite water depth and limited fetch [22, 90].The spectral density function is written as

$$S(\omega) = 155 \frac{H_s^2}{T_1^4} \omega^{-5} \exp\left(\frac{-944}{T_1^4}\omega^{-4}\right)\gamma^Y \tag{5.19}$$

where H_s is the significant wave height, T_1 is the average wave period, $\gamma = 3.3$ and

$$Y = \exp\left[-\left(\frac{0.191\omega T_1 - 1}{\sqrt{2}\sigma}\right)^2\right] \tag{5.20}$$

where

$$\sigma = \begin{cases} 0.07 & \text{for } \omega \leq 5.24/T_1 \\ 0.09 & \text{for } \omega > 5.24/T_1 \end{cases} \tag{5.21}$$

The modal period, T_0, is related to the average wave period through $T_1 = 0.834\,T_0$, [22].

Figure 5.4, produced using MSS Toolbox, shows the JONSWAP spectrum power distribution curve. The parameter values for H_s and T_0 are taken from

[66]. From Figure 5.4, we can see that the JONSWAP spectrum is a narrow band spectrum, and its energy is mainly focused on $0.5 - 1.5\,rad/s$, and the peak frequency is $\omega_0 = 0.7222\,rad/s$.
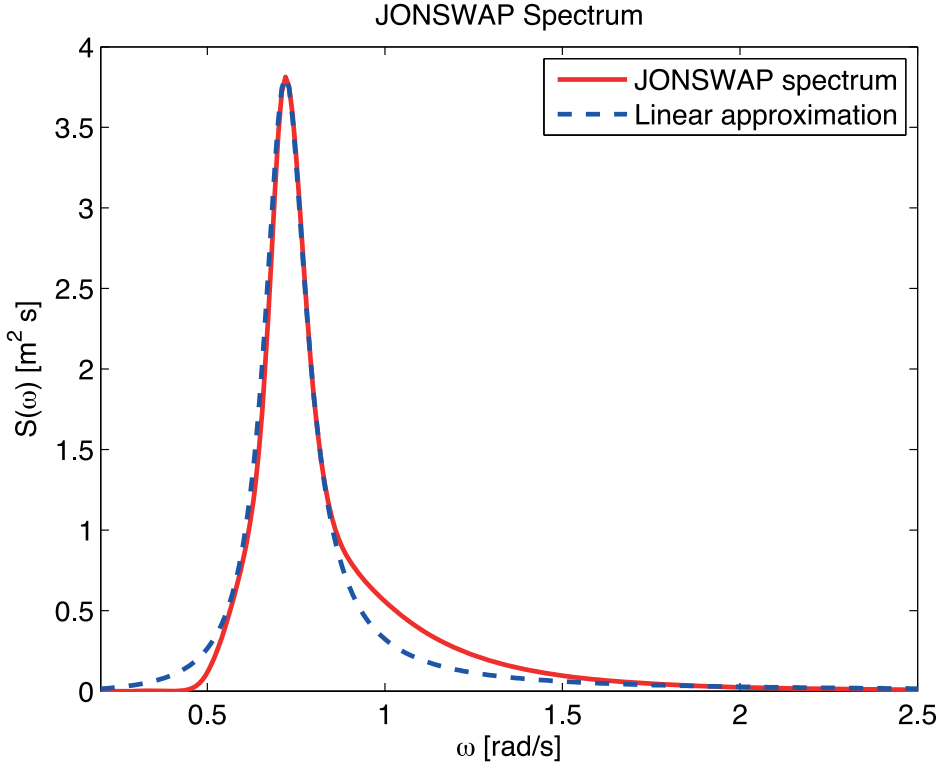
Figure 5.4: JONSWAP spectrum and its approximation.

Second-Order Wave Transfer Function Approximation

As discussed earlier, a finite dimensional,rational transfer function wave response approximation for $H_s(s)$ is usually preferred by ship control systems engineers, because of its simplicity and applicability:

$$h^h(s) = \frac{2\lambda\omega_0\sigma s}{s^2 + 2\lambda\omega_0 s + \omega_0^2} \tag{5.22}$$

where $\lambda = 0.1017$, $\sigma = 1.9528$, $H_s = 4.70$, $T_0 = 8.70$, $\omega_0 = 0.7222$, and $K^h = 9.1$ are typical parameters for heave motion of the drilling rig. The transfer function approximation is shown in Figure 5.4.

5.3   Controller Design

The model described by equations (5.4)-(5.10) is in form of a nonlinear strict feedback system, with an unmatched stochastic disturbance. By considering $a_j = \frac{\beta_j}{A_j l_j}$, $b_j = \frac{A_j}{l_j \rho_j}$, $c_j = \frac{K_{fric}}{\rho_j l_j}$, the model in state-space form would be

$$\begin{cases} \dot{X} = AX + Bu_a + B_1 + Ed \\ y = CX \end{cases} \tag{5.23}$$

where

$$X = \begin{bmatrix} p_1 & q_1 & p_2 & q_2 & p_3 & q_3 & p_4 & q_4 & p_5 \end{bmatrix}^T$$

$$A = \begin{bmatrix} 0 & -a_1 & 0 & 0 & 0 & 0 & 0 & 0 & 0 \\ b_1 & -c_1 & -b_1 & 0 & 0 & 0 & 0 & 0 & 0 \\ 0 & a_2 & 0 & -a_2 & 0 & 0 & 0 & 0 & 0 \\ 0 & 0 & b_2 & -c_2 & -b_2 & 0 & 0 & 0 & 0 \\ 0 & 0 & 0 & a_3 & 0 & -a_3 & 0 & 0 & 0 \\ 0 & 0 & 0 & 0 & b_3 & -c_3 & -b_3 & 0 & 0 \\ 0 & 0 & 0 & 0 & 0 & a_4 & 0 & -a_4 & 0 \\ 0 & 0 & 0 & 0 & 0 & 0 & b_4 & -c_4 & -b_4 \\ 0 & 0 & 0 & 0 & 0 & 0 & 0 & a_5 & 0 \end{bmatrix}$$

$$B = \begin{bmatrix} 0 & 0 & 0 & 0 & 0 & 0 & 0 & 0 & a \end{bmatrix}^T$$

$$B_1 = -263.7814 \begin{bmatrix} 0 & 1 & 0 & 1 & 0 & 1 & 0 & 1 & 0 \end{bmatrix}^T$$

$$E = \begin{bmatrix} -22.0857 & 0 & 0 & 0 & 0 & 0 & 0 & 0 & 0 \end{bmatrix}^T$$

$$C = \begin{bmatrix} 1 & 0 & 0 & 0 & 0 & 0 & 0 & 0 & 0 \end{bmatrix} \tag{5.24}$$

and

$$u_a = q_{bpp} - q_c \tag{5.25}$$

The output $y = p_1$ is the BHP. The heave disturbance v_d in equation (5.4) will be compensated by using constrained MPC as designed in the following section. Note that the hydrostatic pressures in equation (5.9) are included in the states p_i in (5.4)-(5.8).

5.3.1   MPC

The main MPC objective in this chapter is to regulate BHP to desired values (set points) during pipe connection by minimizing the cost function and satisfying output and input constraints.

Constrained MPC design

Consider the discrete-time linear time-invariant input-affine system [equation 5.23] while fulfilling the constraints

$$y_{min} \leq y(k) \leq y_{max}, \ u_{min} \leq u(k) \leq u_{max} \qquad (5.26)$$

at all time instants $k \geq 0$.

In (5.23)-(5.26), n , p and m are the number of states, outputs and inputs respectively, and $x(k) \in \Re^n$, $y(k) \in \Re^p$, $d(k) \in \Re^n$ and $u(k) \in \Re^m$ are the state, output, disturbance and input vectors respectively.

The constrained MPC solves a constrained optimal regulation problem at each time k.

$$\min_{U \triangleq \{u_k, \cdots, u_{k+N}\}} \{ J(u,y,r) = \sum_{i=1}^{N} [(u_{k+i|k}^T R u_{k+i|k} + \Delta u_{k+i|k}^T R_{\delta u} \Delta u_{k+i|k}$$
$$+ (y_{k+i|k} - r_{k+i|k})^T Q (y_{k+i|k} - r_{k+i|k})] \}$$

$$
\begin{aligned}
subject\,to \quad & y_{min} \leq y_{i+k|k} \leq y_{max} \quad i = 1, \cdots, N, \\
& u_{min} \leq u_{i+k|k} \leq u_{max} \quad i = 1, \cdots, N, \\
& \Delta u_{min} \leq \Delta u_{i+k|k} \leq \Delta u_{max} \quad i = 1, \cdots, N, \\
& x_{k|k} = x(k) \qquad\qquad\qquad\qquad\qquad (5.27) \\
& x_{i+k+1|k} = A_{di} x_{i+k|k} + B_{di} u_{i+k|k} + B_{di,1} + E_{di} d_{i+k|k}, \\
& y_{i+k|k} = C_{di} x_{i+k|k}
\end{aligned}
$$

where N, J and r are the finite horizon, cost function and reference trajectory, respectively. The matrices $A_{di}, B_{di}, B_{di,1}, E_{di}$, and C_{di} follow from a discretization of the system. The subscript "$(k + i|k)$" denotes the value predicted for time $k+i$, and it is assumed that $Q, R_{\delta u}$ and R are the positive definite matrices.

Since the states x_k are not directly measurable, predictions are computed from the estimation of states. Since the pair (C, A) is detectable, a state observer is designed to provide estimation of states x_k, as described in the Kalman Filter for State Estimation section. The controller computes the optimal solution U by solving the quadratic programing (QP) [equation 5.27]. If the future value of disturbances and/or measurement of disturbances are not assumed to be known, then disturbances are assumed to be zero in the MPC predictions.

Controller parameters such as weight of inputs, inputs' rate, and outputs and control horizon must be tuned to achieve the good performance and stability in this problem. The prediction horizon should be chosen large enough to ensure the closed-loop stability of the control system.

MPC Constraints

The upper and lower bounds on the input are chosen from the choke opening modes, which are fully opened and fully closed, respectively. Enforcing pressure of the annulus in a certain operating window is the main reason for using MPD. The hydrostatic pressure of the well must be kept between both the reservoir formation pressure and collapsing pressure on one side and the fracturing pressure on the other side. The typical limit for pressure regulation accuracy in MPD is about ± 2.5 *bar*. The controlled output constraints for the limits for pressure regulation accuracy in MPD must be softened by the addition of slack variables.

MPC Cost Function

The cost function [equation 5.27] consists of three standard terms. The first term penalizes the prediction input effort, and the second term in the cost function penalizes variation in the prediction control input. The last term weights the deviations of the output variable from the reference trajectory $r_{k+i|k}$.

5.3.2   Kalman Filter for state estimation

The discrete-time Kalman filter is a recursive algorithm based on discrete linear dynamic systems and known stochastic models of noise and disturbance. The Kalman filter has the ability to estimate states with the minimum variance of the estimation error. This algorithm has two distinct steps: prediction and correction. In the prediction step, predicted state $(\hat{x}_{k|k-1})$ and predicted estimate covariance $(P_{k|k-1})$ are computed. In the correction step with updated measurement, optimal Kalman gain (K_k) is computed. Then, the updated state $(\hat{x}_{k|k}$) and updated estimate covariance $(P_{k|k})$ are computed with optimal Kalman gain. More details on Kalman filtering can be found in [104].

5.4   Simulation Results

The nominal parameters for simulations, identified from the IRIS drill simulator [89], are given in Table 5.1.

Table 5.1: Parameter values

Parameter	Value
a	$2.254 \times 10^8 \, [Pa/m^3]$
b	$4.276 \times 10^{-8} \, [m^4/Kg]$
g (gravitational constant)	$9.806 \, [m/s^2]$
A (annulus area)	$0.0269 \, [m^2]$
A_d (drill string area)	$0.0291 \, [m^2]$
K_f (friction coefficient)	$5.725 \times 10^5 \, [sPa/m^3]$
q_{bpp} (backpressure pump flow)	$369.2464 \, [m^3/s]$
K_c (choke constant)	2.32
c	$14.4982 \, [1/sm^2]$
p_0 (atmospheric pressure)	$101325 \, [pa]$

The time-step used for discretizing the dynamic optimization model was 0.1 s. This is also the sampling interval of measurements and the update prediction of the Kalman filter and MPC. The input weight (R), input rate weight ($R_{\delta u}$), output weight (Q) and prediction horizon (N) are chosen 150, 0, 17 and 100, respectively. In this problem, the prediction horizon (10 s) is relatively large compared with the settling time to ensure the closed-loop stability of the control system. The weights specify trade-offs in the controller design. Choosing a larger output weight or smaller input weight results in overshoot in the closed-loop response and, sometimes, broken constraints. On the other hand, if a larger input weight or smaller output weight is chosen, then the closed-loop response is slower or sometimes unstable.

To compare the impact of MPC on the drilling system with other controllers, a PID controller was applied to the system as well. A PID controller is chosen due to its popularity in the industry. PID gains are chosen as 0.75, 0.002, and −1, respectively. The Bode plot of the loop transfer function with the PID is shown in Figure 5.5. Bandwidth with PID is less than 1.3 rad/s, and the phase drops very quickly. Therefore, it is not realistic to get a bandwidth of about 5 rad/s or more, as would be desirable for this disturbance, which has dominating frequencies of about 0.5–1.5 rad/s.

Several simulations are performed. The first simulation is shown in Figure 5.6, where the nominal model is used for generating the measurements, and there is no heave motion.A soft constraint of ±2.5bar (compared to the reference pressure) and a constraint of choke opening taking its values on the interval [0, 1] are included in the constrained MPC optimization. Figure 5.6(a) compares the responses of the PID controller and constrained MPC to regulate a set point trajectory. In the proposed MPC controller, the BHP approaches to set point quickly without any overshoot. In comparison to the MPC controller, the PID controller has some overshoot and a slower
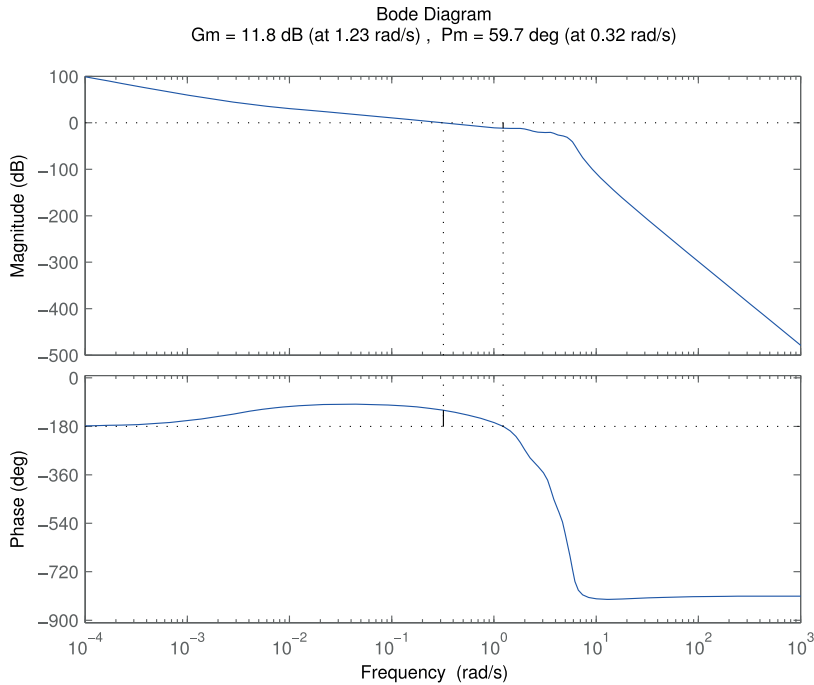
Figure 5.5: Bode plot of the loop transfer function with the PID.

response. The choke control signal in the constrained MPC is illustrated in
Figure 5.6(b).

The second simulation is shown in Figures 5.7 and 5.8, where the nominal model with heave disturbance is used for generating the measurements.
The same constraints as in previous simulation are enforced to the controller. Figure 5.7 compares the responses of constant input ($q_{bpp} = q_c$) and
constrained MPC to track the set point reference with existing heave disturbance. A constant input couldn't reduce the effect of heave disturbance
and track the set point reference. Figure 5.8(a) compares the responses of
PID controller and constrained MPC to track the set point reference with a
heave disturbance. It is found that the MPC controller is capable of maintaining the constraints, whereas the PID controller is not. Performance of
the controller is evaluated through the root mean square (RMS) tracking
error metric. The RMS tracking errors for the MPC and PID controllers are
1.2524 and 1.6273, respectively, which means that the effect of disturbances
is reduced to 77.0% by the MPC compared to the PID. As indicated in
this figure and the RMS tracking error, the constrained MPC shows good
disturbance rejection capabilities. The choke control signal is illustrated in
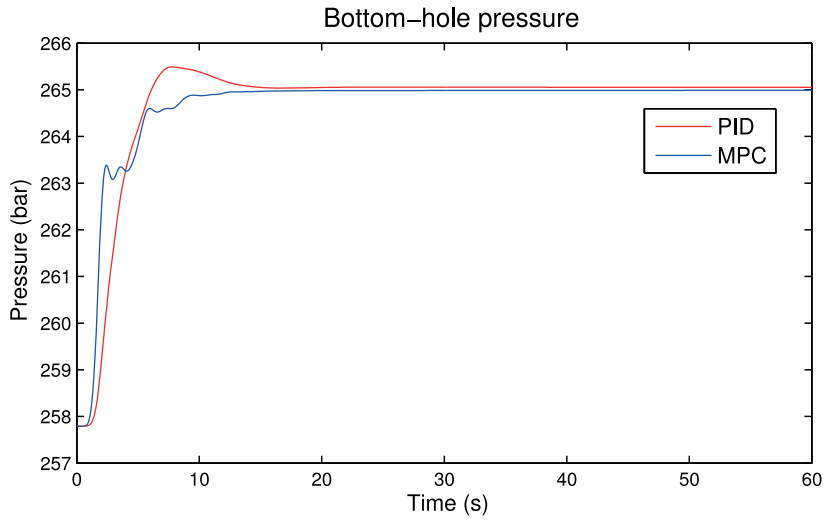
(a) Bottom-hole pressure without disturbance.
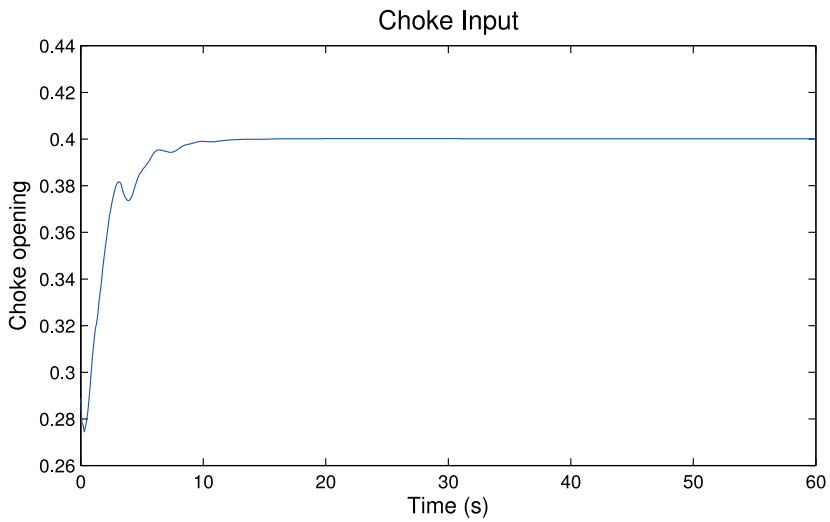
(b) MPC control signal to the choke without disturbance.

Figure 5.6: Output and control signal of MPC without disturbance.

Figure 5.8(b). Figure 5.9 shows heave disturbance pressure variations.
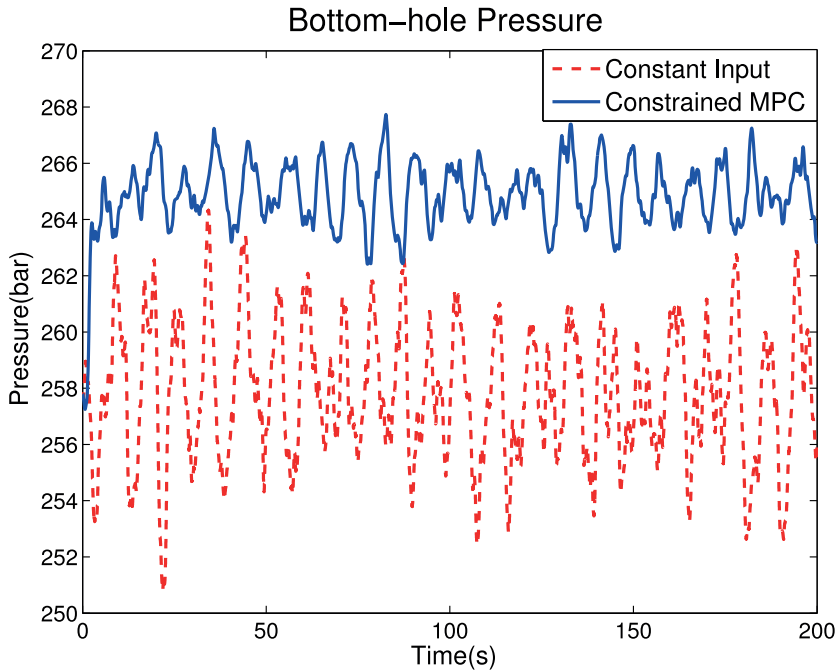
Figure 5.7: Bottom-hole pressure

The next simulation is shown in Figure 5.10 where the nominal model with heave disturbance is used for generating the measurements. The same constraints as in the previous simulation are enforced to the controller. In this simulation, the heave disturbance is assumed to be predictable. The heave disturbance is given by $v_d = cos(2\pi t/12)[m]$, where $2\pi/12$ corresponds closely to the most dominant wave frequency in the North Atlantic, with reference to the JONSWAP spectrum [49, 50]. The input weight for MPC with future knowledge of heave disturbance is chosen $R = 85$. Figure 5.10 compares the responses of MPC controller without future knowledge of heave disturbance and MPC with future knowledge of heave disturbance to track the set point reference. It is found that the MPC controller with future knowledge of heave disturbance reduces the effect of heave disturbance more significantly than the MPC controller without future knowledge of heave disturbance. The MPC can therefore efficiently utilize predictions of future heave disturbance to improve the control.
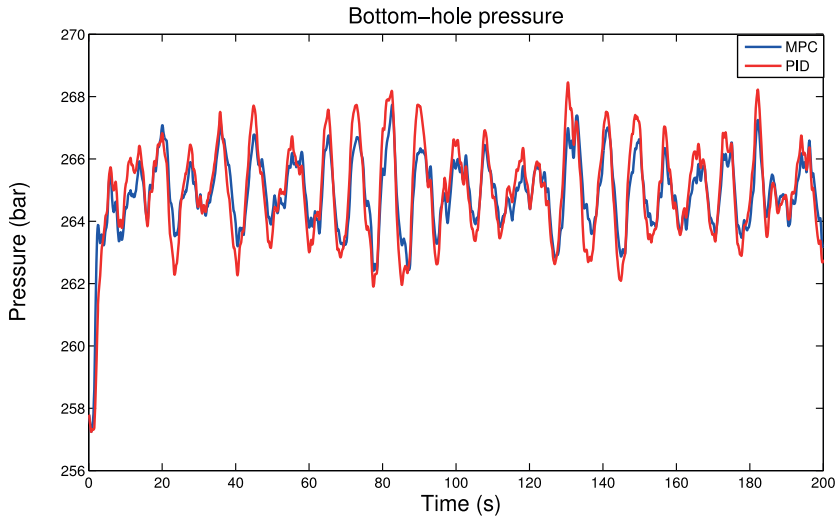
(a) Bottom-hole pressure with heave disturbance.
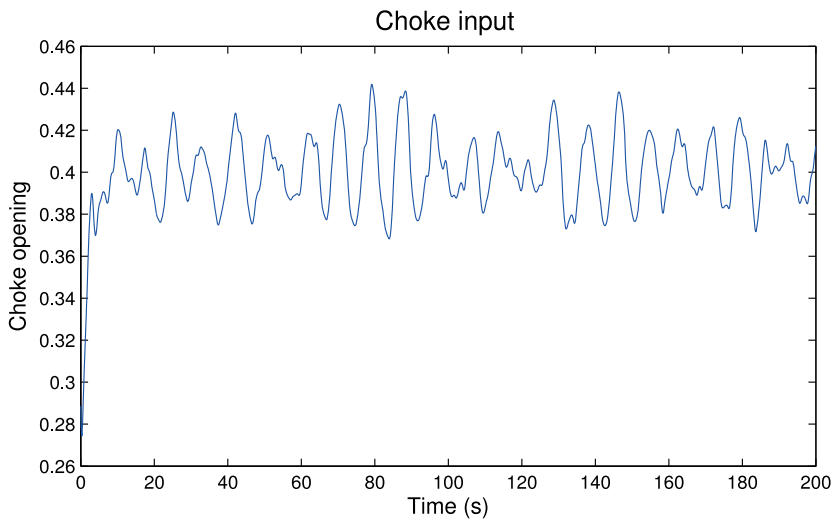
(b) MPC control signal to the choke with heave disturbance.

Figure 5.8: Output and control signal of MPC with heave disturbance.

Figure 5.9: Heave disturbance

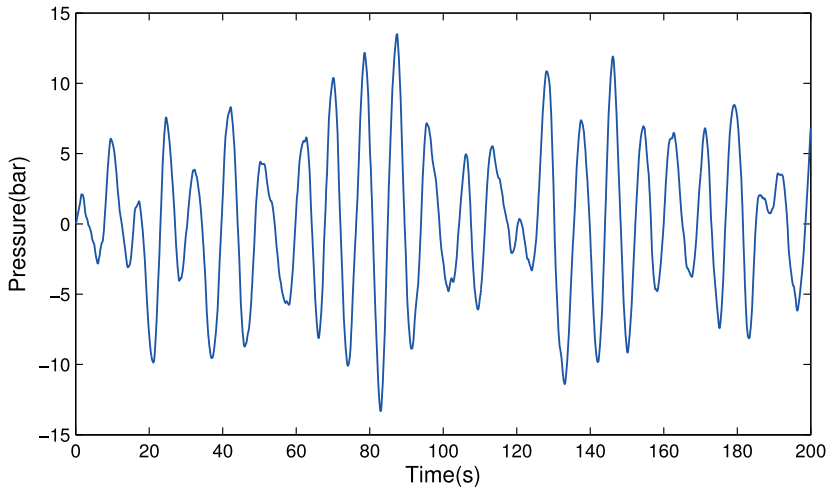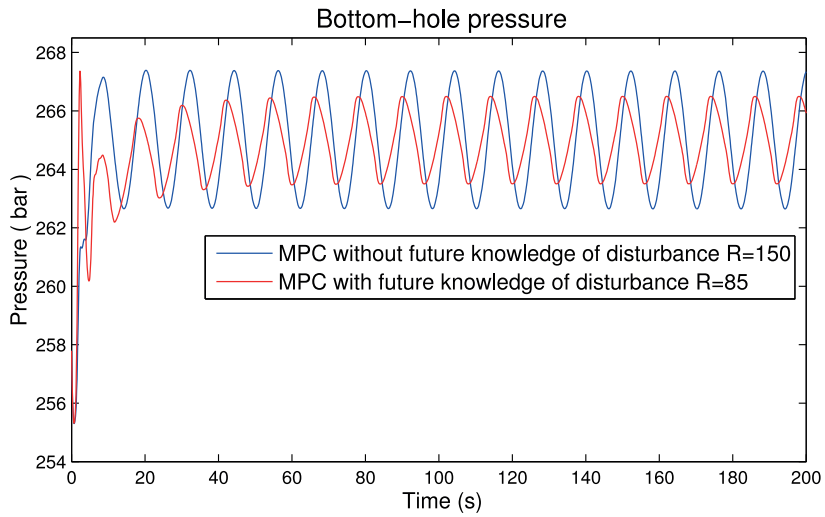Figure 5.10: Bottom-hole pressure with predictable heave disturbance.

5.4.1 Robustness Analysis of Closed-Loop System Using Monte Carlo Simulations

Finally, the robustness of the constrained MPC without future knowledge of heave disturbance with the presence of uncertainties in the friction factor and bulk modulus, 25% each, is evaluated by Monte Carlo simulations. Each simulation time was 200 s, and the simulations were done over 400 Monte Carlo runs in the uncertainty region with uniform distribution. We evaluated the performance by computing the ratio of average of RMS of the tracking error to RMS of the stochastic disturbance. The result indicates that the controller was successful to attenuate the disturbance in the uncertain system to 74.34%.

5.5 Conclusions

In this chapter, a dynamical model describing the flow and pressure in the annulus is used. The model was based on a hydraulic transmission line and is discretized using a finite volume method. The disturbance due to drill string movement is simulated as a stochastic model describing sea waves in the North Sea applied to the flow in the bottom hole of the well.

A constrained MPC for controlling bottom-hole pressure during oil well drilling was designed. It was found that the constrained MPC scheme is able to successfully control the downhole pressure. It was also found that a constrained MPC shows improved attenuation of heave disturbance. Comparing the PID controller results with MPC shows that the MPC controller has a better performance than the PID controller, being able to reduce the effect of disturbances to 77%. Monte Carlo simulations show that the constrained MPC has a good performance to regulate the set point and attenuate the effect of the heave disturbance in case of significant uncertainties in the well parameter values. Finally, it is shown that performance can be further improved by prediction of the heave motion about 10 s into the future.

Conclusions and suggestions for future work

The final chapter presents the conclusions that can be drawn from the work of this thesis, and gives possible directions for future work.

6.1 Conclusions

Since the oil production in Norway decreased from 3.22 million (B/D) in 2001 to 1.46 million (B/D) in 2013 [1], the number of depleted reservoirs and formations with low pressure margins in Norway have increased. In order to increase recovery, it is very vital to invest in developing advanced technologies which can be utilized for depleted reservoir and formations with narrow pressure window. Underbalanced drilling (UBD) and Managed pressure drilling (MPD) are drilling technologies which has been developed to work on challenging reservoir and reducing drilling problems. In order to further advance these technologies, the objectives of this work are to estimate the states and geological properties of the reservoir during UBD operation, and design of a controller to attenuate heave disturbance in offshore MPD system.

Novel methods has been designed and developed to estimate reservoir properties with using only pressure measurements and different lumped and distributed models. Meanwhile, methods to control the pressure during MPD oil well drilling using measurements and predictions of the heave disturbance has been developed.

To achieve the objectives of this work following step has been accomplished:

1. This thesis presents a nonlinear Moving Horizon Observer and joint UKF based on a nonlinear two-phase fluid flow model to estimate the

---

[1] http://www.opec.org/

annular mass of gas and liquid, and production constants of gas and liquid from the reservoir into the well during UBD operations with measuring the choke pressure and the bottom-hole pressure. The performance of the adaptive observers was tested by two different simulations with low and high measurement noise covariance during pipe connection procedure in UBD operations. In all simulations, there is no model mismatch as the same model is used for simulation and estimation. It was found that both methods are capable of identifying the production constants of gas and liquid from the reservoir into the well with sufficient accuracy. The results show that the nonlinear Moving Horizon Observer achieves better convergence and performance than the joint UKF with low and high measurement noise covariance.

2. Both the nonlinear Lyapunov-based adaptive observer and Unscented Kalman filter based on the LOL model, and the Unscented Kalman filter based on the distributed drift-flux model were designed to estimate states and the geological properties of the reservoir by using real-time measurements of the choke and the bottom-hole pressures during UBD operations. The performance of these adaptive observers was evaluated by using OLGA simulations of two drilling scenarios: a pipe connection scenario and a scenario with a changing production index. The results show that reasonable performance for both adaptive observers to detect and track a changing at production constant of gas with sufficient accuracy, while the nonlinear Lyapunov-based adaptive observer has better accuracy than the other methods for estimation of the production constants of gas and liquid from the reservoir into the well. Adaptive observers based on the LOL model are computationally simpler than joint UKF based on drift-flux model. Robustness of the adaptive observers for the scenario with a changing production index was tested in case of uncertainties and errors in the reservoir and well parameters of the model. The results show that adaptive observers based on LOL model are more sensitive to errors in the reservoir and the liquid density value than joint UKF based on drift-flux model. However, it was also found that the LOL model is sufficient for the purpose of reservoir characterization during UBD operations.

3. The Unscented and Extended Kalman filters were applied to the drift-flux model for different number of spatial discretization cells to estimate the unmeasured states, production constant of gas from the reservoir into the well, and slip parameters (S, K) during UBD operations using measurement of the bottom-hole pressure and liquid and gas rate at

the outlet. The results show reasonable performance for both adaptive observers to detect and track a changing gas production coefficient using the simulated scenario with OLGA, while the Unscented Kalman filter is more accurate than the Extended Kalman filter. In addition, both production constants of gas and liquid and distributed unmeasured states were estimated by using only measurements of the choke and the bottom-hole pressures for the pipe connection procedure. It was found that the number of cells in the spatial discretization does not have a significant effect on the accuracy of estimation. Robustness of the adaptive observers with different number of spatial discretization cells was investigated despite uncertainties in the reservoir and well parameters of the models. Since the reservoir pore pressure has a direct effect on the mass flow rates from the reservoir into the well, small inaccuracies in the reservoir pore pressure have a significant effect on the estimation of production constants. Therefore the Unscented and Extended Kalman filters are very sensitive to errors in the reservoir pore pressure value. However, these methods with different number of spatial discretization cells are robust in case of error in the liquid density value of the model.

4. Offshore MPD operation in hostile environment, such as the North Sea, is a challenging problem in drilling, since vertical movement of floating rigs with the waves, called as heave motion, induces severe pressure fluctuations at the bottom of the well. Therefor a constrained finite horizon model predictive control (MPC) scheme is designed to control the annular pressure in a well to deal with heave disturbances during offshore MPD operations. The heave disturbances were simulated as the stochastic model describing sea waves in the North Sea applied to the flow in the bottom hole of the well. The performance of this controller was compared with a standard proportional-integral-derivative (PID) control scheme. The results show that both controllers without disturbance are able to successfully control the downhole pressure. It was found that the MPC controller, with heave disturbances, has a better performance than the PID controller and can reduce the effect of disturbances to 77 %. The results show that the performance can be further improved by prediction of the heave motion about 10 s ahead. Monte Carlo simulations show that the MPC has a good performance to control the downhole pressure and attenuate the effect of the heave disturbance, while it has significant uncertainties in estimation of the well parameter values (the friction factor and bulk modulus).

6.2 Future works

6.2.1 Adaptive observer for UBD operations

Testing proposed adaptive observers with more data:

The adaptive observers proposed in this thesis were evaluated by the high-fidelity OLGA simulator. The future research could be to evaluate these proposed methods with field drilling data and full scale tests of UBD in real-time. The performance of the proposed methods should also be evaluated in scenarios with both field data and experimental data.

Using an adaptive observer for model based controller in UBD operation:

The main focus of this thesis is to estimate reservoir parameters during UBD operations. Since the primary goal of controller in UBD is to control the bottom-hole pressure and influx from the reservoir during UBD operations, the reservoir inflow model has a significant effect on a model based controller. Therefore, even small inaccuracies in the reservoir parameters will affect performance of model based controller significantly. To improve the controller performance, it appears useful to integrate the proposed adaptive observers with model-based controller. Since the LOL model is computationally simpler and faster than the drift flux model, this may be a good motivation to use the LOL model for the prediction part of a model predictive controller.

Modeling:

To improve the modeling , one may extend the simplified LOL model and the simplified drift flux model to capture the effects of cutting transport and dynamic temperature inside the annulus section of the well. For the simplified LOL model further development would be to include the dynamics of mass and momentum balances inside the drill string section of the well. Since the friction pressure loss in the well has a significant effect on the bottom-hole pressure and the reservoir model has a vital role on the influx from the reservoir, a direction of future modeling could be studying on improvement of the transient reservoir model and the model of the friction pressure loss in the well.

Estimation of the friction pressure loss in the well:

The model of the friction pressure loss in the well is function of drilling fluid viscosity, pipe roughness, velocity, Reynolds number, and flow regime (such

as slug flow, churn flow, dispersed bubble flow, Annular flow). Since the parameters of the friction pressure loss in the well have uncertainties during drilling, it is valuable to estimate the friction pressure loss in the well while drilling is performed.

6.2.2 MPC for MPD operations

Implementing the controller in real conditions:

The constrained MPC in this work was tested by simulation. Further work could be to test the constrained MPC in more realistic conditions such as high-fidelity simulator, laboratory experiment or eventually real MPD operations. Furthermore, it would be interesting for industry to implement the constrained MPC on programmable logic controller (PLC). This work may motivate further research on short-term heave motion prediction based on forward-looking sensors such as ocean wave radar.

Using an adaptive observer to constrained MPC in MPD operations:

As mentioned in chapter 5, some elements of the transient hydraulic model such as effective bulk modulus, rheology and viscosity of drilling fluid, and friction factor have significant uncertainties during MPD operations. Therefore, it is worthwhile to design adaptive estimator to estimate uncertain parameters of the transient hydraulic model for future work, and using these estimations to improve the controller performance by calibrating and tuning online the model of the MPC.

Appendices

Unscented Kalman Filter

The Unscented Kalman Filter (UKF) was introduced in[36, 37, 109]. The main idea behind the method is that approximation of a Gaussian distribution is easier than an arbitrary nonlinear function. The UKF estimates the mean and covariance matrix of estimation error with a minimal set of sample points (called sigma points) around the mean by using a deterministic sampling approach known as the unscented transform. The nonlinear model is applied to sigma points instead of a linearization of the model. So, this method does not need to calculate explicit Jacobian or Hessian. More details can be found in [36, 104, 109, 112].

A set of 2L+1 sigma points is derived from the augmented state

$$
\begin{aligned}
(\chi_{k-1})_0 &= \hat{x}_{k-1} \\
(\chi_{k-1})_i &= \hat{x}_{k-1} + (\sqrt{(L+\lambda)P_{K-1}})_i \ , i = 1, ..., L \\
(\chi_{k-1})_i &= \hat{x}_{k-1} - (\sqrt{(L+\lambda)P_{K-1}})_{i-L} \ , i = L+1, ..., 2L
\end{aligned}
\tag{A.1}
$$

where L is the dimension of the augmented states. $(\sqrt{(L+\lambda)P_{K-1}})_i$ is column i of the matrix square root of $(L+\lambda)P_{K-1}$. $(\chi_{k-1})_i$ is the ith column of the sigma point matrix χ_{k-1}. The design parameter λ is defined by

$$
\lambda = \alpha^2(L+\kappa) - L
\tag{A.2}
$$

The spread of the sigma points around the state estimate is denoted by the constant α and usually set to $10^{-4} < \alpha < 1$, κ is a secondary scaling parameter usually set to zero[109]. The UKF has two distinct steps: prediction and correction. In UKF prediction step, compute the predicted

state mean $\hat{x}_k^-$ and the predicted error covariance P_k^- as

$$(\chi_k)_i = f^a((\chi_{k-1})_i) \qquad , i = 0, ..., 2L \tag{A.3}$$

$$\hat{x}_k^- = \sum_{i=0}^{2L} W_i^{(m)} (\chi_k)_i \tag{A.4}$$

$$P_k^- = \sum_{i=0}^{2L} W_i^{(c)} [(\chi_k)_i - \hat{x}_k^-][(\chi_k)_i - \hat{x}_k^-]^T + Q_k \tag{A.5}$$

where Q is the process covariance matrix. $W_i^{(m)}$ and $W_i^{(c)}$ are defined by

$$W_0^{(m)} = \frac{\lambda}{(L + \lambda)} \tag{A.6}$$

$$W_i^{(m)} = \frac{1}{2(L + \lambda)} \qquad , i = 1, ..., 2L$$

$$W_0^{(c)} = \frac{\lambda}{(L + \lambda)} + (1 - \alpha^2 + \beta) \tag{A.7}$$

$$W_i^{(c)} = \frac{1}{2(L + \lambda)} \qquad , i = 1, ..., 2L$$

$W^{(m)}$ and $W^{(c)}$ are the weighting matrix for the state mean calculation and the covariance calculation, respectively. The scaling parameter β is used to incorporate part of the prior knowledge of the distribution of state vector . For Gaussian distribution, $\beta = 2$ is optimal [36]. In UKF correction step, the predicted weighted mean measurement can be computed as follows

$$(Y_k)_i = h((\chi_k)_i) \qquad , i = 0, ..., 2L \tag{A.8}$$

$$\hat{y}_k^- = \sum_{i=0}^{2L} W_i^{(m)} (Y_k)_i \tag{A.9}$$

In the UKF formulation, the Kalman gain is computed as follows

$$K_k = P_{\hat{x}_k \hat{y}_k} P_{\hat{y}_k \hat{y}_k}^{-1} \tag{A.10}$$

where

$$P_{\hat{x}_k \hat{y}_k} = \sum_{i=0}^{2L} W_i^{(c)} [(\chi_k)_i - \hat{x}_k^-][(Y_k)_i - \hat{y}_k^-]^T \tag{A.11}$$

$$P_{\hat{y}_k \hat{y}_k} = \sum_{i=0}^{2L} W_i^{(c)} [(Y_k)_i - \hat{y}_k^-][(Y_k)_i - \hat{y}_k^-]^T + R_k \tag{A.12}$$

covariance of the measurement and the cross-covariance of the state and measurement are denoted by $P_{\hat{y}_k \hat{y}_k}$ and $P_{\hat{x}_k \hat{y}_k}$, respectively. R_k is the measurement noise covariance matrix. Finally, the last step is to compute the updated state mean $\hat{x}_k$ and the updated error covariance P_k given by

$$\hat{x}_k = \hat{x}_k^- + K_k(y_k - \hat{y}_k^-) \tag{A.13}$$

$$P_k = P_k^- - K_k P_{\hat{y}_k \hat{y}_k} K_k^T \tag{A.14}$$

Calculation of derivative of the Lyapunov function

$$\dot{V}(e,\tilde{\theta}) = -l_1 g\cos(\Delta\theta)(e_1+e_2)^2 + \frac{e_1 e_2 w_{out}}{m_g + m_l} - \frac{e_1^2 w_{out}}{m_g + m_l} - \frac{e_2^2 w_{out}}{m_g + m_l}$$

$$-\frac{\hat{m}_g e_1 K_c Z\sqrt{\frac{p_c - p_{c0}}{V_a}}(\sqrt{m_g + m_l} - \sqrt{\hat{m}_g + \hat{m}_l})}{\hat{m}_g + \hat{m}_l}$$

$$-\frac{\hat{m}_l e_2 K_c Z\sqrt{\frac{p_c - p_{c0}}{V_a}}(\sqrt{m_g + m_l} - \sqrt{\hat{m}_g + \hat{m}_l})}{\hat{m}_g + \hat{m}_l}$$

$$+\frac{\hat{m}_l e_2^2 w_{out}}{(m_g + m_l)(\hat{m}_g + \hat{m}_l)} + \frac{\hat{m}_g e_1^2 w_{out}}{(m_g + m_l)(\hat{m}_g + \hat{m}_l)}$$

$$\implies \dot{V}(e,\tilde{\theta}) = -l_1 g\cos(\Delta\theta)(e_1+e_2)^2 + \frac{e_1 e_2 w_{out}}{m_g + m_l} - \frac{\hat{m}_g e_2^2 w_{out}}{(m_g + m_l)(\hat{m}_g + \hat{m}_l)}$$

$$-\frac{\hat{m}_l e_2 K_c Z\sqrt{\frac{p_c - p_{c0}}{V_a}}(e_1+e_2)}{(\hat{m}_g + \hat{m}_l)(\sqrt{m_g + m_l} + \sqrt{\hat{m}_g + \hat{m}_l})} - \frac{\hat{m}_l e_1^2 w_{out}}{(m_g + m_l)(\hat{m}_g + \hat{m}_l)}$$

$$-\frac{\hat{m}_g e_1 K_c Z\sqrt{\frac{p_c - p_{c0}}{V_a}}(e_1+e_2)}{(\hat{m}_g + \hat{m}_l)(\sqrt{m_g + m_l} + \sqrt{\hat{m}_g + \hat{m}_l})}$$

$$\implies \dot{V}(e,\tilde{\theta}) = -l_1 g\cos(\Delta\theta)(e_1+e_2)^2 + \frac{e_1 e_2 w_{out}}{m_g + m_l} - \frac{\hat{m}_g e_2^2 w_{out}}{(m_g + m_l)(\hat{m}_g + \hat{m}_l)}$$

$$- \frac{\hat{m}_l e_2^2 K_c Z \sqrt{\frac{p_c - p_{c0}}{V_a}}}{(\hat{m}_g + \hat{m}_l)(\sqrt{m_g + m_l} + \sqrt{\hat{m}_g + \hat{m}_l})} - \frac{e_1 e_2 K_c Z \sqrt{\frac{p_c - p_{c0}}{V_a}}}{(\sqrt{m_g + m_l} + \sqrt{\hat{m}_g + \hat{m}_l})}$$

$$- \frac{\hat{m}_l e_1^2 w_{out}}{(m_g + m_l)(\hat{m}_g + \hat{m}_l)} - \frac{\hat{m}_g e_1^2 K_c Z \sqrt{\frac{p_c - p_{c0}}{V_a}}}{(\hat{m}_g + \hat{m}_l)(\sqrt{m_g + m_l} + \sqrt{\hat{m}_g + \hat{m}_l})}$$

$$\implies \dot{V}(e, \tilde{\theta}) = -l_1 g \cos(\Delta\theta)(e_1 + e_2)^2 + \frac{e_1 e_2 w_{out}}{m_g + m_l} - \frac{\hat{m}_g e_2^2 w_{out}}{(m_g + m_l)(\hat{m}_g + \hat{m}_l)}$$

$$- \frac{\hat{m}_l e_2^2 w_{out}}{(\hat{m}_g + \hat{m}_l)(m_g + m_l + \sqrt{\hat{m}_g + \hat{m}_l}\sqrt{m_g + m_l})}$$

$$- \frac{\hat{m}_g e_1^2 w_{out}}{(\hat{m}_g + \hat{m}_l)(m_g + m_l + \sqrt{\hat{m}_g + \hat{m}_l}\sqrt{m_g + m_l})}$$

$$- \frac{e_1 e_2 w_{out}}{(m_g + m_l + \sqrt{\hat{m}_g + \hat{m}_l}\sqrt{m_g + m_l})} - \frac{\hat{m}_l e_1^2 w_{out}}{(m_g + m_l)(\hat{m}_g + \hat{m}_l)}$$

$$\implies \dot{V}(e, \tilde{\theta}) = -l_1 g \cos(\Delta\theta)(e_1 + e_2)^2 - \frac{\hat{m}_l e_1^2 w_{out}}{(m_g + m_l)(\hat{m}_g + \hat{m}_l)}$$

$$- \frac{\hat{m}_l \ e_2^2 \ w_{out}}{(m_g + m_l + \sqrt{m_g + m_l}\sqrt{\hat{m}_g + \hat{m}_l})(\hat{m}_g + \hat{m}_l)}$$

$$- \frac{\hat{m}_g \ e_1^2 \ w_{out}}{(m_g + m_l + \sqrt{m_g + m_l}\sqrt{\hat{m}_g + \hat{m}_l})(\hat{m}_g + \hat{m}_l)}$$

$$+ \frac{e_1 e_2 \ w_{out}\sqrt{m_g + m_l}\sqrt{\hat{m}_g + \hat{m}_l}}{(m_g + m_l + \sqrt{m_g + m_l}\sqrt{\hat{m}_g + \hat{m}_l})(m_g + m_l)}$$

$$- \frac{\hat{m}_g e_2^2 w_{out}}{(m_g + m_l)(\hat{m}_g + \hat{m}_l)}$$

$$\implies \dot{V}(e, \tilde{\theta}) < - \frac{e_2^2 \ w_{out}}{m_g + m_l + \sqrt{m_g + m_l}\sqrt{\hat{m}_g + \hat{m}_l}} - l_1 g \cos(\Delta\theta)(e_1 + e_2)^2$$

$$+ \frac{e_1 e_2 \ w_{out}\sqrt{m_g + m_l}\sqrt{\hat{m}_g + \hat{m}_l}}{(m_g + m_l + \sqrt{m_g + m_l}\sqrt{\hat{m}_g + \hat{m}_l})(m_g + m_l)}$$

$$- \frac{e_1^2 \ w_{out}}{m_g + m_l + \sqrt{m_g + m_l}\sqrt{\hat{m}_g + \hat{m}_l}}$$

$$\implies \dot{V}(e, \tilde{\theta}) < - l_1 g \cos(\Delta\theta)(e_1 + e_2)^2 - \frac{w_{out}(\ e_1^2 + e_2^2 - e_1 e_2 \frac{\sqrt{\hat{m}_g + \hat{m}_l}}{\sqrt{m_g + m_l}})}{m_g + m_l + \sqrt{m_g + m_l}\sqrt{\hat{m}_g + \hat{m}_l}}$$

References

[1]   O. M. Aamo, G. Eikrem, H. Siahaan, and B. A. Foss. Observer design for multiphase flow in vertical pipes with gas-lift—-theory and experiments. *Journal of process control*, 15(3):247–257, 2005.

[2]   U. J. F. Aarsnes, O. M. Aamo, F. Di Meglio, and G.-O. Kaasa. Fit-for-purpose modeling for automation of underbalanced drilling operations. In *SPE/IADC Managed Pressure Drilling & Underbalanced Operations Conference & Exhibition*. Society of Petroleum Engineers, 2014.

[3]   U. J. F. Aarsnes, F. Di Meglio, S. Evje, and O. M. Aamo. Control-oriented drift-flux modeling of single and two-phase flow for drilling. In *ASME 2014 Dynamic Systems and Control Conference*. American Society of Mechanical Engineers, October 2014.

[4]   L. E. Advantage, O. S. Church, and A. Bucksburn. Introduction to underbalanced drilling. *Leading Edge Advantage Ltd., Aberdeen*, 2002.

[5]   S. Alajmi and J. Schubert. Optimum selection of underbalanced techniques. In *SPE/IADC Middle East Drilling Technology Conference and Exhibition*, 2003.

[6]   R. Asgharzadeh Shishavan, C. Hubbell, H. Perez, J. Hedengren, D. S. Pixton, A. P. Pink, et al. Multivariate control for managed pressure drilling systems using high speed telemetry. In *SPE Annual Technical Conference and Exhibition*. Society of Petroleum Engineers, 2014.

[7]   R. Asgharzadeh Shishavan, C. Hubbell, H. Perez, J. Hedengren, D. S. Pixton, et al. Combined rate of penetration and pressure regulation for drilling optimization using high speed telemetry. In *SPE Deepwater Drilling and Completions Conference*. Society of Petroleum Engineers, 2014.

[8]   K. H. Bendiksen, D. Maines, R. Moe, S. Nuland, et al. The dynamic two-fluid model olga: Theory and application. *SPE production engineering*, 6(02):171–180, 1991.

[9]   D. Bennion, F. Thomas, R. Bietz, and D. Bennion. Underbalanced drilling, praises and perils. In *Permian Basin Oil and Gas Recovery Conference*, 1996.

[10]   D. B. Bennion. Underbalanced drilling technology candidate selection for optimal application. *Calgary, Canada: Hycal Energy Research Laboratories Ltd*, 1990.

[11]   H. Bloemen, S. Belfroid, W. Sturm, and F. Verhelst. Soft sensing for gas-lift wells. *SPE Journal*, 11(December):454–463, 2006.

[12]   Ø. Breyholtz, G. Nygaard, H. Siahaan, and M. Nikolaou. Managed pressure drilling: A multi-level control approach. In *SPE Intelligent Energy Conference and Exhibition*, number 128151-MS, Utrecht, The Netherlands, March 2010. Society of Petroleum Engineers.

[13]   L. A. Carlsen, G. Nygaard, and M. Nikolaou. Evaluation of control methods for drilling operations with unexpected gas influx. *Journal of Process Control*, 23(3):306–316, 2013.

[14]   R. Carroll and D. Lindorff. An adaptive observer for single-input single-output linear systems. *Automatic Control, IEEE Transactions on*, 18(5):428–435, 1973.

[15]   F. Di Meglio, D. Bresch-Pietri, and U. J. F. Aarsnes. An adaptive observer for hyperbolic systems with application to underbalanced drilling. In *IFAC World Congress 2014*, pages 11391–11397, 2014.

[16]   K. Do and J. Pan. Nonlinear control of an active heave compensation system. *Ocean Engineering*, 35(5–6):558–571, April 2008.

[17]   J. Eck-Olsen, M. Golan, and A. Wilhelmsen. Iadc rigpass for statoil, underbalanced drilling orientation. statoil, Bergen, Norway, 2003.

[18]   S. Evje. Weak solutions for a gas-liquid model relevant for describing gas-kick in oil wells. *SIAM Journal on Mathematical Analysis*, 43(4): 1887–1922, 2011.

[19]   S. Evje and K. K. Fjelde. Hybrid flux-splitting schemes for a two-phase flow model. *Journal of Computational Physics*, 175:674–701, 2002.

[20]   D. B. Finley, S. Shayegi, J. Ansah, I. Gil, et al. Reservoir knowledge and drilling-benefits comparison for underbalanced and managed pressure drilling operations. In *SPE/IADC Indian Drilling Technology Conference and Exhibition*. Society of Petroleum Engineers, 2006.

[21] F. Florence and F. Iversen. Real-time models for drilling process automation: Equations and applications. In *IADC/SPE Drillng Conference and Exhibition*, number 128958-MS, Louisiana, USA, February 2010. Society of Petroleum Engineers.

[22] T. I. Fossen. *Handbook of Marine Craft Hydrodynamics and Motion Control*. John Wiley & Sons, April 2011.

[23] C. E. García, D. M. Prett, and M. Morari. Model predictive control: Theory and practice—a survey. *AUTOMATICA*, 25(3):335–348, May 1989.

[24] J.-M. Godhavn. Control requirements for automatic managed pressure drilling system. *SPE Drilling & Completion*, 25(3):336–345, September 2010.

[25] J.-M. Godhavn, A. Pavlov, G.-O. Kaasa, and N. L. Rolland. Drilling seeking automatic control solutions. In *Proceedings of the 18th World Congress*, volume 18, pages 10842–10850, Milano, Italy, September 2011. The International Federation of Automatic Control, IFAC.

[26] R. A. Graham and M. S. Culen. Methodology For Manipulation Of Wellhead Pressure Control For The Purpose Of Recovering Gas To Process In Underbalanced Drilling Applications. In *Proc. SPE/IADC Underbalanced Technol. Conf. Exhib.*, Houston, Texas, October 2004. Society of Petroleum Engineers.

[27] J. E. Gravdal, R. J. Lorentzen, K. K. Fjelde, and E. H. Vefring. Tuning of computer model parameters in managed-pressure drilling applications using an unscented-kalman-filter technique. *SPE Journal*, 15(3): 856–866, 2010. doi: 10.2118/97028-PA.

[28] A. N. Gryzlov. *Model-based estimation of multi-phase flows in horizontal wells*. PhD thesis, Technische Universiteit Delft, 2011.

[29] A. Hasan and L. Imsland. Moving horizon estimation in managed pressure drilling using distributed models. In *Control Applications (CCA), 2014 IEEE Conference on*, pages 605–610. IEEE, 2014.

[30] E. Hauge, O. Aamo, J.-M. Godhavn, and G. Nygaard. A novel model-based scheme for kick and loss mitigation during drilling. *Journal of Process Control*, 23(4):463–472, 2013.

[31] M. Hernandez, D. MacNeill, M. Reeves, A. Kirkwood, S. Lemke, J. Ruszka, and R. Zaeper. High-speed wired drillstring telemetry network delivers increased safety, efficiency, reliability, and productivity

to the drilling industry. In *SPE Indian Oil and Gas Technical Conference and Exhibition*, number 113157-MS, Mumbai, India, March 2008. Society of Petroleum Engineers.

[32] S. O. Hutchison. Foam workovers cut costs 50%. *World Oil;(United States)*, 169(6), 1969.

[33] P. A. Ioannou and J. Sun. *Robust adaptive control.* Prentice Hall, 1996.

[34] S. S. Jang, B. Joseph, and H. Mukai. Comparison of two approaches to on-line parameter and state estimation of nonlinear systems. *Industrial & Engineering Chemistry Process Design and Development*, 25(3):809–814, 1986.

[35] T. A. Johansen, D. Sui, and R. Nybø. Regularized nonlinear moving horizon observer with robustness to delayed and lost data. *IEEE TRANSACTIONS ON CONTROL SYSTEMS TECHNOLOGY*, 21 (6):2114–2128, 2013.

[36] S. J. Julier and J. K. Uhlmann. Unscented filtering and nonlinear estimation. *Proceedings of the IEEE*, 92(3):401 – 422, March 2004.

[37] S. J. Julier, J. K. Uhlmann, and H. F. Durrant-Whyte. A new method for the nonlinear transformation of means and covariances in filters and estimators. *IEEE Transactions on Automatic Control*, 45(3):477–482, March 2000.

[38] G.-O. Kaasa, Ø. N. Stamnes, O. M. Aamo, and L. S. Imsland. Simplified hydraulics model used for intelligent estimation of downhole pressure for a managed-pressure-drilling control system. *SPE Drilling and Completion*, 27(1):127–138, March 2012.

[39] C. Kardolus and C. van Kruijsdijk. Formation testing while underbalanced drilling. In *SPE annual technical conference*, pages 521–528, 1997.

[40] H. K. KHALIL. *Nonlinear Systems.* Prentice Hall, 3rd edition, 2002.

[41] W. Kneissl. Reservoir characterization whilst underbalanced drilling. In *SPE/IADC drilling conference*, pages 41–49, 2001.

[42] U. A. Korde. Active heave compensation on drill-ships in irregular waves. *Ocean Engineering*, 25(7):541–561, July 1998.

[43] G. Kreisselmeier. Adaptive observers with exponential rate of convergence. *Automatic Control, IEEE Transactions on*, 22(1):2–8, 1977.

[44] S. Kuchler, T. Mahl, J. Neupert, K. Schneider, and O. Sawodny. Active control for an offshore crane using prediction of the vessel's motion. *IEEE/ASME Transactions on Mechatronics*, 16(2):297–309, April 2011.

[45] A. Lage, E. Nakagawa, R. Time, E. Vefring, and R. Rommetveit. Full-scale experimental study for improved understanding of transient phenomena in underbalanced drilling operations. In *SPE/IADC Drilling Conference*, number 52829-MS, Amsterdam, Netherlands, March 1999. Society of Petroleum Engineers.

[46] A. Lage, R. Rommetveit, and R. Time. An experimental and theoretical study of two-phase flow in horizontal or slightly deviated fully eccentric annuli. In *IADC/SPE Asia Pacific Drilling Technology*, number 62793-MS, Kuala Lumpur, Malaysia, September 2000. Society of Petroleum Engineers.

[47] A. C. Lage, K. K. Fjelde, and R. W. Time. Underbalanced drilling dynamics: Two-phase flow modeling and experiments. *SPE Journal*, 8 (1):61–70, March 2003.

[48] I. S. Landet, H. Mahdianfar, U. J. F. Aarsnes, A. Pavlov, and O. M. Aamo. Modeling for mpd operations with experimental validation. In *IADC/SPE Drilling Conference and Exhibition*, number SPE-150461, San Diego, California, March 2012. Society of Petroleum Engineers.

[49] I. S. Landet, A. Pavlov, O. M. Aamo, and H. Mahdianfar. Control of heave-induced pressure fluctuations in managed pressure drilling. In *American Control Conference (ACC)*, pages 2270–2275, Montréal, Canada, June 2012. IEEE.

[50] I. S. Landet, A. Pavlov, and O. M. Aamo. Modeling and control of heave-induced pressure fluctuations in managed pressure drilling. *IEEE Transactions on Control Systems Technology*, 21(4):1340–1351, 2013.

[51] G. Li, Y. Meng, Y. Chen, K. Zhu, X. Xu, et al. Study on pressure measuring and formation evaluation methods while underbalanced drilling. In *SPE/IADC Middle East Drilling Technology Conference and Exhibition*. Society of Petroleum Engineers, 2011.

[52] G. Li, H. Li, Y. Meng, N. Wei, C. Xu, L. Zhu, and H. Tang. Reservoir characterization during underbalanced drilling of horizontal wells based on real-time data monitoring. *Journal of Applied Mathematics*, 2014, 2014.

[53] H. P. Lohne, J. E. Gravdal, E. W. Dvergsnes, G. Nygaard, and E. H. Vefring. Automatic calibration of real-time computer models in intelligent drilling control systems - results from a north sea field trial. In *International Petroleum Technology Conference*, number 12707-MS, Kuala Lumpur, Malaysia, December 2008. International Petroleum Technology Conference.

[54] R. Lorentzen, K. Fjelde, F. Johnny, A. Lage, N. Geir, and E. Vefring. Underbalanced drilling: real time data interpretation and decision support. In *SPE/IADC drilling conference*, 2001.

[55] R. Lorentzen, K. Fjelde, F. Jonny, A. Lage, N. Geir, and E. Vefring. Underbalanced and low-head drilling operations: Real time interpretation of measured data and operational support. In *SPE Annual Technical Conference and Exhibition*, 2001.

[56] R. Lorentzen, G. Nævdal, and A. Lage. Tuning of parameters in a two-phase flow model using an ensemble kalman filter. *International Journal of Multiphase Flow*, 29(8):1283–1309, August 2003.

[57] R. J. Lorentzen, A. Stordal, G. Nævdal, H. A. Karlsen, and H. J. Skaug. Estimation of Production Rates With Transient Well-Flow Modeling and the Auxiliary Particle Filter. *SPE Journal*, 19(01):172–180, February 2014.

[58] X. Luo, R. J. Lorentzen, A. S. Stordal, and G. Nævdal. Toward an enhanced bayesian estimation framework for multiphase flow soft-sensing. *Inverse Problems*, 30(114012), 2014.

[59] W. C. Lyons et al. *Air and Gas Drilling Manual: Applications for Oil and Gas Recovery Wells and Geothermal Fluids Recovery Wells*. Gulf Professional Publishing, 2009.

[60] J. M. Maciejowski. *Predictive Control with Constraints*. Prentice Hall, 2002.

[61] H. Mahdianfar, O. M. Aamo, and A. Pavlov. Attenuation of heave-induced pressure oscillations in offshore drilling systems. In *American Control Conference (ACC)*, pages 4915–4920, Montréal, Canada, June 2012. IEEE.

[62] H. Mahdianfar, O. M. Aamo, and A. Pavlov. Suppression of heave-induced pressure fluctuations in mpd. In *Proceedings of the 2012 IFAC Workshop on Automatic Control in Offshore Oil and Gas Production*, volume 1, pages 239–244, Trondheim, Norway, May 2012. IFAC.

[63] H. Mahdianfar, A. Pavlov, and O. M. Aamo. Joint unscented kalman filter for state and parameter estimation in managed pressure drilling. In *European Control Conference*, pages 1645 – 1650, Zurich, Switzerland, July 2013. IEEE.

[64] D. Q. Mayne, J. B. Rawlings, and P. O. Rao, C. V.and Scokaert. Constrained model predictive control: Stability and optimality. *AUTOMATICA*, 36(6):789–814, 2000.

[65] H. Michalska and D. Q. Mayne. Moving horizon observers and observer-based control. *Automatic Control, IEEE Transactions on*, 40(6):995–1006, 1995.

[66] W. H. Michel. Sea spectra revisited. *Marine Technology*, 36(4):211–227, 1999.

[67] M. Morari and J. H. Lee. Model predictive control: past, present and future. *AUTOMATICA*, 23(4-5):667–682, May 1999.

[68] K. Narendra and A. Annaswamy. *Stable adaptive systems*. DoverPublications. com, 2012.

[69] T. Nazari, V. Mostafavi, and G. Hareland. Ukf-based estimation fusion of underbalanced drilling process using pressure sensors. In *Instrumentation and Measurement Technology Conference, 2009. I2MTC'09. IEEE*, pages 1006–1011. IEEE, 2009.

[70] R. Nersesian. *Energy for the 21st century: a comprehensive guide to conventional and alternative sources*. Routledge, 2014.

[71] A. Nikoofard, F. R. Salmasi, and A. K. Sedigh. An adaptive observer for linear systems with reduced adaptation laws and measurement faults. In *Control and Decision Conference (CCDC), 2011 Chinese*, pages 1105–1109. IEEE, May 2011.

[72] A. Nikoofard, T. A. Johansen, H. Mahdianfar, and A. Pavlov. Constrained mpc design for heave disturbance attenuation in offshore drilling systems. In *OCEANS-Bergen, 2013 MTS/IEEE*, pages 1–7, June 2013.

[73] A. Nikoofard, T. A. Johansen, and G.-O. Kaasa. Design and comparison of adaptive estimators for under-balanced drilling. In *American Control Conference (ACC)*, pages 5681–5687, Portland, Oregon, USA, June 2014.

[74] A. Nikoofard, T. A. Johansen, and G.-O. Kaasa. Nonlinear moving horizon observer for estimation of states and parameters in under-balanced drilling operations. In *ASME 2014 Dynamic Systems and Control Conference*. American Society of Mechanical Engineers, October 2014.

[75] A. Nikoofard, T. A. Johansen, H. Mahdianfar, and A. Pavlov. Design and comparison of constrained mpc with pid controller for heave disturbance attenuation in offshore managed pressure drilling systems. *Marine Technology Society Journal*, 48(2):90–103, March/April 2014.

[76] A. Nikoofard, U. J. F. Aarsnes, T. A. Johansen, and G.-O. Kaasa. Estimation of states and parameters of drift-flux model with unscented kalman filter. In *Proceedings of the 2015 IFAC Workshop on Automatic Control in Offshore Oil and Gas Production*, volume 2, pages 171–176, Florianópolis, Brazil, May 2015.

[77] A. Nikoofard, U. J. F. Aarsnes, T. A. Johansen, and G.-O. Kaasa. State and parameter estimation of a drift-flux model for under-balanced drilling operations. *IEEE Transactions on Control Systems Technology (submitted)*, 2015.

[78] A. Nikoofard, T. A. Johansen, and G.-O. Kaasa. Evaluation of lyapunov-based adaptive observer using low-order lumped model for estimation of production index in under-balanced drilling. In *9th International Symposium on Advanced Control of Chemical Processes (ADCHEM)*, pages 69–75, Whistler, British Columbia, Canada, June 2015. IFAC.

[79] A. Nikoofard, T. A. Johansen, and G.-O. Kaasa. Reservoir characterization in under-balanced drilling using low-order lumped model. *Journal of Process Control (submitted)*, 2015.

[80] G. Nygaard and G. Nævdal. Modelling two-phase flow for control design in oil well drilling. In *Control Applications, 2005. CCA 2005. Proceedings of 2005 IEEE Conference on*, pages 675–680. IEEE, 2005.

[81] G. Nygaard and G. Nævdal. Nonlinear model predictive control scheme for stabilizing annulus pressure during oil well drilling. *Journal of Process Control*, 16(7):719–732, August 2006.

[82] G. Nygaard, G. Nævdal, and S. Mylvaganam. Evaluating nonlinear kalman filters for parameter estimation in reservoirs during petroleum well drilling. In *Computer Aided Control System Design, 2006 IEEE*

International Conference on Control Applications, 2006 IEEE International Symposium on Intelligent Control, pages 1777–1782. IEEE, 2006.

[83] G. Nygaard, L. Imsland, and E. A. Johannessen. Using nmpc based on a low-order model for control pressure druing oil well drilling. In *8th International Symposium on Dynamics and Control of Process Systems*, volume 8. IFAC, 2007.

[84] G. H. Nygaard, E. H. Vefring, K. K. Fjelde, G. Nævdal, R. J. Lorentzen, and S. Mylvaganam. Bottomhole pressure control during pipe connection in gas-dominant wells. In *SPE/IADC Underbalanced Technology Conference and Exhibition*, number 91578-MS, Houston, Texas, October 2004. Society of Petroleum Engineers.

[85] G. H. Nygaard, L. S. Imsland, and E. A. Johannessen. Using nmpc based on a low-order model for controlling pressure during oil well drilling. In *8th International IFAC Symposium on Dynamics and Control of Process Systems*, volume 1, pages 159–164, Mexico, June 2007.

[86] G. H. Nygaard, E. Johannessen, J. E. Gravdal, and F. Iversen. Automatic coordinated control of pump rates and choke valve for compensating pressure fluctuations during surge and swab operations. Number 108344-MS, IADC/SPE Managed Pressure Drilling and Underbalanced Operations Conference and Exhibition, March 2007. Society of Petroleum Engineers.

[87] G. H. Nygaard, E. H. Vefring, K.-K. Fjelde, G. Nævdal, R. J. Lorentzen, and S. Mylvaganam. Bottomhole pressure control during drilling operations in gas-dominant wells. *SPE Journal*, 12(1):49–61, March 2007.

[88] O. G. H. Nygaard. *Multivariable process control in high temperature and high pressure environment using non-intrusive multi sensor data fusion*. PhD thesis, Norwegian University of Science and Technology (NTNU), 2006.

[89] G. Nyggard and J. Gravdal. Wemod for matlab user's guide. Technical Report 2007/234, International Research Institute of Stavanger AS (IRIS), Bergen, Norway, 2007.

[90] M. K. Ochi. *Ocean Waves - The Stochastic Approach*. Cambridge University Press, 2005.

[91] K. Ostroot, S. Shayegi, D. Zoontjes, and R. Lovorn. Comparison and advantages of underbalanced and managed-pressure drilling techniques: When should each be applied? In *Offshore Technology Conference*, 2007.

[92] M. Paasche, T. A. Johansen, and L. Imsland. Regularized and adaptive nonlinear moving horizon estimation of bottomhole pressure during oil well drilling. In *IFAC World Congress, Milano*, 2011.

[93] A. Pavlov, G.-O. Kaasa, and L. Imsland. Experimental disturbance rejection on a full-scale drilling rig. In *8th IFAC Symposium on Nonlinear Control Systems*, pages 1338–1343, University of Bologna, Italy, September 2010. IFAC.

[94] C. Perez-Tellez. *Improved bottomhole pressure control for underbalanced drilling operations*. PhD thesis, Universidad Nacional Autonoma de Mexico, 2003.

[95] C. Perez-Tellez, J. Smith, J. Edwards, et al. Improved bottomhole pressure control for underbalanced drilling operations. In *IADC/SPE Drilling Conference*. Society of Petroleum Engineers, 2004.

[96] J. Petersen, R. Rommetveit, K. S. Bjørkevoll, and J. Frøyen. A general dynamic model for single and multi-phase flow operations during drilling, completion, well control and intervention. In *IADC/SPE Asia Pacific Drilling Technology Conference and Exhibition*, number 114688-MS, Jakarta, Indonesia, August 2008. Society of Petroleum Engineers.

[97] M. Rafique. Underbalanced drilling:" remedy for formation-damage, lost-circulation, and other related conventional-drilling problems". In *SPE Western Regional and Pacific Section AAPG Joint Meeting*, 2008.

[98] C. V. Rao and J. B. Rawlings. Nonlinear moving horizon state estimation. In *Nonlinear model predictive control*, pages 45–69. Springer, 2000.

[99] O. S. Rasmussen and S. Sangesland. Evaluation of mpd methods for compensation of surge-and-swab pressures in floating drilling operations. Number 108346-MS, Texas, U.S.A., March 2007. IADC/SPE Managed Pressure Drilling & Underbalanced Operations, IADC/SPE.

[100] S. Raza, S. Marsden, et al. The streaming potential and the rheology of foam. *Society of Petroleum Engineers Journal*, 7(04):359–368, 1967.

[101] B. Rehm, J. Schubert, A. Haghshenas, A. S. Paknejad, and J. Hughes. *Managed Pressure Drilling*. Gulf Publishing Company, 2008.

[102] B. Rehm, A. Haghshenas, A. S. Paknejad, A. Al-Yami, and J. Hughes. *Underbalanced Drilling: Limits and Extremes*. Elsevier, 2013.

[103] H. Shi, J. A. Holmes, L. J. Durlofsky, K. Aziz, L. Diaz, B. Alkaya, G. Oddie, et al. Drift-flux modeling of two-phase flow in wellbores. *Spe Journal*, 10(01):24–33, 2005.

[104] D. Simon. *Optimal state estimation: Kalman, H infinity, and nonlinear approaches*. Wiley. com, 2006.

[105] Ø. N. Stamnes, J. Zhou, O. M. Aamo, and G.-O. Kaasa. Adaptive observer design for nonlinear systems with parameteric uncertainties in unmeasured state dynamics. In *IEEE Conference on Decision and Control*, 2009. doi: 10.1109/CDC.2009.5400944.

[106] E. Storkaas, S. Skogestad, and J.-M. Godhavn. A low-dimensional dynamic model of severe slugging for control design and analysis. In *11th International Conference on Multiphase flow (Multiphase03)*, pages 117–133, 2003.

[107] D. Sui and T. A. Johansen. Moving horizon observer with regularisation for detectable systems without persistence of excitation. *International Journal of Control*, 84(6):1041–1054, 2011.

[108] B. O. Teixeira, W. S. Castro, A. F. Teixeira, and L. a. Aguirre. Data-driven soft sensor of downhole pressure for a gas-lift oil well. *Chemical Engineering Practice*, 22:34–43, January 2014.

[109] R. van der Merwe. *Sigma-Point Kalman Filters for Probabilistic Inference in Dynamic State-Space Models*. PhD thesis, Oregon Health & Science University, April 2004.

[110] E. H. Vefring, G. Nygaard, R. J. Lorentzen, G. Nævdal, K. K. Fjelde, et al. Reservoir characterization during ubd: Methodology and active tests. In *IADC/SPE Underbalanced Technology Conference and Exhibition*. Society of Petroleum Engineers, 2003.

[111] E. H. Vefring, G. H. Nygaard, R. J. Lorentzen, G. Naevdal, K. K. Fjelde, et al. Reservoir characterization during underbalanced drilling (ubd): methodology and active tests. *SPE Journal*, 11(02):181–192, 2006.

[112] E. A. Wan and R. van der Merwe. *The Unscented Kalman Filter, in Kalman Filtering and Neural Networks (ed S. Haykin)*, chapter 7. John Wiley & Sons, New York, USA, March 2002.

[113] J. Zhou and G. Nygaard. Automatic model-based control scheme for stabilizing pressure during dual-gradient drilling. *Journal of Process Control*, 21(8):1138–1147, September 2011.

[114] J. Zhou, Ø. N. Stamnes, O. M. Aamo, and G.-O. Kaasa. Switched control for pressure regulation and kick attenuation in a managed pressure drilling system. *IEEE Transactions on Control Systems Technology*, 19(2):337–350, 2011. doi: 10.1109/TCST.2010.2046517.